Silk Fibroin – Characterization and Chemical Modification of a Unique Biomaterial for Controlled Release

Inauguraldissertation

zur

Erlangung der Würde eines Doktors der Philosophie

vorgelegt der

Philosophisch-Naturwissenschaftlichen

Fakultät der Universität Basel

von

Kira Helga Maria Nultsch

aus Buchen (Odenwald), Deutschland

Basel, 2018

Genehmigt von der Philosophisch-Naturwissenschaftlichen Fakultät

auf Antrag von

Fakultätsverantwortlicher Prof. Dr. Georgios Imanidis

Korreferentin Prof. Dr. Dagmar Fischer

Basel, den 18.09.2018

Prof. Dr. Martin Spiess
Dekan

In der Wissenschaft gleichen wir alle nur den Kindern, die am Rande des Wissens hie und da einen Kiesel aufheben, während sich der weite Ozean des Unbekannten vor unseren Augen erstreckt.

- Sir Isaac Newton -

Table of Contents

I. Abbreviations

BSA	Bovine serum albumin
CLSM	Confocal laser scanning microscopy
CuAAC	Copper (I)-catalyzed alkyne-azide cycloaddition
DEAE-dextran	Diethylaminoethyl-dextran
DDS	Drug delivery system
DLS	Dynamic light scattering
EGF	Epidermal growth factor
FDA	Food and drug administration
FITC	Fluorescein isothiocyanate
FT-IR	Fourier-transform infrared spectroscopy
HPLC	High performance liquid chromatography
IEF	Isoelectric focusing
IgE	Immunoglobulin E
IGF	Insulin-like growth factor
MMP	Matrix metalloproteinase
NGF	Nerve growth factor
PEG	Poly (ethylene glycol)
PGA	Poly (glycolic acid)
PLA	Poly (lactic acid)
PVA	Poly (vinyl alcohol)
SDS PAGE	Sodium dodecyl sulfate poly (acrylamide) gel electrophoresis
SEC	Size exclusion chromatography
SEM	Scanning electron microscopy
siRNA	Small interfering ribonucleic acid

SF	Silk Fibroin
TGA	Thermogravimetric analysis
USP	United States Pharmacopeia
VEGF	Vascular endothelia growth factor
WAX	Weak anion exchange chromatography

II. Abstract

Around 100 years ago, Paul Ehrlich postulated the “magic bullet”, a personalized and tailored drug that can hit the affected tissue like a bullet from a gun. Since then on a lot of research has been conducted to develop such “magic bullets”. To deliver a drug to the target location, usually a carrier/vehicle is needed (drug delivery system). Conventional ways to administer drugs are by tablets or parenterals, whereas the latter often suffers from high plasma concentration for a short time period, followed by a more or less fast decrease of the plasma concentration. Depending on the elimination constant, repeated drug administration can lead either to a diminished effect if the active ingredient is fast eliminated, or to side effects if the active ingredient cumulates. To control the release, local drug release might be considered with the advantage that systematic side effects can be reduced. As a result, local drug delivery systems gain more and more interest with the challenge to achieve a sustained release without impacting the surrounding healthy tissue. In order to achieve this controlled drug delivery and an optimal therapeutic effect, a lot of research has been carried out for targeted delivery with a controlled release rate. However, a drug delivery system has to meet several requirements, e.g. mechanical stability, controllable structure and degradation. Due to its extraordinary properties (e.g. mechanical strength, biocompatibility, biodegradability into non-toxic products, FDA-approved), silk fibroin (SF) has been in the focus of research since a long time, especially in terms of sustained release drug delivery systems. One of the major advantages of SF compared to other biomaterials is that it can be assembled into a variety of matrices (e.g. particles, foams, gels, electrospun mats) [1, 2].

The objective of the first study was to characterize silk fibroin in more detail. The focus was set on different purification processes of SF in order to efficiently remove sericin and a method to detect residual sericin was established. This is important to ensure biocompatibility since the combination of sericin and silk fibroin can cause allergic reactions. The degumming process significantly affected SF integrity, particularly mechanical strength and molecular weight distribution. These factors are crucial for the preparation of drug delivery systems, since they can influence the degradation rate of the drug delivery system and as a result, the release rate of the drug.

The second study aimed to investigate the release behaviour of differently charged macromolecular drugs from SF films. Since biologicals and nucleic acids (respectively nucleic acid/polymer complexes)

are becoming an emerging field, the importance to understand the release behaviour of these macromolecular, charged compounds is growing. Therefore, differently charged, high molecular weight dextran derivatives, used as model drugs, were encapsulated into SF films and their release behaviour was studied. Additionally, the effect of SF purification process, with focus on degumming time, on drug release was elucidated. The release rate was found to be highly dependent on matrix properties, controllable via the purification process.

In the third part, silk fibroin films were chemically modified via copper (I)-catalyzed alkyne-azide cycloaddition (CuAAC) to further control drug release. The already existing, extraordinary features of silk fibroin can be enlarged by chemical modification, extending their range of applications. By varying the modification degree, the release was controlled, aiming a more pronounced sustained release, and additionally, the surface properties with regard to hydrophilicity were tuned.

III. Zusammenfassung

Vor rund 100 Jahren prägte Paul Ehrlich den Begriff "Zauberkugel", ein personalisiertes und maßgeschneidertes Medikament, das genau wie eine Kugel aus einer Waffe nur ein bestimmtes Gewebe trifft, ohne gesundes Gewebe zu beschädigen. Seit jeher bestrebt die Forschung, dieses Ziel zu erreichen. Um ein Medikament an den Zielort zu transportieren, wird üblicherweise ein Träger benötigt (Wirkstofffreisetzungssystem oder auch Drug Delivery System). Häufig vorkommende Darreichungsformen für Wirkstoffe sind, z.B. Tabletten oder Parenteralia, wobei Letztere den Nachteil besitzen, dass sie häufig die gesamte Wirkstoffmenge auf einmal freisetzen, was zu einer hohen Plasmakonzentration für eine kurze Zeitdauer führt. Je nach Eliminationskonstante kann es dann nach erneuter Wirkstoffapplikation zu einer mehr oder weniger schnellen Abnahme des Plasmaspiegels führen und somit auch zu einem Nachlassen der Wirkung, oder zu einer Wirkstoffakkumulierung und somit zu unerwünschten Nebenwirkungen. Um diesen Nachteil zu umgehen, kann die lokale Applikation in Betracht gezogen werden, so dass systemische Nebenwirkungen reduziert werde. Daher gewinnen Wirkstofffreisetzungssysteme, die lokal verabreicht werden können, immer mehr Interesse mit der Herausforderung eine gleichmäßig anhaltende Freisetzung zu erzielen, ohne dabei das umliegende, gesunde Gewebe zu beeinträchtigen. Um diese kontrollierte Arzneimittelabgabe und einen optimalen therapeutischen Effekt zu erreichen, wurde viel in diesem Bereich geforscht, so dass Wirkstoffe mit einer kontrollierten Freisetzungsrate an ihren Zielort im Körper transportiert werden. Ein Wirkstofffreisetzungssystem muss jedoch verschiedene Anforderungen erfüllen, z.B. eine hohe mechanische Stabilität, eine definierte Struktur und bekannte Abbauprodukte. Aufgrund der außergewöhnlichen Eigenschaften (z. B. mechanische Festigkeit, Biokompatibilität, biologische Abbaubarkeit zu ungiftigen Produkten, FDA-Zulassung), ist Seidenfibroin (SF) seit langem im Fokus der Forschung, insbesondere in Bezug auf Systeme mit verzögerter Wirkstoffabgabe. Einer der Hauptvorteile von SF im Vergleich zu anderen Biomaterialien besteht darin, dass es als Basis für eine Vielzahl unterschiedlicher Darreichungsformen verwendet werden kann (z. B. Partikel, Schäume, Gele, elektrogesponnene Fasermatten).

Ziel der ersten Studie war es, das Seidenfibroin detaillierter zu charakterisieren. Der Fokus lag auf verschiedenen Aufreinigungsprozessen von Seidenfibroin, um das Sericin effizient zu entfernen und

eine Methode zum Nachweis von Rest-Sericin zu etablieren. Dies ist wichtig, um die Biokompatibilität sicherzustellen. Der Aufreinigungsprozess beeinflusste signifikant die SF-Integrität, insbesondere die mechanische Festigkeit und die Molekulargewichtsverteilung. Diese Faktoren müssen bei der Herstellung von Wirkstofffreisetzungssystemen bedacht werden, da sie Einfluss auf die Freisetzungsrate und auf den Abbau des Wirkstofffreisetzungssystems haben können.

Die zweite Studie untersuchte das Freisetzungsverhalten von makromolekularen, unterschiedlich geladenen Modellwirkstoffen aus SF-Filmen. Da Biologika zu einem aufstrebenden Gebiet werden, wächst auch die Nachfrage, das Freisetzungsverhalten dieser Verbindungen besser voraussagen zu können. Daher wurden Dextran-Derivate mit hohem Molekulargewicht und unterschiedlicher Ladung aus SF-Filmen freigesetzt und die Freisetzungsraten untersucht. Zusätzlich wurde der Effekt des SF-Aufreinigungsprozesses, vor allem hinsichtlich der Kochzeit der Seidenfibroin-Fasern, auf die Wirkstofffreisetzung untersucht.

Im dritten Teil wurden SF-Filme über eine Kupfer (I) –katalysierte Huisgen-Cycloaddition (CuAAC) chemisch modifiziert, um eine verzögerte Freisetzung zu erreichen. Die bereits vorhandenen, außergewöhnlichen Eigenschaften von SF konnten durch chemische Modifikation ergänzt werden, wodurch auch der Anwendungsbereich erweitert werden. Die Freisetzung kann durch chemische Modifikation gesteuert werden und zusätzlich kann die Oberfläche maßgeschneidert werden, um somit die Wechselwirkung des Gewebes am Zielort und SF zu steuern.

1. Aim of the Work

Naturally derived polymers can substitute inorganic and plastic materials. One of the major challenges is to identify a biopolymer that is capable to remain its chemo-physical properties as drug delivery system while fitting the current requirements of the technology and realizing a cost-competitive and convenient supply chain. Due to their mechanical stability along with other excellent properties (e.g. biocompatibility, biodegradability), silk materials are well suited for biomedical applications including drug delivery systems. Since chronic wounds are an emerging field due to the ageing population, the aim of this thesis was to produce a silk-based drug delivery system for topical applications. In general, the milieu of chronic wounds is characterized by overexpression of specific enzymes (matrix metalloproteinase MMP). The basic idea was to invent a drug delivery system with bioresponsive properties, meaning that a high amount of inflammatory enzymes in the wound can upregulate the release of anti-inflammatory drugs. As the characterization of the starting material is the critical step for the quality of the product, especially for naturally derived materials (due to the batch-to-batch variability), in a first study the silk material was characterized in detail. The main focus was set on an effective protein purification while retaining the silk fibroin (SF) integrity. Especially for early stage and scale-up production, it is essential to develop a robust and scalable SF purification and processing process, as well as the establishment of an analytical tool that allows material characterization. Besides various morphologies (particles, gels, foams, nonwovens, etc.), films are very interesting in terms of tissue engineering, for implant coatings and topical applications. Therefore, in a next step, SF films were loaded with model compounds in order to investigate release behaviour of drugs with different physicochemical properties (high molecular weight and different charges). In a last step, a way to chemically modify and thus, crosslink SF films was investigated and release behaviour of high molecular weight and differently charged model compounds was studied.

2. Theoretical Section

2.1. Silk Fibroin as Biomaterial

2.1.1. Biomaterials

The most accepted definition of biomaterial is currently defined by the American National Institute of Health, describing a biomaterial as “any substance or combination of substances, other than drugs, synthetic or natural in origin, which can be used for any period of time, which augments or replaces partially or totally any tissue, organ or function of the body, in order to maintain or improve the quality the quality of life of the individual” [3]. The range of use for biomaterials with synthetic and natural origin continues growing. Besides the traditional use of biomaterials for medical devices, implants and for tissue engineering, the application is widened to smart drug delivery systems and hybrid organs [4]. In general, biomaterials should be non-immunogenic and provide a broad range to control structure, morphology and function, while retaining their mechanical stability [5]. The major advantages of biomaterials are their biocompatibility and their biodegradability into non-toxic, water soluble products that can be excreted from the body [6]. Synthetic polymers, such as poly (glycolic acid) (PGA) and poly (lactic acid) (PLA), offer characteristics for sustained release up to several months, but they often need harsh conditions and organic solvents for their processing, limiting the biocompatibility [7]. Besides, the acidic degradation products restrict their use for protein therapeutics, since this may affect the product stability [8]. In contrast, natural polymers, such as collagen, albumin and elastin can be processed under mild conditions with the drawback that biopolymers tend to rapidly resolubilize in aqueous environment, since they are often hydrophilic, resulting in burst release profiles [9]. In addition, naturally derived materials are characterized by a wide batch-to-batch variety and concerns regarding sourcing. To meet these expectations, a natural-based product should provide enhanced product stability and tunable sustained release kinetics and as starting material, it should be well-characterized [7].

Silk as the “queen of all fabrics” was discovered around 2700 BCE in China and since then silk is a symbol of royalty and health [10]. Silk from mulberry silkworm *Bombyx mori* has been used for thousands of years to produce textiles due to its luster, softness, dyeability and light weight. In general, silk is produced by several worms of the order *Lipedoptera* (e.g. Bombycidae, Saturniidae) and by

members of *Arachnida* (more than 30 000 spider species) [11]. Among all these different silks, silk from the domesticated silkworm *Bombyx mori* and the spider silk of *Nephila clavipes* and *Araneus diadematus* are the most studied. In contrast to silkworms, spiders are able to produce seven different kinds of silk, e.g. for the nests, webs, egg protection, safety lines etc. [12]. In the fifth instar, the silkworm starts producing a large amount of silk in its inner pair of silk glands, within three days a cocoon is spun consisting of one fiber (300-1200m) [13]. After 15 to 20 days, the pupae hatches and emerges from the cocoon with a complete new physiology and morphology.

Silk provides a unique combination of properties, beneficial for drug delivery (**Table 1**), including biocompatibility, biodegradation into non-toxic products [14], aqueous-based processing [15], and high mechanical strength [16]. On the basis of the background given above and the fact, that silk fibroin is already FDA approved, the following work focuses on silk derived from the domesticated silkworm *Bombyx mori*.

Table 1. *The unique combination of properties of silk for sustained drug delivery in distinction to synthetic polymer systems (e.g. PLGA), highlighted in* ***bold****. Reprinted from [7] with permission from Elsevier.*

Structure	Predominantly hydrophobic blocks, block copolymeric and modifiable sequence Self-assembly into β-sheet rich supramolecular structures Strong intra-/intermolecular physical interactions Stimuli-responsive crystal polymorphism High and tunable molecular weight
Processing	**Aqueous-based ambient purification and processing capabilities** Versatile material forms **Suitability with common sterilization technologies**
Physicochemical properties	Controllable network density, hydration resistance and swelling Controllable surface charge through sequence modifications **High thermal stability** **Robust mechanical properties** Tunable aqueous solubility
Biological properties	Low inflammatory/cytotoxic/immunogenic potential **Enzymatic, surface mediated biodegradation** Slow, controllable biodegradation rates **Non-toxic, neutral biodegradation products (amino acids and peptides)**

Pharmacological properties	Tunable release via diffusion- and biodegradation-controlled release Encapsulation of poorly soluble drugs **Drug stabilization**

2.1.2. Structural Properties of Silk

Silk comprises mainly two proteins, silk fibroin (SF) and sericin, whereas the latter forms a glue-like envelope around two fibroin brins (**Figure 1**). Sericin accounts for approximately 20 to 30% of the silk fiber, soluble in hot water due to the high content of hydrophilic amino acids (**Table 2**). Sericin is characterized by a broad molecular weight distribution (40-400 kDa) and reduces the shear stress during spinning [17].

Figure 1. *The raw silk consists of two fibroin fibers glued together with a layer of sericin on their surfaces. Reprinted from [1] with permission from Elsevier.*

The SF itself consists of a heavy (approx. 350 kDa) and a light chain (approx. 25 kDa), connected via a disulfide bond at the C-terminus of the heavy chain and this disulfide bond might play a key role in β-sheet formation [14].

Additionally, a glycoprotein p25 (30 kDa) binds to the SF in a ratio of 6:1 (SF:p25) via hydrophobic interactions. The glycoprotein is important, on the one hand, for the maintenance of the structural integrity of the heavy and light chain complex, and on the other hand, for the formation of micellar structure, allowing the transportation of large fibroin amounts through the silk gland before spinning [18, 19].

The amino acid composition of fibroin is primarily composed of approximately 45% glycine, 30% alanine and 12% serine, whereas tyrosine occurs at approximately 5% as one of the larger amino acid with a polar side chain (**Table 2**) [20].

***Table 2**. Amino acid composition of the polypeptides sericin and fibroin. Reprinted from [20] with permission from Elsevier.*

Amino acid	**Sericin**	**Fibroin**
Glycine	13.9	44.5
Alanine	4.6	29.3
Valine	3.2	2.2
Leucine	1.2	0.5
Isoleucine	0.7	0.7
Serine	32.3	12.1
Threonine	8.4	0.9
Aspartic acid	14.5	1.3
Glutamic acid	4.8	1.0
Lysine	8.4	0.3
Arginine	2.3	0.5
Histidine	1.6	0.2
Tyrosine	2.6	5.2
Phenylalanine	0.4	0.6
Proline	0.4	0.3
Methionine	0.1	0.1
Cysteine	0.3	0.2

The light chain of SF is formed by 262 amino acids. As its size is much smaller compared to the heavy chain, the light chain plays a minor role in mechanical properties of SF. The heavy chain, as the major structural component of the protein, is characterized by amphiphilic, alternating block polymers, allowing the formation of β-sheets [20]. This co-polymer consists of 12 repetitive oligopeptide motifs GAGAGX (where X = alanine, serine or tyrosine), responsible for β-sheet formation, and 11 less repetitive, hydrophilic and bulky, amino acids, responsible for amorphous domains [2, 7]. These amorphous regions together with the hydrophilic C- and N-terminus (**Figure 2a**) give the molecule an overall negative charge (pI ~ 4) at physiological pH [19]. The crystalline regions form antiparallel β-sheets in aqueous solution (silk II), where methyl side groups of alanine are pointing alternatively toward both sides of the β-sheet structure [21], allowing inter- and intramolecular intersheet stacking [22]. At air/water interface a helical structure is formed (silk III), involving an hexagonal packing of the SF molecules in a threefold helical conformation [23]. In contrast, the silk I structure is a water soluble

form of SF (glandular state prior to crystallization) and is converted into the silk II structure upon exposure to heat or shear forces, or after methanol, ethanol or water vapor treatment [15, 24, 25]. The β-sheet structure is soluble in aqueous, chaotropic agents (lithium bromide, lithium thiocyanate, calcium chloride etc.), which are able to disrupt intermolecular hydrogen bonds between SF chains [26, 27]. After dilution, the solution is subsequently dialyzed in order to obtain an aqueous solution (see chapter 2.1.3 Applications of Silk Fibroin) [24].

However, the primary sequence of SF with its hydrophobic, repetitive and hydrophilic, non-repetitive domains allows the formation of micellar structures (**Figure 2b**), where the hydrophilic, terminal blocks define the outer structure of the micelle. The hydrophilic domains between the hydrophobic domains enable the micelles to remain soluble in water. Increasing SF concentration leads to increasing inter-micellar interaction, resulting in the formation of globular structures and further in gelation (**Figure 2c**) [2].

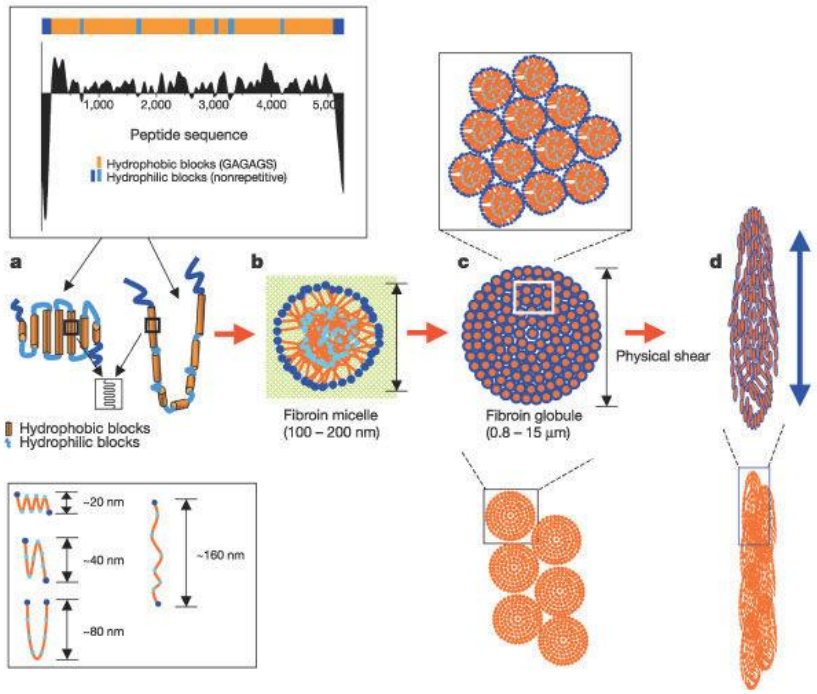

***Figure 2**. a Heavy chain of Silk Fibroin with hydrophobic and hydrophilic blocks. b SF micelle. c SF globule, consisting of several micelles. d Fibrillar arrangement after application of physical shear. Reprinted from [2] with permission from Elsevier.*

These hierarchical structures, especially the ability of SF to form β-sheets, give the material its extraordinary strength and stiffness, exceeding the breaking strength and toughness of Kevlar and other

natural and synthetic polymers [28, 29]. In **Table 3**, the mechanical properties of silk and other fibrous materials are compared.

Table 3*. Comparison of mechanical properties of silk, and synthetic and natural fibers. Table adopted from [1] with permission from Elsevier.*

Material	**Young's Modulus / GPa**	**Ultimate Strength / %**	**Breaking Strain / %**
Silkworm (*Bombyx mori*)	10-17	300-740	4-26
β-sheet crystallites (*Bombyx mori*)	22.6	-	-
Spider silk	10	1100	27
Nylon	1.8-5	430-950	18
Kevlar	130	3600	2.7

The hydrogen bonds and Van der Waals interactions, present in the SF structure, contribute mainly the stability of this structure and result in strength and stiffness [30]. In contrast, the semi-amorphous matrix allows extensibility and toughness of the SF fiber. Upon tensile loading, the β-sheet structures orientate along the fiber axis (**Figure 2d**), whereas the semi-amorphous structures start to unravel [31].

2.1.3. Applications of Silk Fibroin

Textile industry. Silk fibroin with its unique properties provides a wide variety of application, not only as material for textiles but also as biomaterial in the medical and pharmaceutical field. Today, there are different natural (e.g. silk, wool) and synthetic (e.g. polyester) materials available for the textile industry. Due to its exceptional appearance and properties (soft texture, luster, dyeability and moisture-absorbance ability), silk is still an attractive textile choice, especially for luxurious clothing. To achieve the softness and luster of the silk fabrics, the sericin has to be removed by a so-called degumming process (degumming, since the sericin constitutes the glue between the two fibroin filaments). During unreeling of the cocoons and followed by knitting or weaving into fabrics, the sericin remains on the fiber in order to protect it. In contrast to fibroin, sericin is soluble in hot water due to high amount of hydrophilic amino acids (**Table 2**). After the production of the silk textile, the degumming is traditionally carried out in Marseille soap and elevated temperature (90-95°C). However, this treatment takes up to six hours and might affect SF fibers [32].

SF purification. For an effective sericin removal for biomedical applications, the purification of SF is commonly carried out using a 0.2 M sodium carbonate solution at 100°C for at least one hour (**Figure 3a**). After drying, the SF fibers are dissolved in a highly concentrated salt solution (e.g. 9 M lithium bromide) and in a next step, the salt is removed via dialysis (**Figure 3a**). Further treatments for an effective removal of sericin are discussed in 3.1 Effects of Degumming Process on Physicochemical and Mechanical Properties of Silk Fibroin. The sericin removal is not only for optical but also for health purposes, since the combination of both silk proteins, fibroin and sericin, can lead to allergies (see following paragraph).

Bio-response to silk. Biological responses to silk have been reported mainly related to allergic reactions, especially type I allergic responses and elevated immunoglobulin E (IgE) level, when patients had contact with silk sutures [33, 34]. Additionally, respiratory response, e.g. asthma, was manifested after silk contact and sericin was accused to trigger T-cell mediated allergic response [35, 36]. Nevertheless, sericin features several biological properties, e.g. anti-oxidant, anti-inflammatory, collagen promoting and tumor inhibitory effects, and, thus, has been investigated for its use in medical applications [37]. Due to the weak structural properties and the high water solubility, sericin is more applicable in the field of neural applications. Unfortunately, the simultaneous presence of both proteins, silk fibroin and sericin, decrease the biocompatibility and limit the application of the virgin silk. Hence, the sericin has to be removed by the above-mentioned degumming process. However, further investigations regarding the immune response and extensive characterization of macrophage invasion and locally released cytokines is needed to pioneer the application of SF based drug delivery systems [38].

Suture material. Low bacterial adherence and the high mechanical strength enable the use of SF as suture material since centuries. As defined by the US Pharmacopeia (USP), silk fibroin (suture) material is absorbable ("loses most of its tensile strength within 60 days") and non-degradable [1]. Nonetheless, SF was shown to be degradable in recent studies but over a longer period, e.g. SF suture material loses the majority of its tensile strength within one year [5, 39], depending strongly on the purification process of fibroin (short vs. long degumming), the kind of system (porous vs. dense) and the implantation site. Due to the fact, that silk fibroin is used as a suture material for surgeries, it is already FDA approved, making it an attractive basis for drug delivery systems, tissue engineering and other medical devices. One fibroin

based scaffold, which passed the regulatory scrutiny, is the Seri® Surgical Scaffold (Allergan, MA, USA), which is functionalized with RGD motifs to promote cellular growth. This scaffold is used for soft tissue repair and crucial ligament repair [40], paving the way for further application of SF-based drug delivery systems.

A lot of research has been conducted for SF based drug delivery systems, since SF can be assembled in a variety of matrices, e.g. particles, hydrogels sponges, fibers and meshes (**Figure 3a**), delivering a wide range of active molecules, such as genes, small molecules and biologicals. The purified silk fibroin solution can be processed into a variety of morphologies with attractive features, e.g. large surface area and high porosity [41].

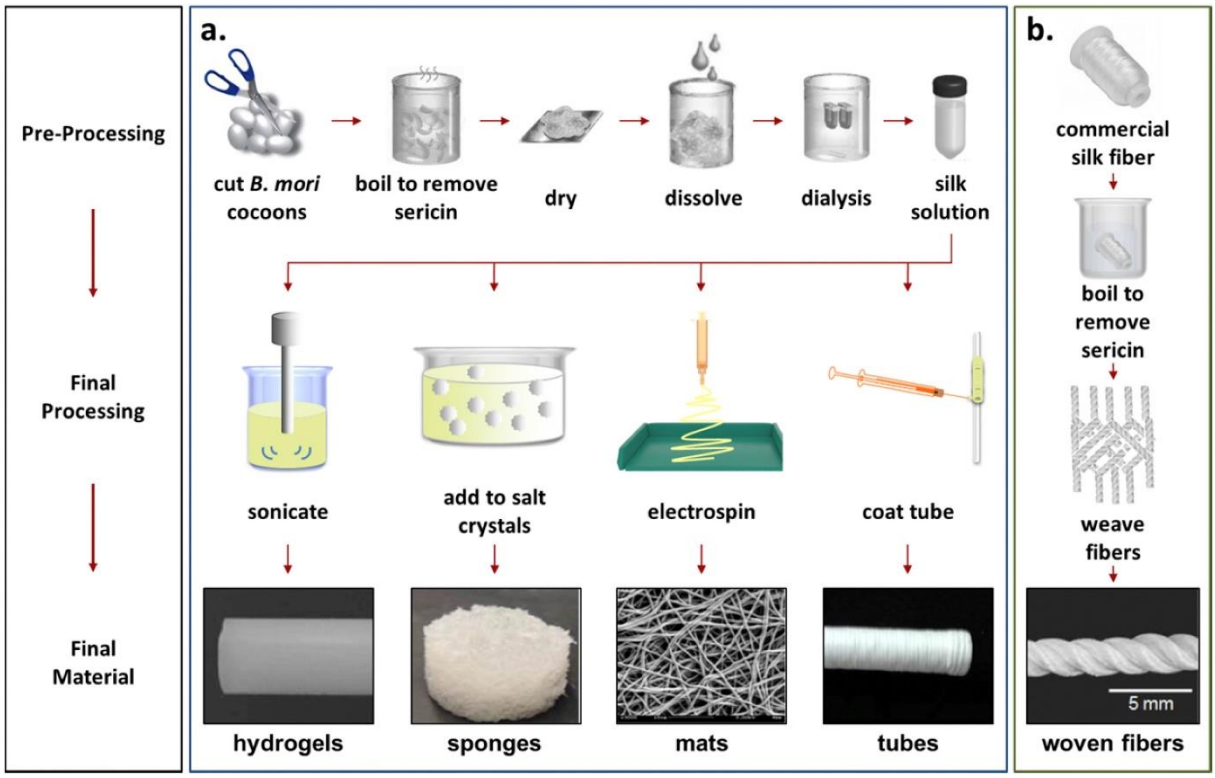

Figure 3*. Purification of Silk Fibroin, a. made from silkworm cocoons and b. solubilized fibers, which are left intact (to keep the stability) until the final processing. Reprinted with permission of Elsevier [38].*

Hydrogels. Silk fibroin hydrogels are characterized by their ability to swell in water without dissolution, imitating the physical and mechanical properties of tissue (skin, cartilage). The gelation of SF is controllable via pH, temperature and calcium ion concentration, and in addition via protein concentration, where increasing protein concentration leads to faster gelation. Besides, the pore size of the hydrogel can be impacted by the protein concentration [42]. Especially for minimally invasive surgeries, injectable hydrogels are attractive scaffolds as well as for the delivery of cells and cytokines.

Sponges. SF sponges with a high porosity (up to 97%) can be prepared by lyophilization, porogens and gas foaming, and by leaching of solvents (e.g. hexafluoro-2-propanol) [43]. Sponges provide a high interior surface area with interconnected spaces and a defined three-dimensional volume, allowing the invasion of cells, their attachment and growth. In addition, nutrients and oxygen can easily diffuse into the sponges [28, 44]. These properties together with the possibility to produce different pore sizes make them an attractive scaffold for tissue engineering.

Mats. Electrospinning is a favourable process to produce SF fiber mats with a wide range of fiber diameter (nanometer to a few micrometers), depending on the mode of processing and resulting in high surface area [45]. Briefly, for the production of SF fibers a strong electrical field is applied between the polymer solution and a collector plate [46, 47]. As mentioned before, the high surface area is important for cell attachment and enables the imitation of extracellular matrix of natural tissue.

Particles. SF particles can range from high nanometer up to several micrometers with a spherical shape, allowing a wide variety of applications for controlled drug delivery. The ability of SF to self-assemble can be utilized to form microspheres, e.g. by salting out with potassium phosphate [48]. The particle size can be varied by the type of salt and the ionic strength, leading to displacement of protein-water interaction and the ease of hydrophobic protein-protein interactions. A second method to produce particles is a technique so-called prilling or laminar jet break-up method. In brief, the aqueous SF solution is pumped with a syringe pump through a vibrating nozzle, so that the jet turns into droplets. In order to avoid agglomeration of the particles, a high voltage is applied and as a result, the droplets are repulsing each other. The droplets are falling into a hardening bath to induce water insolubility (e.g. with methanol) or are immediately frozen with liquid nitrogen [49]. The size of the prilled particles is dependent on the nozzle size and ranges between 100 and 400 µm. An additional method for particle production is the use of lipid vesicles as templates or by blending with poly (vinyl alcohol) (PVA) [48, 50].

Films. SF films can be casted from aqueous and organic solvent systems, aiming a straightforward biomaterial with a less complex nature compared to the systems mentioned before. Depending on the content of silk I or II, SF films are water vapour and oxygen permeable [51]. Furthermore, the diffusity through the film and the degradation rate can be controlled via the purification process (see also 3.2 Silk

Fibroin Degumming affects Scaffold Structure and Release of Macromolecular Drugs). Particularly for controlled drug delivery, the release kinetics are a key factor to control the drug level in the body within the therapeutic window. SF films offer a number of advantages due to the ease of production and the consistency of the material. In addition, proteins and enzymes are stabilized within the SF matrix, allowing the release of fully active proteins and enzymes [8].

In general, all the above-mentioned matrices can be loaded with an active pharmaceutical ingredient, ranging from small molecules to high molecular weight biologicals. **Table 4** provides an overview of a small section of the research already carried out [7]. The encapsulation can be achieved by simple mixing of the SF solution with the compound and subsequently, further processing.

Table 4. *Silk-based formulations of small molecule and biological drugs with their sustained release data in vitro. VEGF = vascular endothelial growth factor, EGF = epidermal growth factor, NGF = nerve growth factor, IGF = insulin-like growth factor, BSA = bovine serum albumin. Table adopted from [7] with permission from Elsevier.*

Formulation	**Drug**	**Sustained release duration / days**
Hydrogels	Penicillin	2-4
	Dexamethasone	2
	Inulin	45
	VEGF	42
Electrospun fibers/mats/tubes/scaffolds	EGF	7
	NGF	28
Particles	Salicylic acid	1
	Propranolol HCl	28
	Insulin	<< 1
	IGF-1	14-49
Films	Clopidogrel	28
	Gentamicin	5
	BSA	28
	EGF	22

2.2. Matrix Metalloproteinase Triggered Bioresponsive Drug Delivery Systems – Design, Synthesis and Application

The writing of the manuscript was my contribution. The manuscript was finalized by Prof. Dr. Oliver Germershaus.

– Kira Nultsch –

Published in: European Journal of Pharmaceutics and Biopharmaceutics, October 2018

Matrix Metalloprotease Triggered Bioresponsive Drug Delivery Systems – Design, Synthesis and Application

Kira Nultsch [a, b], *Oliver Germershaus* [b, *]

[a] University of Basel, Department of Pharmaceutical Sciences, Klingelbergstrasse 50, CH-4059 Basel, Switzerland

[b] University of Applied Sciences and Arts Northwestern Switzerland, School of Life Sciences, Institute of Pharma Technology, Gründenstrasse 40, CH-4132 Muttenz, Switzerland

* To whom correspondence should be addressed:

Prof. Dr. Oliver Germershaus

University of Applied Sciences and Arts Northwestern Switzerland, School of Life Sciences, Institute for Pharma Technology, Gründenstrasse 40, CH-4132 Muttenz, Switzerland

+41 61 467 44 48

oliver.germershaus@fhnw.ch

Abstract

Engineering of drug delivery systems has evolved in recent decades from comparably simple designs that merely controlled drug release to complex, often multistage systems that respond to multiple biological or environmental stimuli. Matrix metalloproteases (MMPs) are a family of proteolytic enzymes that are involved in numerous physiologic and pathophysiologic processes, including cancer. Therefore, these enzymes represent highly relevant targets for the development of novel bioresponsive drug delivery systems. The first part of this review summarizes major developments of the various types of MMP responsive drug delivery systems that have been achieved in the last decade and highlights promising strategies. The selection and incorporation of MMP sensitive elements into drug delivery systems as well as the interaction between MMP, drug delivery system and drug require additional scrutiny to avoid common pitfalls. Thus, the second part of this review focusses on strategies for successful selection and incorporation of MMP sensitive elements and on important design parameters related to the drug delivery system and the drug. This review will therefore provide a broad overview of successful MMP-sensitive drug delivery system designs and will inform about important design criteria for novel systems.

1. Introduction

Paul Ehrlich's vision of the "magic bullet" that targets a defined cellular structure, resulting in specific and efficient attack of pathogens or diseased tissue while leaving healthy tissue unaffected does not fail to inspire scientists even today [52]. Since Ehrlich's days however, the knowledge on the origin and progression of diseases, most notably various forms of cancer, has evolved significantly. Despite still being the most important strategy, chemical targeting of the drug molecule alone frequently is insufficient to obtain a true "magic bullet". Drug delivery systems (DDS) can introduce additional targeting functionalities, which are virtually independent from the chemical characteristics of the therapeutic drug molecule. This includes diverse strategies such as localized drug delivery, systemic targeting (e.g. by ligand-receptor mediated targeting and locally activated delivery systems) and intracellular targeting [53, 54]. Among those strategies, locally activated delivery systems appear interesting due to their broad applicability in systemic targeting and localized delivery alike, and the high specificity achievable with this strategy. Local activation may be achieved by changes of the pH value, through reduction or oxidation or by enzymatic degradation or numerous other principles. Within this review, targeting strategies based on enzymatic activation using matrix metalloproteinases (MMP) will be discussed.

MMPs are a family of zinc-dependent endopeptidases with at least 24 different types which play a central role in numerous physiological and pathological processes [55]. The different MMP types are frequently categorized into four main classes according to their substrate specificity and their cellular localization: collagenases (MMP-1, MMP-8 and MMP-13), gelatinases (MMP-2 and MMP-9), stromelysins (MMP-3, MMP-10, MMP-12) and membrane-type MMPs (MT1-MMP, MT2-MMP, MT3-MMP, MT4-MMP) [56]. While MMPs were initially recognized for their role in extracellular matrix (ECM) degradation in the context of cancer cell invasion and metastasis, this simplistic view was later revised and the importance of MMPs in regulating the entire extracellular signaling milieu was identified [57, 58]. MMPs consequently are involved in numerous physiological processes such as cell proliferation, differentiation, adhesion, migration, survival, and in cell-cell interactions.

In the context of MMP activity it is important to note that proteases do not simply act in a linear fashion, but their actions are concerted within the so called "protease web" consisting of MMPs and MMP

inhibitors, their substrates and other proteases and resulting in tissue homeostasis. Homeostatic balance, however, might be disturbed by inhibition of a whole class of proteases or of a single member of the network. Subsequently, other proteases can either compensate for lost activity or even inhibition of a single protease may unleash a cascade of events that results in deleterious consequences for the tissue or the entire body [59]. As a result, great care must be exercised and the entire interplay between the target MMP and other members of the protease web must be understood not only in the case of broad spectrum MMP inhibition but also with highly selective MMP inhibitors.

Alternatively, MMP overexpression may be employed as a trigger for drug delivery systems, leading to localized, on-demand drug release without the necessity of direct MMP inhibition. Because of accumulation of MMPs in the extracellular space and significance of MMP overexpression in various diseases, MMPs are excellent target molecules for triggered drug release.

The design and application of such MMP-activated systems may be approached from different angles and the complexity of the delivery systems ranges from comparably simple, low molecular weight molecules to sophisticated multi-stage drug delivery systems. The concept of protease-activated prodrugs (PAP) that are activated specifically by proteases overexpressed in tumor tissue was established already in 1980 and has been applied in various iterations since then [60]. The original concept of PAP was based on peptidyl prodrugs where an anticancer agent was coupled to a protease sensitive peptide. However, it was found that differences in protease expression between tumor and normal tissues alone might not result in sufficient tumor specificity and that short drug half-life in circulation limited efficient distribution to the target site. The blood half-life and preferential accumulation of PAP therapies at the target site was further improved through conjugation of macromolecular compounds such as albumin, N-(2-hydroxypropyl) methacrylamide copolymer or dextran [61]. More recently, even larger and more complex delivery systems such as various protease-sensitive nanoparticles and hydrogels were developed. As an example, MMP-sensitive multi-stage nanoparticles are capable of efficient extravasation into the tumor, followed by MMP triggered disassembly and size reduction, improving diffusion in the interstitial space of the tumor [62].

In their review published in 2007, Vartak and Gemeinhart provided an insightful summary on the development of MMP-activated drugs [55]. After more than 10 years of research in the field, we herein

review the current state of MMP activated drug delivery systems from prodrugs to complex protein and nucleic acid delivery systems. Furthermore, design considerations and general challenges associated with MMP-activated drug delivery systems will be discussed in detail to guide readers to successful implementation of MMP activation. Finally, we will address issues around synthesis of MMP activatable elements and discuss their successful incorporation into DDS.

2. Drug delivery systems utilizing MMP responsive elements

Enzymes such as MMP exhibit high efficiency on substrates and are frequently overexpressed in specific tissues and/or specific disease states [63]. These characteristics can be exploited for the design of "smart" linkers between the drug and a carrier, which are designed to be stable during storage, administration, in the blood circulation or under physiologic conditions but are enzymatically cleaved upon contact with specific MMPs. This ideally leads to increased local concentrations at the site of disease. Such "smart" systems can be applied in various ways in the design of drug delivery systems. The recent progress in the development of bioresponsive, MMP-activated systems will be described in the following sections with regards to different categories of drug delivery systems.

2.1. Carrier-peptide-drug conjugates

Targeting of systemically administered low molecular weight drugs e.g. to tumor tissue is complicated by drug instability in the circulation, rapid clearance and distribution to non-target tissues.

Overexpression of several members of the MMP family is characteristic for numerous tumors. Hence, protease activated prodrugs (PAP), where a MMP cleavable peptide substrate was linked to a drug molecule, were developed to trigger release and activation of the drug only at the tumor site [64]. Since PAPs frequently suffered from non-specific activation and fast clearance, the basic concept was expanded to include macromolecular carrier molecules to allow a longer circulation time, improved tissue accumulation, protection from degradation and premature drug release [65]. This type of bioresponsive, long-circulating delivery system was first introduced by Kratz et al. and Mansour et al. by combining PAP incorporating doxorubicin (DOX) with albumin as macromolecular carrier, either by synthesis of albumin-PAP conjugates or by rapid binding of an activated PAP to circulating albumin [66, 67].

In recent years, the concept of carrier modified PAP has evolved further. On the one hand, synthetic polymers were introduced as macromolecular carriers, on the other hand, additional functionalities have been added to the delivery systems. Various synthetic carrier molecules were studied instead of natural carriers such as albumin, allowing for synthesis of well-defined products at high purity and simplifying further modification, e.g. for tailored solubility, improved pharmacokinetics or intracellular delivery of the cargo [68, 69].

As an example, PAPs have been modified with cell penetrating peptides (CPP) to induce cellular uptake at the target site [70-73]. In these delivery systems, CPP activity is reduced or entirely inhibited as long as the conjugate is intact. After cleavage of MMP-specific peptide linkers at the target site, CPP are released and facilitate cellular uptake of cytotoxic drugs (e.g. DOX or protoporphyrin).

Building on this concept, multistage drug delivery systems, combining MMP-cleavable elements with CPPs and active targeting moieties were developed. Chen et al. set out to deliver trichosanthin (TCS), a ribosome-inactivating protein with reported high antitumor activity, to malignant glioma [74]. To achieve this goal the macromolecular drug delivery system must overcome the blood-brain-barrier (BBB) as well as the cell membrane of glioma cells. Furthermore, unspecific toxicity from TCS must be curtailed. The authors therefore combined TCS with lactoferrin (LF), assisting with penetration of the BBB and targeting. An MMP-2 sensitive peptide was used to conjugate LF to TCS/CPP. Upon reaching its target, elevated MMP-2 levels at the tumor site induce the release of TCS/CPP portion of the DDS and CPP facilitates the delivery of TCS into the cytoplasm of glioma cells (**Figure 1**).

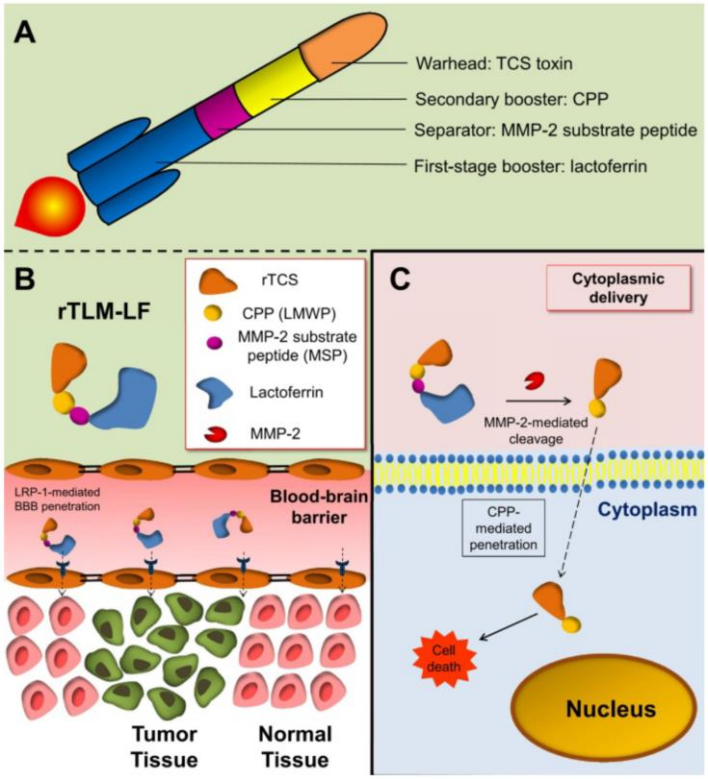

Figure 1. *(A) Multistage DDS combining cytotoxic drug (TCS toxin) with CPP and lactoferrin. (B) Lactoferrin facilitates targeting and penetration of the BBB through binding to low-density lipoprotein receptor-related protein 1 (LRP-1). (C) Elevated MMP-2 levels at the tumor site result in separation of TCS/CPP portion from lactoferrin and CPP mediates TCS delivery to the cytosol of glioma cells. Reproduced under the terms of CC BY-NC from [74].*

Besides cytotoxic drugs, also cytolytic peptides are candidate drugs for smart, MMP-activated delivery system. Cytolytic peptides can oligomerize on the cell surfaces, resulting in transient pore formation and cell lysis. However, very similar to highly potent cytotoxic drugs, the therapeutic application of these natural weapons, e.g. wasp venom, is complicated by cytotoxicity resulting from non-specific lytic activity and rapid elimination after injection [75]. The major challenges associated with application of cytolytic peptides have been tackled by conjugation to polymeric carriers (e.g. poly (L-glutamic acid), PGA) via MMP-sensitive linker peptides. On the one hand, conjugation to the carrier molecule renders cytolytic peptides inactive, on the other hand, circulation half-life of the conjugate is increased. Specific cleavage of the MMP sensitive linker at the tumor site releases the cytolytic peptide and reestablishes cytolytic activity. After three hours of *in vitro* incubation with target cells a significant amount of the modified peptide-mitoparan-PGA conjugate had been endocyted and mitoparan was released after proteolytic cleavage [75]. The authors concluded that overall loading of the conjugate could represent a challenge from a pharmacological point of view. Nevertheless, active and passive targeting as well as

spatially controlled activation could result in sufficiently high local concentrations at the tumor site and appropriate pharmacological effects.

These considerations represent critical issues, which may be valid for the majority of carrier-peptide-drug conjugates described in this chapter. These delivery systems are generally chemically well-defined and simply constructed and hence, response to their environment can be tightly controlled. On the other hand, drug load is often and possibly inherently low, therefore requiring highly efficient targeting as well as spatiotemporal activation to result in sufficient efficacy. Furthermore, and in conjunction with the previous point, these systems critically depend on highly efficient drug molecules, which exert their effect already at very low concentration. This, on the other hand, frequently results in severe systemic or unspecific toxicity, which must be tackled by the delivery system. Finally, efficiency frequently depends on intracellular delivery of the cargo, which often requires incorporation of CPP.

2.2. MMP-responsive, particulate drug delivery systems

Similar bioresponsive elements as described above (**Section 2.1.**) have also been introduced into particulate drug delivery systems, e.g. micelles, complexes or nanoparticles. These delivery systems allow drug encapsulation as well as chemical coupling of the drug to its building blocks or both, resulting in higher drug load compared to carrier-peptide-drug conjugates. Like carrier-peptide-drug conjugates, these delivery systems are primarily employed to improve circulation half-life and solubility of the drug, reduce off-target toxicity and to achieve targeting to specific tissues and/or to improve cellular uptake. As with carrier-peptide-drug conjugates, different MMP responsive drug delivery systems of different complexity have been developed. In the following chapters, the recent progress is reviewed, focusing on the most common systems, i.e. self-assembled systems and solid nanoparticles.

2.2.1. MMP responsive, self-assembled drug delivery systems

The majority of self-assembled MMP-responsive drug delivery systems represent micelles, liposomes or polymersomes, which are all based on amphiphilic building blocks. Micelles are spontaneous self-assemblies with a core-shell structures consisting of a hydrophobic core, frequently used for drug loading, and a hydrophilic shell. Liposomes, on the other hand, are self-assembled from lipids, forming bilayer or multilayer structures and allowing encapsulation of both hydrophobic and hydrophilic drugs.

Finally, polymersomes typically consist of diblock- or triblock copolymers, forming liposome-like structures but are characterized by higher stability and increased ease of chemical modification.

One of the main disadvantages of peptide-drug conjugates, i.e. short circulation half-life, led Lee et al. to synthesize MMP-2 sensitive PEG-peptide-DOX conjugates, which spontaneously formed micelles [76]. The efficacy of these micelles was further enhanced by loading with free DOX. Like peptide-drug conjugates, micelles disassembled in the presence of MMP-2, triggering release of the drug. High loading efficiency of > 98 % and drug load of > 60 wt% was achieved due to hydrophobic interactions between the loaded and conjugated DOX. The unloaded and DOX loaded micelles showed lower cytotoxicity and improved half-lives ($t_{1/2}$ = 11.4 – 15.2 min) compared to free DOX ($t_{1/2}$ = 1.6 min). Similar delivery systems were developed based on PEGylated lipids in conjunction with MMP-9 cleavable lipopeptide, which also disassembled in the presence of elevated MMP levels [77]. In this case, drug release was triggered by two consecutive steps: firstly, the PEG shell was shed in the presence of elevated glutathione concentrations, followed by degradation of MMP-sensitive peptide leading to disassembly and drug release. The authors confirmed efficiency of the delivery system *in vitro*, showing that MMP-9 was required for efficient uptake and drug release in a cell spheroid model. In addition, efficient and localized drug release was observed in the tumor microenvironment and *in vivo* tumor growth was better controlled with MMP-9 sensitive vesicles compared to vesicles without MMP substrate. Protease and reduction-triggered drug release in the tumor microenvironment was also investigated by Xu et al. through combination of MMP-sensitive, drug containing micelles which were incorporated into reduction-sensitive liposomes [78] and by Hou et al. through self-assembly of a conjugate consisting of a photosensitizer (chlorin e6), a MMP-2 sensitive peptide and reduction sensitive PEG [79].

Complex, multistage systems offer the possibility to combine multiple drug delivery- and targeting strategies and hence improve specificity and reduce side effects. As an example, Zhu et al. developed micelles composed of a PEG-MMP-2-sensitive peptide-paclitaxel conjugate as drug carrier, a TATp-PEG-phosphoethanolamine (PE) conjugate to facilitate cell internalization and PEG-PE as micelle building block [80]. Significant accumulation of the rhodamine-labeled micelles was found in the liver and the tumor of non-small cell lung cancer xenograft mice due to substantial expression of MMP-2 in

these tissues. The high local concentration might be explicable by cell internalization, whereas tumor accumulation was contingent on enhanced penetration and retention (EPR) effect and high MMP-2 expression. When non-sensitive micelles and MMP-2 sensitive micelles were administered, no significant difference of paclitaxel (PTX) accumulation was found in the major organs and blood, while tumor accumulation was 2.5 times higher for MMP-2 sensitive micelles. A similar strategy was applied for a liposomal system by the same group [81]. Two functional PEG-lipid conjugates, TATp-PEG-lipid and mAb-PEG-MMP2 cleavable peptide-lipid were synthesized and used to prepare liposomes. In this case, besides de-shielding of TATp, the liposome also contained a cancer-specific mAb enabling active targeting to tumor cells and subsequent receptor-mediated endocytosis. The authors, however, concluded that from a practical point of view the combination of active targeting and MMP2-sensitive de-shielding of TATp may not be required since the EPR effect in combination with MMP-triggered TATp de-shielding could result in sufficient delivery efficiency to tumor cells. Yet again a very similar approach was chosen by Gao et al., who used tumor microenvironment-sensitive polypetides (TMSP) which consisted of polycationic CPP and polyanionic shielding peptide, connected by a MMP-sensitive linker [82]. Docetaxel loaded lipid carriers were prepared using TMSP-PEG-lipid and folate-PEG-lipid conjugates and were tested *in vitro* in cell culture and cell spheroids as well as *in vivo* in tumor bearing mice. Interestingly, in this study MMP-triggered de-shielding of CPP and active targeting to folate receptors appeared to show additive effects, suggesting that the combination of these two delivery modalities could further increase efficacy and specificity of drug delivery systems.

MMP-specific PEG disassembly or de-shielding is a strategy quite frequently employed for self-assembled drug delivery systems by several research groups, either alone or in combination with cell penetration enhancers, RGD motifs or other targeting moieties [83-88].

In addition to size reduction through PEG disassembly, alternative morphological transitions such as aggregation and network formation may be triggered by MMP activity. This approach has been proposed by Chien et al. and Nguyen et al., who used amphiphilic block copolymers for micelle formation which were modified with brush like, hydrophilic and MMP-degradable peptides (**Figure 2 A and B**) [89, 90]. Micelles were able to freely circulate until extravasation at a site with elevated MMP

expression. Upon contact with MMP, micelles were transformed into network-like scaffolds (**Figure 2 C-F**) which were retained in the tissue up to 28 days post injection.

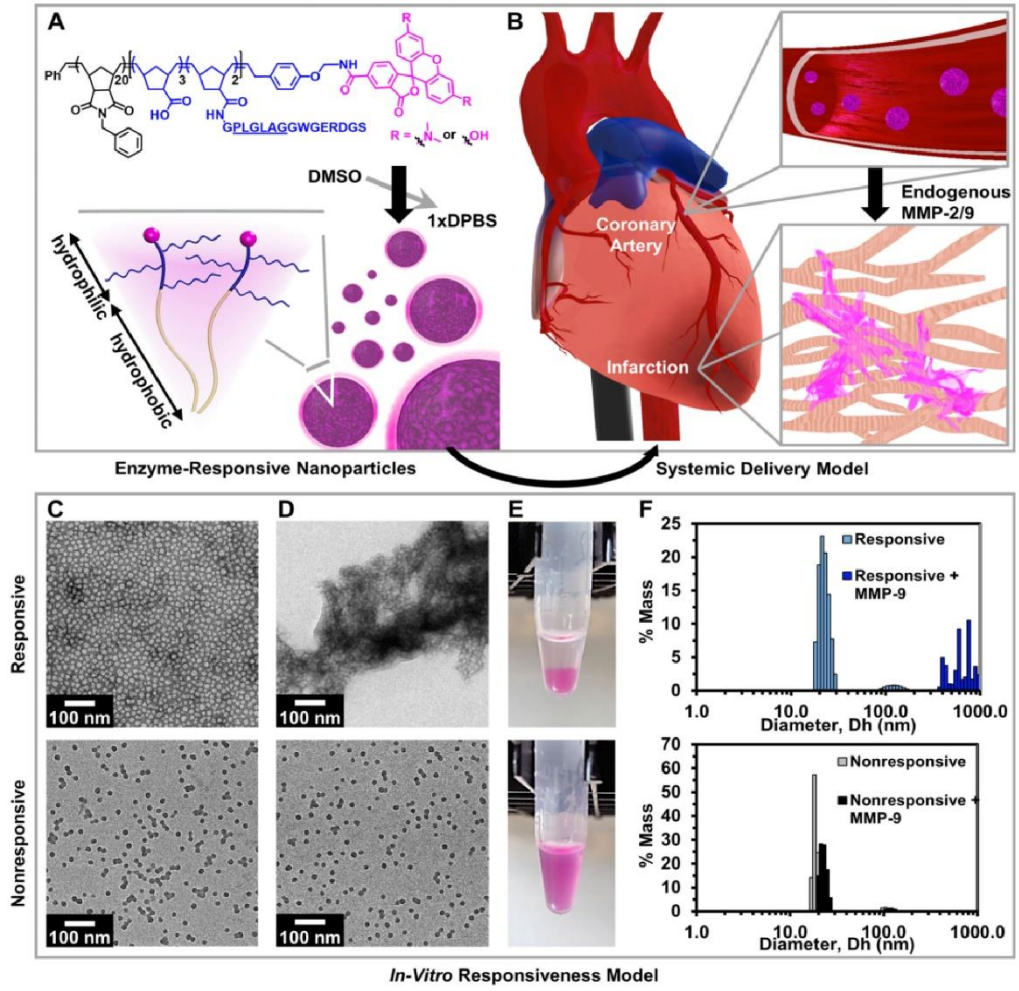

Figure 2. *(A) Structure of brush peptide-polymer amphiphile with MMP-sensitive peptide sequence (underlined). Upon dialysis into aqueous buffer, these amphiphilic polymers self-assemble into nanoparticles. (B) Schematic of nanoparticles circulating in the bloodstream, followed by extravasation through leaky vasculature at myocardial infarction site and formation of aggregate-like network due to MMP activity. (C-E) MMP responsive nanoparticles (top) show morphological transition in the presence of MMP (C vs. D and E) while nonresponsive control nanoparticles (bottom) morphology is unaffected. (F) Hydrodynamic diameters of MMP responsive (top) and nonresponsive (bottom) nanoparticles prior to and after MMP addition. Reprinted from [91] with permission from Wiley.*

Finally, active targeted delivery of lipid micelles to MMPs was published by Ngyuen et al. for therapy of coronary heart disease [92]. After myocardial infarction drug delivery is limited by low permeability of vasculature and short-time upregulation of specific cardiac markers [93]. Since MMPs play a key role in remodeling and restructuring after myocardial infarction [94], a novel micelle was developed containing an MMP targeting peptide (MMP-TP micelles), which facilitated specific accumulation due to myocardium-specific MMP upregulation [92]. One day after systemic injection no significant

superiority of the MMP-TP micelles over non-targeted micelles was found, but at day 3 and 7, accumulation of MMP-TP micelles exceeded non-targeted micelles by a factor of 2 to 3. The micelles showed the ability to efficiently accumulate in the infarcted area of the heart while leaving healthy tissue unaffected. Similarly, Fab fragments against MT1-MMP have been used to actively target DOX loaded liposomes *in vitro* and *in vivo* [95, 96]. This approach represents a very interesting alternative strategy to classic MMP-responsive drug delivery utilizing specific overexpression of MMPs in certain disease states.

2.2.2. MMP-responsive micro- and nanoparticles

MMP-responsive elements have been widely used not only in self-assembled drug delivery systems but also in various nano- and microparticulate systems for therapeutic, diagnostic or theranostic purposes. Nanoparticles are frequently prepared from biodegradable polyesters such as polylactide (PLLA) or polylactide-co-glycolide (PLGA). A simple yet elegant strategy for preparation of MMP-responsive nanoparticles was developed by Dorresteijn et al. who synthesized a PLLA based triblock copolymer where a MMP-sensitive peptide sequence was introduced as a linker between two PLLA blocks during preparation of nanoparticles by emulsion polymerization (**Figure 3 A**) [91]. The authors showed that incubation with MMP2 results in specific enzymatic cleavage of the linker peptide, leading to a reduction of the glass transition temperature below body temperature (**Figure 3 B**) which potentially triggers cargo release. MMP-2 expressing C2C12 cells were shown to stimulate release of 5-fluorouracil (5-FU) from nanoparticles resulting in comparable cytotoxicity to free 5-FU, while nanoparticles prepared with scrambled peptide sequence and loaded with 5-FU remained nontoxic (**Figure 3 C**). This strategy may allow for facile development of custom-designed bioresponsive nanoparticulate delivery systems based on triblock copolymers with various peptide sequences.

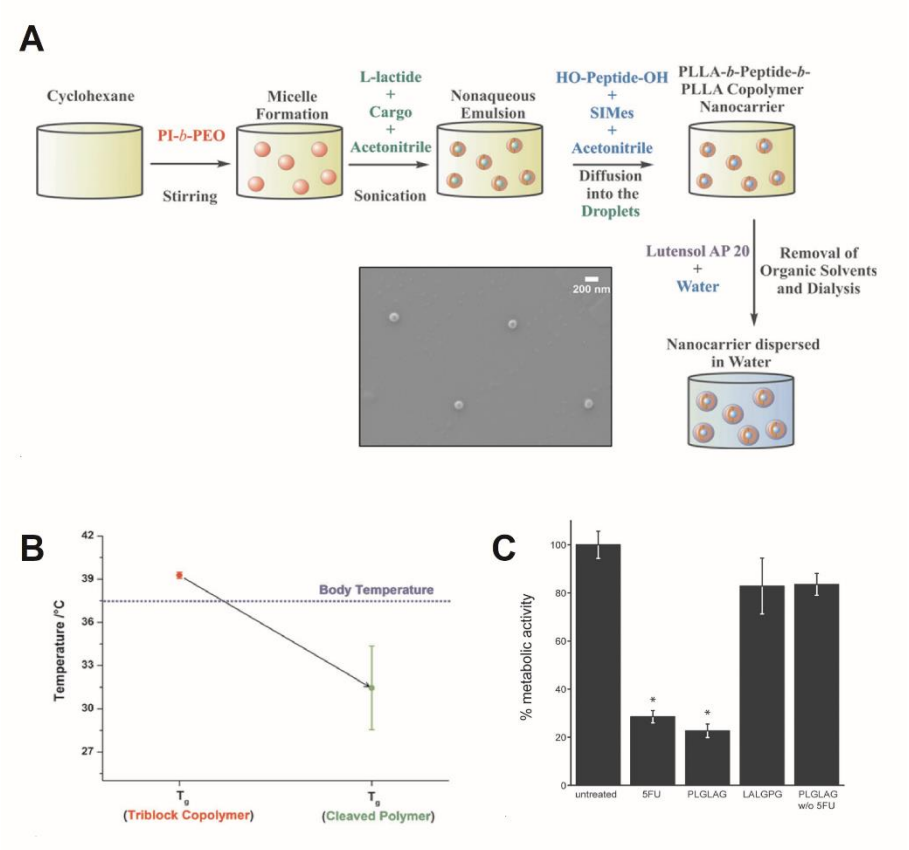

Figure 3. *(A) Preparation of nanoparticles by nonaqueous emulsion polymerization. Acetonitrile is emulsified in cyclohexane in the presence of poly (isoprene)-block-poly (ethylene oxide) (PI-b-PEO) as a stabilizer. Emulsion polymerization of L-lactide is initiated by MMP-cleavable peptide with two terminal serine units. Nanoparticles are then transferred inti aqueous solution. (B) Incubation with MMP2 results in cleavage of the triblock copolymer and reduction of the glass transition temperature below body temperature. (C) Cytotoxicity of 5-fluorouracil (5-FU) loaded nanoparticles in MMP-2 expressing C2C12 cells. PLGLAG represents 5-FU loaded nanoparticles with MMP-2 cleavable peptide sequence, LALGPG represents 5-FU loaded nanoparticles with scrambled peptide sequence, and PLGLAG w/o 5FU represent unloaded nanoparticles with MMP-2 cleavable peptide sequence. Reprinted with adaptations from [91] with permission from Wiley.*

As detailed for self-assembled drug delivery systems (**Section 2.2.1.**), shedding of PEG- or alternative polymer shells and/or size reduction of particulate drug delivery systems are common ways to incorporate MMP responsiveness into nanoparticulate systems. This concept may be exemplified by the study of Grünwald et al., who prepared poly (lactic-co-glycolic acid) (PLGA) nanoparticles with MMP-sensitive PEG coating for efficient tumor targeting [97]. The targeting strategy relied on long circulation half-life of PEGylated particles, passive accumulation of particles in the tumor due to the EPR effect and subsequent specific shedding of the PEG corona by tumor-secreted MMPs (**Figure 4 A**). Nanoparticles were prepared from PLGA-b-PEG by nanoprecipitation and concurrently loaded with iron oxide nanoparticles. Then, nanoparticles were further modified with PEG via a MMP-sensitive

peptide linker. Specific targeting to pancreatic tumor was confirmed by Prussian Blue staining of nanoparticles (**Figure 4 B**) and MMP-9 dependent uptake was verified *in vivo* using Mmp9 deficient mice (**Figure 4 C**).

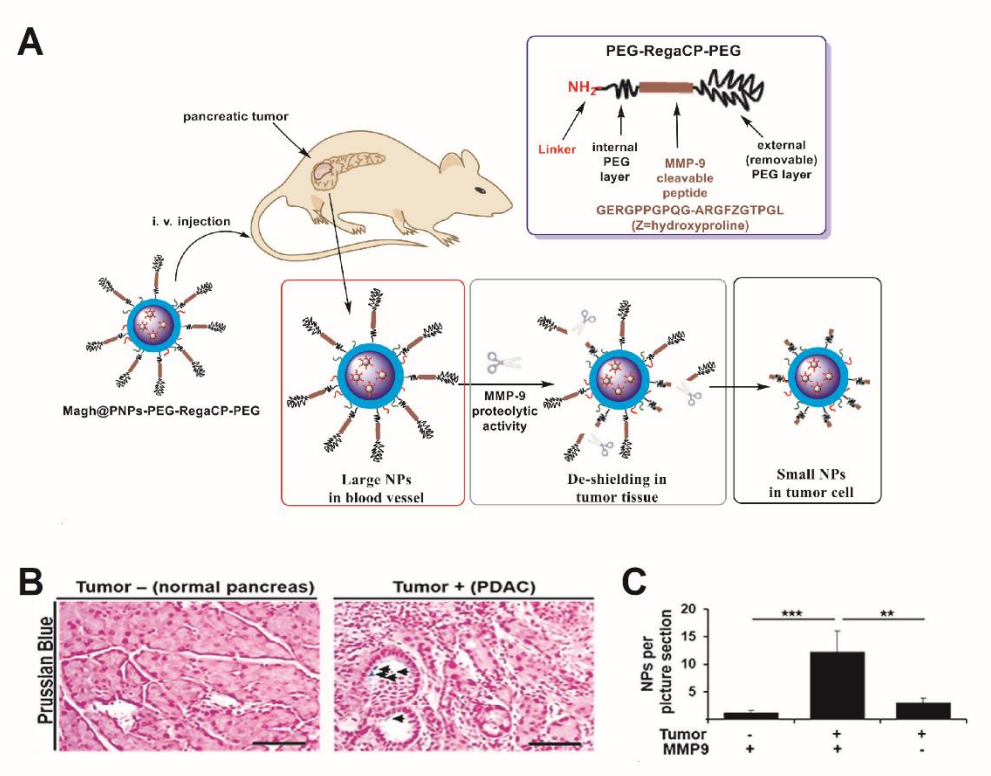

Figure 4. *(A) Schematic of MMP-9 induced in vivo de-shielding of nanoparticles. (B) Uptake of nanoparticles into pancreatic tissue without and with tumors. Nanoparticles (arrows) were stained by Prussian blue. Scale bar represent 100 µm. (C) Uptake of nanoparticles into pancreatic tissue in the presence and absence of tumor or MMP-9, respectively as determined by Prussian blue staining-based counting. Reprinted with adaptations from [97] with permission from Elsevier.*

Similarly, Gullotti et al. prepared PTX loaded PLGA nanoparticles, which were coated with polydopamine and modified with CPP and a PEG-MMP-sensitive peptide conjugate [98]. The authors confirmed MMP dependence of cellular uptake in vitro. However, they also noted that premature drug release from PLGA nanoparticles, which was virtually independent from surface modification, represented a significant issue, which ultimately resulted in statistically insignificant difference of cytotoxicicty of MMP-sensitive nanoparticles in the presence and absence of MMP. To overcome this problem, covalent conjugation of the cytotoxic drug to the particle matrix via hydrolysable or enzymatically degradable linkers was proposed.

Numerous alternative modification strategies based on shedding of PEG shells have been developed with different types of solid nanoparticles. Gold nanoparticles have been widely used, assumingly due

to ease of modification and straightforward preparation and imaging. Suresh et al. modified gold nanoparticles with a conjugate consisting of PEG and a MMP-sensitive peptide with a terminal cysteine for efficient attachment to the surface of gold nanoparticles [99]. The modified particles were stabilized by the PEG shell but formed larger aggregates after treatment with MMP. Cellular uptake of gold nanoparticles was up to 100-fold increased after incubation with MMP compared to uptake of particles with non-cleavable PEG shell. Nazli et al. used iron oxide nanoparticles as a template for MMP-triggered release of DOX [100]. Iron oxide nanoparticles were coated with an MMP-sensitive PEG hydrogel shell via surface-initiated photopolymerization and modified with an integrin binding motif. Doxorubicin was loaded into the hydrogel shell by soaking. Interestingly, this design resulted in MMP-dependent drug release with 60% DOX release in the presence of MMP and 36% release in its absence. Furthermore, active targeting through integrin binding resulted in improved cellular uptake in tumor cells. With this approach, the authors showed that targeted intracellular delivery of cytotoxic drugs by nanocarriers and intracellular MMP-dependent drug release could be successfully combined. A facile and simple approach to MMP-sensitive PEGylation of nanoparticles was developed by Choi et al., which relied on layer-by-layer (LbL) assembly instead of chemical conjugation [101]. Heparin-Pluronic nanogels were used as template nanoparticles onto which multiple layers of poly (ethylenimine) (PEI) and heparin were deposited. As a final layer, a PEI-MMP sensitive peptide-PEG conjugate was employed. The authors showed that this approach resulted in MMP-dependent improvement of cellular uptake of nanoparticles *in vitro*. In principle, this LbL coating strategy could be used as a straightforward and simple platform to incorporate bioresponsive elements into drug delivery systems. LbL coating can be applied with alternative materials as well (e.g. polyester-based nanoparticles), especially if the nanoparticle surface is negatively or positively charged.

The general concept of using MMPs to trigger a reduction of particle size was also applied using gelatin nanoparticles since MMP-2 and MMP-9 not only hydrolyze specific peptide sequences but also efficiently degrade gelatin. As an example, Wong et al. used 10 nm quantum dots as model nanoparticles for encapsulation into 100 nm gelatin nanoparticles [102]. Gelatin nanoparticles were efficiently degraded *in vitro* and *in vivo* in the presence of MMP-2, releasing quantum dots and resulting in improved interstitial transport within tumor tissue after intratumoral injection. A more complex drug

delivery system for MMP-sensitive release of DOX modified gold nanoparticles from gelatin nanoparticles was developed by Ruan et al. (**Figure 5**) [103]. In this case, PEG- and DOX-modified gold nanoparticles were attached onto gelatin nanoparticles, which were hydrolyzed in the presence of MMP-2, releasing drug-loaded gold nanoparticles. This design was developed to allow long circulation and accumulation in the tumor using the EPR effect. Within the tumor tissue, gold nanoparticles are released by MMP leading to improved transvascular and interstitial distribution. Gold nanoparticles were modified with DOX via a pH labile hydrazine bond, allowing release of free DOX only in the acidic microenvironment of the tumor and/or within lysosomes after cellular uptake.

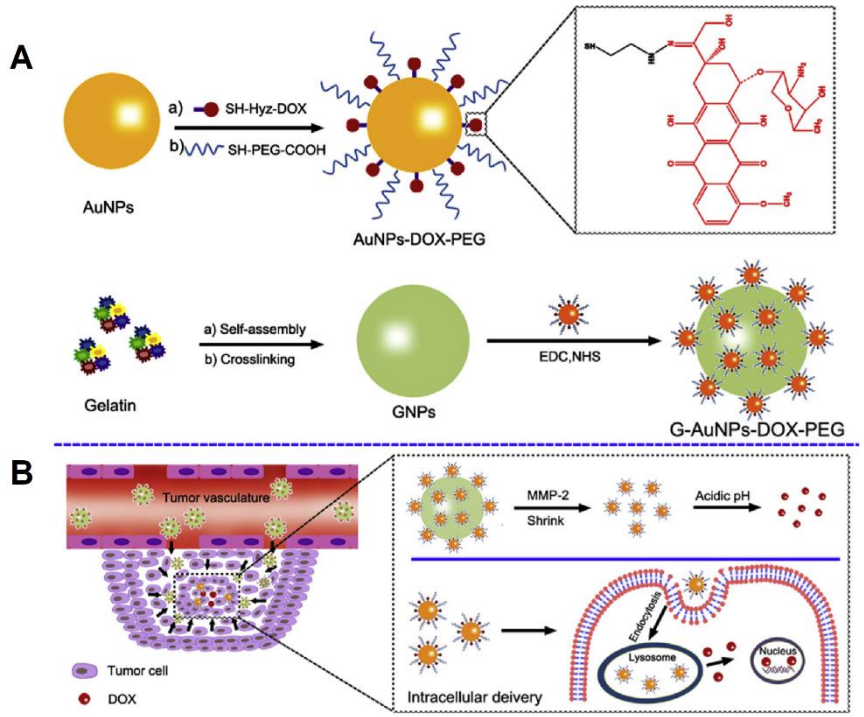

Figure 5. *(A) Schematic of drug delivery system design. Gold nanoparticles were modified with DOX via pH labile hydrazine bond and with PEG. Gelatin nanoparticles were prepared and decorated with modified gold nanoparticles via EDC/NHS chemistry. (B) Schematic of delivery strategy. Nanoparticles extravasate at tumor site via EPR effect, MMP activity degrades gelatin nanoparticles and releases modified gold nanoparticles. Modified gold nanoparticles show improved interstitial penetration of tumor tissue and DOX is released after cleavage of hydrazine bond in the acidic tumor microenvironment or after cellular uptake of gold nanoparticles in the lysosomal compartment. Reprinted from [103] with permission from Elsevier.*

Expression of MMP may also be exploited for active targeting of nanoparticles to the site of disease or to specific cells. As detailed in **Section 2.2.1.** such active targeting to MT-MMP has been applied in the case of targeted treatment after myocardial infarction. Similarly, glioblastoma is signified by overexpression of MT1-MMP on angiogenic blood vessels as well as glioma cells. Gu et al. therefore

designed PEG-PLA nanoparticles decorated with a peptide with high binding affinity to MT1-MMP [104]. Nanoparticles were also modified with iRGD, facilitating binding to the tumor vasculature, extravasation and tumor tissue penetration. Targeted nanoparticles were loaded with PTX and compared to non-targeted PTX loaded nanoparticles and Taxol. The targeted nanoparticles showed improved antiproliferative activity, higher apoptosis rate and stronger inhibition of glioma spheroid growth *in vitro*. Finally, targeted nanoparticles with iRGD modification resulted in longest survival of glioma bearing mice. Another nanoparticle design for glioma targeting was proposed by Locatelli et al. [105]. In this study, polymeric nanoparticles were loaded with Alisertib, a selective aurora A kinase inhibitor, and silver nanoparticles as cytotoxic drug payload and modified with a MMP-2 targeting peptide. Despite showing some effect on cell viability in vitro and tumor growth in vivo, unfortunately MMP-2 dependent accumulation or targeting was not directly confirmed in this study, especially due to the lack of untargeted controls.

Finally, numerous studies use MMP-specific responsive systems for diagnostic and theragnostic purposes. Exemplary theragnostic systems based on MMP activity are drug loaded gold nanoparticle assemblies developed by the group of Yoo [106, 107]. In both cases, MMP-2 cleavable peptides were employed for crosslinking of modified gold nanoparticles into nanoclusters. Drug loading was achieved either through thiolation of DOX followed by direct loading onto gold nanoparticles or through covalent, pH-sensitive attachment onto the PEG shell of gold nanoparticles. Modified gold nanoparticles were then crosslinked either directly via MMP sensitive peptides or via peptide-modified quantum dots. Both systems were specifically disassembled in the presence of MMP-2 and released DOX under reducing conditions in the cytosol or in acidic environment of the tumor tissue or lysosomes. The quantum dots incorporated in the theragnostic system can be either employed for traditional fluorescence imaging or can be used in conjunction with gold nanoparticles for Förster resonance energy transfer (FRET) [107]. The alternative approach of solely using gold nanoparticle presented later is advantageous with regards to toxicity associated with quantum dots but still allows *in vivo* imaging by computer tomography [106].

Lastly, an entirely different and novel approach on using MMP responsive elements for diagnostic purposes was recently published by Ritzer et al. [108]. In this study, the authors modified microparticles with bitter substances using a MMP sensitive peptide as linker. Microparticles were incorporated into

chewing gum to generate a diagnostic device, which uses the tongue as a sensor and therefore allows diagnosis by “anyone, anywhere, anytime”. Sensing of bitter taste is linked to the detection of poisons, which potentially explains why bitter substances are very sensitively recognized, some substances even in the nanomolar range. The design of the diagnostic system ensured that in the absence of MMP, bitter substances remained attached to the microparticles and therefore were not detectable. However, in the presence of elevated MMP levels, e.g. due to peri-implant disease, periodontitis or gingivitis, peptide linkers were cleaved and low molecular weight, water soluble, bitter substances were released which could be immediately detected by the bitter sensors of the tongue.

In conclusion, MMP sensitive particulate delivery systems have evolved and diversified significantly in the last decade. Based on our analysis, the most widely employed strategy for incorporation of MMP responsiveness was based on using MMP sensitive linkers to induce shedding of PEG shells or structural transition upon linker cleavage by MMP. Numerous authors developed particulate systems, which showed prolonged circulation due to the presence of a stable, hydrophilic (PEG-) shell and appropriate particle size distribution. Frequently, passive targeting to the tumor was achieved utilizing the EPR effect. After extravasation, MMP activity resulted in de-PEGylation and/or other structural transitions, resulting in improved interstitial penetration, deposition within the tissue and/or cellular uptake. Apart from this general design, frequently additional elements, such as active targeting moieties or CPPs, were incorporated to further improve specificity or cellular internalization. Such multifunctional delivery systems generated promising results in several studies, especially in the case of addition of CPP [109]. With regards to addition of active targeting elements, it still appears to be controversial, and seems to depend on the actual indication or use case, if these are advantageous or redundant [81, 82, 104]. It should also be reiterated here that besides MMPs enzymatic activity, MMPs have also been successfully used as target structures for active targeting of delivery systems. Finally, MMP sensitive system offer a plethora of possibilities for diagnostic and theragnostic use.

2.3. MMP-responsive hydrogels

Hydrogel-based DDS are ideally suited for local application, e.g. at tumor sites and allow localized, on-demand drug release, thereby reducing systemic side effects [54]. These systems frequently are advantageous concerning their hydrophilicity and biocompatibility and, if properly designed, mimic

extracellular matrix (ECM) structure, providing the natural environment for cell invasion and proliferation. These processes are tightly associated with MMP activity. Therefore, addition of MMP responsive elements may be regarded a logical and straightforward choice for hydrogel-based tissue engineering scaffolds and drug delivery systems alike. Hyaluronic acid, a non-sulfated glucosaminoglycan, is a major component of the ECM and abundantly present in load-bearing joints due to its viscoelastic properties. Its biocompatibility, biodegradability and hydrophilicity has attracted significant attention as a matrix for drug delivery of sensitive drugs [110]. Hydrogels composed of low molecular weight hyaluronic acid and MMP sensitive peptide crosslinkers were developed by Kim et al. for tissue defect regeneration [111]. While in this case no drug was encapsulated into the hydrogels, the authors showed that mechanical properties as well as degradation rate of the hydrogels could be tailored by hyaluronic acid molecular weight and MMP sensitivity of crosslinking.

Purcell et al. achieved MMP-responsive delivery of recombinant tissue inhibitor of MMPs (rTIMP-3) from an injectable hydrogel consisting of modified hyaluronic acid and modified dextran sulfate [112]. Modification of the polysaccharides was such that both components could be crosslinked directly as well as via MMP sensitive peptide linkers. Recombinant TIMP-3 was encapsulated within the hydrogel through electrostatic interactions with modified dextran sulfate and was released in response to matrix degradation in the presence of elevated MMP levels. The design of this delivery system thus introduces a feedback loop where elevated MMP levels result in increased release of rTIMP-3, which itself inhibits MMP activity. Therefore, this “intelligent” drug delivery system results in on-demand, well-regulated release as opposed to the majority of simpler bioresponsive delivery systems.

An alternative strategy for the generation of MMP-responsive hydrogels for drug release relies on natural or semi-synthetic matrices such as gelatin. Sutter et al. modified a recombinant gelatin derivative with methacrylate residues for crosslinking and encapsulated lysozyme and trypsin inhibitor as model proteins [113]. Release of the model drugs was found to be primarily diffusion-controlled and to depend on hydrogel mesh size and degree of gel swelling. Degradation of hydrogels was also investigated in the presence of MMP-1 and MMP-9. While no hydrogel degradation occurred with MMP-9, MMP-1 resulted in complete degradation within 5 days. However, unfortunately in this study release of model drugs was not investigated in the presence of MMP.

Drug release from *in situ* forming, poly (ethylenoxide)-poly (propylenoxide)-poly (ethylenoxide)triblock copolymer (Pluronic®) based, MMP sensitive hydrogels was investigated by Garripelli et al. [114]. Pluronic thermogels can be tailored to display gelation temperatures in the range of body temperature and hence, can be applied as a liquid while gel formation immediately takes place at elevated temperature. PTX was incorporated into the thermogels as a model drug. Drug release from MMP sensitive hydrogels was slow in the absence of MMP but increased dramatically in the presence of MMP.

Another example for localized application of MMP-sensitive hydrogels is focused on myocardial infarction, which is characterized by limited intrinsic regeneration and a high mortality rate [115]. Kraehenbuehl et al. developed an injectable MMP-sensitive hydrogel, delivering the pro-angiogenic and pro-survival factor thymosin β4 (Tβ4) along with human embryonic stem cells (hESC) to infarcted myocardium of rats [115]. *In situ* gel formation from liquid 8-arm PEG-vinylsulfone precursors occurred after minutes during surgery, allowing injection in the liquid form. In vivo release of Tβ4 was observed over a period of 6 weeks. After six weeks rats treated with the combination Tβ4 and hESC showed better aligned cardiomyocytes in the infarcted zone compared to PBS treated rats.

In summary, hydrogel systems for localized therapy show numerous advantages: they reduce systemic side effects while maximize local drug concentration and require less complicated designs compared to particulate delivery systems. MMP sensitive elements have been successfully used to introduce on-demand drug or even stem cell release. Notably, the MMP-sensitive release of MMP inhibitors from hydrogels results in a feedback-loop that might be used to further improve therapy, especially in cases were a well-balanced reduction of MMP activity is essential.

2.4. MMP-sensitive nucleic acid delivery

Nucleic acid (NA) delivery represents a specific challenge for drug delivery systems since nucleic acids not only must be protected from degradation, e.g. by nucleases, during delivery but must also be delivered into the cytosol (e.g. siRNA) or nucleus (e.g. plasmid DNA) [54]. These challenges are addressed by specialized delivery systems such as non-viral gene delivery systems that, on the one hand, encapsulate or complex NAs to offer protection from degradation and, on the other hand, ensure cellular uptake. However, requirements regarding sufficient circulation time, active or passive targeting,

biocompatibility and potentially bioresponsiveness are broadly comparable to delivery systems for chemical or biological drugs. For this reason, strategies discussed above for MMP triggered structural changes, such as shedding of PEG shell, resulting in improved tumor uptake by the EPR effect and efficient distribution within the tumor tissue are also applied for NA delivery system. Furthermore, inclusion of CPPs to improve cellular uptake as well as MMP triggered unshielding of these moieties are frequently applied in the context of MMP sensitive NA delivery. The system developed by Wang et al. represent an excellent example, combining MMP induced structural changes, i.e. shedding of the PEG corona of micelles with CPP in a NA delivery system [116]. The chemical structure of this system and the general concept is illustrated in **Figure 6**. A block copolymer from PEG and PCL is used as the amphiphile, enabling self-assembly of micelles. The two blocks are connected via a peptide sequence containing an MMP-sensitive element and a polycationic polyarginine element for complexation of siRNA and for improved penetration of target cell membranes. A similar system was developed by Veiman et al. using stearylated peptides containing polyarginine repeats, which were PEGylated via a MMP-sensitive linker [117]. Another micellar siRNA carrier system used dimethylaminoethyl methacrylate (DMAEMA) as charged building block for siRNA condensation and a terpolymer block resulting in pH-responsive, endosome disruption [118]. Again, PEG was attached via MMP-cleavable linker resulting in improved circulation time and masking of the polycationic and membrane disruptive elements of the micelles. The authors showed that in the presence of elevated MMP levels zetapotential of nanoparticles increased due to shedding of the PEG corona and release from endosomal compartment was improved due to the core forming terpolymer block.

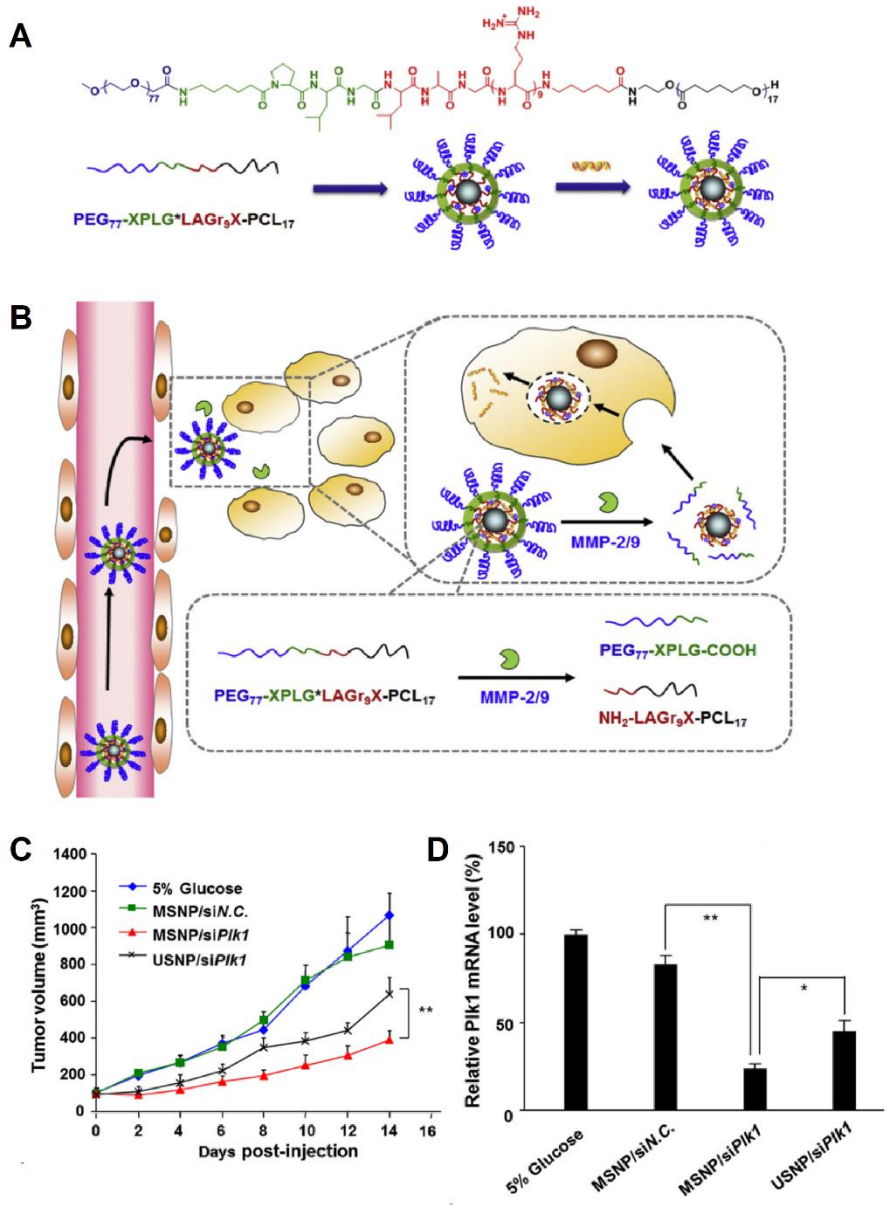

Figure 6. *(A) Chemical structure of block copolymer consisting of PEG and PCL with a MMP-2/9 degradable linker (PLG*LAGr9) which contains a poly arginine repeating sequence for siRNA complexation and membrane penetration. (B) Schematic function of the delivery system showing long term circulation, extravasation at the tumor site, MMP triggered shedding of the PEG corona, cellular uptake and delivery of siRNA into the cytosol. (C) In vivo inhibition of MDA-MB-231 tumor xenograft growth in mice and (D) expression of Plk1 mRNA in tumors 48 hours after the last injection. MSNP: MMP-sensitive micellar nanoparticles; USNP: MMP-insensitive micellar nanoparticles; siN.C. negative control siRNA; siPlk1: siRNA targeting Plk1 mRNA. Reprinted with adaptations from [116], with permission from Elsevier.*

Several authors investigated co-delivery of low molecular weight chemical drugs and NA, mainly targeting at tumor therapy. In this regard, the delivery platform must accommodate both NA and chemical drugs, e.g. by combining neutral lipids with polycations. Zhu et al. approached this challenge by synthesis of a conjugate consisting of PEI modified with PEG via MMP-cleavable peptide linker and

modified with dioleoylphosphatidylethanolamine (DOPE) [119]. This conjugate self-assembled into nanoparticles encapsulating PTX in its lipidic core and complexing siRNA with PEI, while the outermost layer consisted of a MMP-responsive PEG shell. Combining PTX with anti-survivin siRNA with a MPP-sensitive delivery system proved to be an efficient strategy, resulting in IC50 value of 96 nM for PTX alone, 28 nM for PTX loaded nanoparticles and 15 nM for PTX and siRNA loaded nanoparticles. Salzano et al. also combined a chemotherapeutic drug (DOX) with NA (miRNA-34a) in a single delivery system [120]. However, in this case several different conjugates were synthesized and assembled into nanoparticles (**Figure 7A**). The authors combined MMP-sensitive DOX release (PEG2k-CLV-Dox) with reduction-sensitive release of miRNA (miRNA-34a-S-S-PE) and a CPP conjugate (TAT-PEG1k-PE) to form self-assembled micellar nanoparticles. Again, the authors showed that the combination of DOX and miRNA was more effective than each single treatment, both in 2D monolayer culture (**Figure 7 B**) and in a 3D spheroid tumor model (**Figure 7 C**).

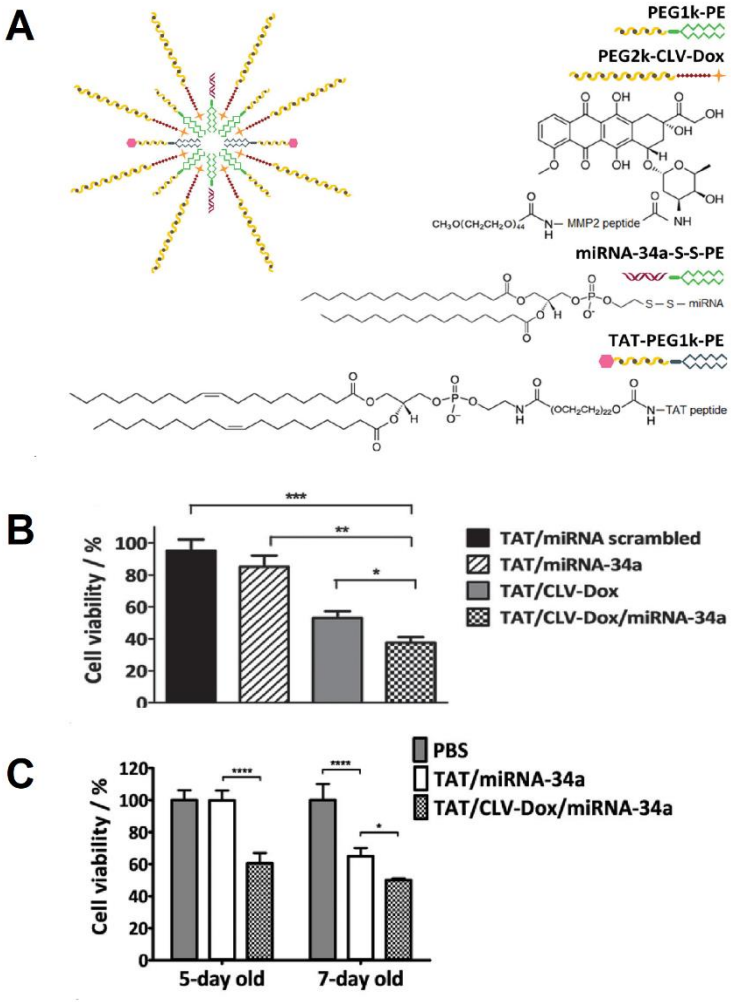

Figure 7. *A) Schematic representation of the structure of the individual conjugates as well as the hypothetical structure of the self-assembled nanoparticle. B) Cell viability 2D cell culture after treatment with different formulations. C) Cell viability in 3D spheroid model after treatment with different formulations. Reprinted with adaptations from [120], with permission from Wiley.*

MMP responsive elements have also successfully been used for localized, on-demand delivery of DNA and siRNA from nanofibrous matrices for treatment of diabetic ulcers in a series of papers by Kim et al. [121-123]. Diabetic ulcers are characterized by a disbalance in remodeling of ECM accompanied with elevated MMP levels. Therefore, the authors focused on local delivery of NA, either silencing overexpression of MMP [122] or delivering genes for growth factor expression [121]. The matrix was produced by electrospinning of polycaprolactone-polyethylene glycol (PCL-PEG) block copolymer, whose surface was modified with a conjugate consisting of MMP-sensitive peptide and PEI. DNA or siRNA was then electrostatically bound to PEI. Once the MMP-sensitive peptide is cleaved, NA/PEI nanoparticles are released and are endocytosed by the wound bed. Here, chemical immobilization on

the surface allows for homogenously distributed, well-accessible agents and attenuated release linked with physiological signals (inflammation, growth factors). In the absence of MMP, release of NA/PEI complex remained low, only a part was adsorbed on the surface and was released by simple diffusion. Significant higher release rate could be achieved in presence of MMP (approximately 47 % compared to 15 % without MMP). In an in vivo study in cutaneous wounds of streptozotocin-induced diabetic mice MMP-sensitive meshes for NA delivery showed the best healing results and the highest hEGF expression up to 14 days meaning that a single treatment was already sufficient [121].

In summary, MMP responsive elements have been successfully applied for nucleic acid delivery, both for systemic as well as local application. In addition to the general design strategies outlined above, NA delivery systems are characterized by additional polycationic elements that ensure proper complexation of NA and improve cellular uptake.

4. Challenges in synthesis and incorporation of MMP-sensitive peptides into drug delivery systems

Despite the numerous successful designs described in the preceding sections and the numerous advantages of inclusion of bioresponsive elements, the identification of suitable MMP-cleavable peptides and their incorporation into drug delivery systems remains challenging.

The first step in the development of MMP-sensitive drug delivery systems is to evaluate which MMP is specifically overexpressed and overactive in the particular tissue or disease state. A specific MMP may represent a target for one disease but counter target for another disease and additionally, some MMPs have similar substrate specificity (e.g. MMP-2 and MMP-9) [55]. Knowledge of the cleavage site is therefore highly important. Interestingly, the structural features of the cleavage site are similar for all MMPs, containing a zinc ion in the catalytic domain and a deep S_1' pocket as docking point [124]. In general, the peptide linker itself should be rapidly cleaved once the DDS reaches the target site. These linkers can be rationally designed based on the literature [125-128]. One approach to identify protease cleavage sites is the proteomic identification of protease cleavage sites (PICS) method [129]. This method employs proteome-based peptide libraries and allows identification of prime and non-prime cleavage sites within one single experiment, enabling high throughput approaches, e.g. identification of

4300 cleavage sites of nine MMPs. The main advantage of this method is the specificity profiling without any knowledge of structure, sequence preferences or the physical role of MMP [126]. Once the targeted MMP is identified and a desired set of MMP-sensitive linkers is chosen, enzyme kinetic studies should be conducted in order to ensure appropriate catalytic efficiency. Such studies were performed by Patterson and Hubbell for MMP-responsive PEG hydrogels [130]. The authors investigated degradation kinetics (k_{cat}) of 17 different MMP-1 and MMP-2 substrate peptides both in solution and after incorporation into hydrogels. Variation of MMP substrate sequence strongly affected hydrogel degradation, cell spreading and cell invasion in vitro, allowing tuning of hydrogel degradation characteristics. As a last step in the selection of a MMP-specific linker, the selectivity should be investigated for a successful targeting approach, since the cleavage of the linker by other enzymes would lead to unspecific drug release and potential side effects [55].

The incorporation of MMP-sensitive peptides itself but also the interaction between MMP, drug delivery system and drug require additional scrutiny. The active site of MMP is predominantly negatively charged [131, 132], which might lead to charge repulsion with negatively charged DDS scaffold. Besides such accessibility issues of MMP substrate to MMPs catalytic domain, the MMP itself in numerous cases must diffuse into drug delivery systems, hence mesh size and rigidity of DDS play an important role. Furthermore, mild synthesis conditions are frequently required to protect the integrity and therapeutic efficacy of the drug molecule. But, conjugates should also show sufficient stability, fast cleavage and generate biocompatible cleavage products [63]. Lastly, the drug should stay active after cleaving from the MMP-sensitive peptide even though some amino acids might remain linked to the drug.

Different synthetic options for incorporation of the peptide into the drug delivery system or between the drug and the drug delivery system via covalent conjugation have been published. One possibility is Michael addition, the nucleophilic addition to an α,β-unsaturated carbonyl compound. Tauro et al. used the sulfhydryl group of cysteine as nucleophile and acrylate group as unsaturated carbonyl compound, yielding 74.1 to 76.1 % efficiency after overnight incubation [133]. However, such reaction scheme might result in peptide dimerization due to disulfide formation as well as other side reactions, overall low drug loading and nonspecific release [134, 135]. Side reactions and disulfide formation can be

largely eliminated by introducing the MMP-sensitive peptide using EDC (1-ethyl-3-(3-dimethylaminopropyl) carbodiimide)/NHS (N-hydroxysuccinimide) chemistry [135]. In addition, this coupling chemistry produces water soluble by-products that can be easily removed via gel-filtration or dialysis. Braun et al. used the EDC/NHS chemistry to couple a myostatin inhibitor via MMP-sensitive peptide to poly (methyl methacrylate) microparticles [136]. This strategy lead to high incorporation efficiency after 2 hours of incubation. However, one disadvantage of this method is the relative non-specificity, leading to random coupling of primary amino groups with carboxyl groups. This can, on the one hand, result in self-polymerization leading to covalent aggregates and increasing the risk of an immunological response, and on the other hand, in a heterogeneous outcome with unclear stoichiometry [136, 137]. Maleimide coupling can be conducted between primary amines and thiols. This approach shows a lot of potential for biomolecules, carrying a free thiol or amine group. The disadvantage of this method is the hydrolysis of the maleimide ring over long reaction times and increasing pH (pH ≥ 8) [75, 138] . Finally, numerous authors used click chemistry, also known as copper (I)-catalyzed azide-alkyne cycloaddition (CuAAC), to synthesize peptide-carrier- or drug-peptide-carrier conjugates [86, 136, 139]. Due to their specific properties (weak acid/base) the functional group, namely alkyne and azide groups, are mostly inert towards biological molecules and the reaction can be carried out under broad reaction conditions (pH 4-12, aqueous solution, 0-120 °C) [137, 140]. The main disadvantage of CuAAC is the use of copper as a catalyst. Although the human body is in need of copper to function, excessive intake can lead to different diseases (kidney diseases, Alzheimer's disease, hepatitis) [140].

Besides the covalent binding, physical interactions (electrostatic and hydrophobic interactions) represent another option, having the advantage that biomolecules do not have to be modified. However, these conjugations are frequently less easy to control, less stable and less reproducible compared to covalent binding. Tauro et al. complexed cisplatin to aspartic acid residues of MMP-sensitive spacer, binding the chemotherapeutic drug to the hydrogel matrix [133]. Complexed cisplatin was slowly released even in the absence of MMP, indicating that complexation was successful but not sufficient to achieve full retention (50 % release within the first 24 h). When cisplatin was only entrapped into hydrogels, 95 % was released within one hour, showing that by complexation the release could be retained but not fully

controlled. After addition of MMP to the drug delivery system, cisplatin was released at an accelerated rate.

Aside from the conjugation strategy, the possible interaction of the carrier and MMP may play an important role. To gain insights into these effects, Chau et al. varied the charge of carboxymethyl dextran, coupled via MMP-sensitive linker to methotrexate, by reacting with ethanolamine under different conditions [141]. The charge had significant influence on the cleavage rate by MMP-2, resulting in more efficient cleavage if the negative charge of carboxymethyl dextran was masked. On the other hand, enzymatic digestion rate by MMP-9 was insensitive to dextran charge [141]. If the MMP-sensitive peptide is incorporated into a 3-D matrix, the MMP must diffuse into the matrix to cleave the peptide. In order to understand the influence of mesh sizes of hydrogels, Ross et al. compared poly (ethylene glycol) diacrylate (PEGDA) with different molecular weights (3.4, 10 and 20 kDa) and different concentrations, resulting in mesh sizes between approx. 5 to 20 nm [142]. PEGDA hydrogels of 3.4 kDa produced mesh sizes smaller than the dimensions of MMP-2 (9.75 nm length by 6.75 nm breadth) and therefore prohibited the diffusion of MMP-2 into the hydrogel and release of the model drug [133, 142]. No significant difference between model drug release was observed for 10 and 20 kDa PEGDA, potentially due to the inability of acrylate groups to form further crosslinks due to the increasing viscosity and physical restriction after gel formation had started. It can be concluded that especially for 3D systems, diffusion of MMP into the hydrogel becomes a key factor for controlled release, in addition to the kinetics of peptide cleavage.

MMP-7 is prone to interact with charged macromolecular surfaces which might influence the stability of the catalytic domain [143]. Catalytic activity remained unaffected by the interaction with anionic and neutral liposomes, whereas it was impaired in the presence of positively charged liposomes (**Figure 8 A**) [144]. If MMP-7 was bound to anionic or neutral liposomes, the active site pocket of the enzyme remained accessible (**Figure 8 B**) and therefore, active, while binding of the cationic liposome lead to obstruction of the active site pocket.

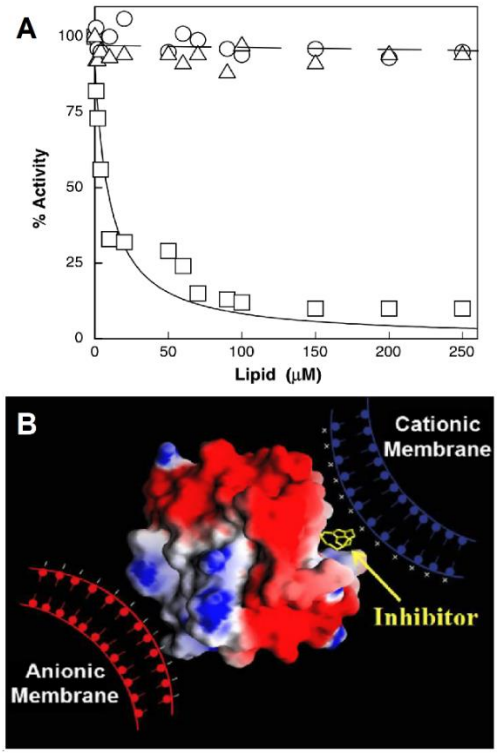

Figure 8. *A) MMP-7 activity in the presence of ○-○ anionic, Δ-Δ neutral, and □-□ cationic liposomes. B) Schematic representation of electrostatic surface potentials of MMP-7 with bound hydroxamate inhibitor and its potential interaction with anionic and cationic liposomes. Reprinted with adaptations from [144], with permission from Wiley.*

Not only the charge of the carrier and the charge distribution in the enzyme play a vital role, but also the constitution of the carrier, meaning the adaptability of the carrier might influence the structural and functional integrity of the enzyme. Differently charged liposomes (flexible) were compared to differently charged gold nanoparticles (rigid) [143]. The results showed that cationic and anionic gold nanoparticles influenced the MMP-7 activity, whereas the former even led to loss of the secondary structure of the enzyme. Therefore, besides the charge, rigidity and surface curvature appear to influence catalytic binding. Hence, understanding of biological structures of MMP, chemical insertion of MMP-sensitive peptide and interactions of MMP and the carrier are essential for bioengineering applications.

5. Utility of MMP responsive elements in the development of commercial products

Currently, only a few stimuli-responsive nanosystems, i.e. magnetic iron oxide particles (Nanotherm®) and thermosensitive liposomes (ThermoDox®), have progressed to clinical phases [145], but no MMP-sensitive DDS are in clinical trials or on the market. In the case of MMP-sensitive drug delivery systems, precise control of the initial response time of the DDS is critical to achieve drug release within the

therapeutic window [4]. Response to MMP is not as prompt as the response to other stimuli and therefore, the enzymatic specificity and sensitivity to activate the drug delivery systems must be optimized [146]. In addition to the basic performance (high sensitivity and selectivity, precise timing of the response), clinical performance is a key factor for successful industrial development, this includes biocompatibility and biodegradability, stability of the DDS both, during storage and application and the ability to scale-up the production to industrial scale [147, 148].

6. Conclusions

The development of MMP responsive drug delivery systems has attracted substantial interest, with numerous novel published designs and a plethora of different applications. MMP sensitive drug delivery started with comparably simple protease activated prodrugs, which frequently suffered from insufficient blood half-life, degradation and premature drug release. Introduction of high molecular weight carrier significantly improved circulation time and stability but was limited to highly active drugs. The development of particulate drug delivery systems then opened entirely new possibilities with regards to loading of different drugs as well as introduction of multiple release mechanisms. In recent years, numerous multifunctional drug delivery systems have been developed, e.g. combining MMP sensitive elements with penetration enhancers or active targeting moieties. Similarly, MMP sensitive systems accommodating different drug types, e.g. cytotoxic, low molecular weight chemical drugs and high molecular weight nucleic acids have been developed. Finally, MMP sensitive hydrogels may be employed for delivery of stem cells.

The functionality of MMP sensitive delivery systems strongly depends on optimal incorporation of MMP sensitive elements concerning the conjugation to the scaffolds and/or drug, the interaction of MMP sensitive elements with scaffold and/or drug and regarding accessibility of those elements to MMP. Therefore, designing MMP responsive drug delivery systems requires knowledge of these interactions and thoughtful selection and optimization of materials and synthetic strategies.

7. Acknowledgements

The financial support from Swiss National Science Foundation (grant number 157890) is gratefully acknowledged.

3. Results and Discussion

3.1. Effects of Degumming Process on Physicochemical and Mechanical Properties of Silk Fibroin

The experimental part (except for refractive index measurements, which were conducted by Livia Bast (Adolphe Merkle Institute, Fribourg) and tensile testing, which was in part conducted by Muriel Näf within the scope of her Bachelor thesis), data analysis and writing of the manuscript were my contribution. The manuscript was finalized by Prof. Dr. Oliver Germershaus.

– Kira Nultsch –

Published in: Macromolecular Materials and Bioscience, September 2018

Effects of silk degumming process on physicochemical, tensile, and optical properties of regenerated silk fibroin

*Kira Nultsch [1, 2], Livia K. Bast [3], Muriel Näf [2], Salima El Yakhlifi [2], Nico Bruns [3], Oliver Germershaus [2, *]*

[1] Department of Pharmaceutical Sciences, University of Basel, Klingelbergstrasse 50, 4056 Basel, Switzerland

[2] Institute of Pharma Technology, University of Applied Sciences and Arts Northwestern Switzerland, Gründenstrasse 40, 4132 Muttenz

[3] Adolphe Merkle Institute, University of Fribourg, Chemin des Verdiers 4, 1700 Fribourg, Switzerland

* Corresponding author:

E-mail address: oliver.germershaus@fhnw.ch (Oliver Germershaus)

Abstract

The removal of sericin from virgin silk (degumming) is the first step in the preparation of regenerated silk fibroin for its many applications as biomaterial, in drug delivery or as optical material. The process significantly affects the material characteristics of the protein. Degumming of silk is most commonly achieved by incubation in sodium carbonate solution at elevated temperature but numerous alternative methods employing enzymes, soap, and ionic liquids have been used. Herein, a systematic comparison of various degumming methods is provided. Sodium carbonate, sodium oleate, trypsin and 1-butyl-3-methyl-imidazolium bromide (ionic liquid) were used for degumming of virgin silk and resulting materials have been characterized with regards to mass loss, silk fibroin content by amino acid analysis, integrity of silk fibroin by size exclusion- and anion exchange chromatography, refractive index, and tensile properties. While complete degumming was achieved within 30 minutes using sodium carbonate, it was also found that this process resulted in significant reduction of molecular weight, shift towards less acidic charge variants and substantial reduction of yield- and rupture strength. Sodium oleate and trypsin were inefficient degumming reagents and negatively affected tensile properties. Degumming using ionic liquid showed good efficiency and marginal degradation of silk fibroin but also reduced yield- and rupture force. The refractive index of silk fibroin did not change by the various degumming methods. These results allow rational selection of the degumming method and tuning of silk fibroin material characteristics towards specific biomedical applications.

1. Introduction

Silk fibroin (SF), a protein produced by the mulberry silkworm *Bombyx mori*, has numerous advantages as scaffold for drug delivery systems, and for biomaterials. It is biocompatible, biodegradable into non-toxic products and possesses superior mechanical strength [28, 110]. Not surprisingly, silk fibroin has been largely explored as a natural material for various technical and biomedical applications such as drug delivery, tissue engineering, biosensors, electronics and optics [149-153]. Silkworm silk fibers (bave) consist of a pair of filaments (brin) composed of SF which are coated and held together by the glue-like protein sericin. SF consists of a hydrophobic heavy (~370 kDa) and a hydrophilic light (~25 kDa) chain, connected by a disulfide bond. The heavy chain is formed by highly repetitive crystalline fractions, GAGAGS, GAGAGY and GAGAGVGY (Gly-X domains), and responsible for the formation of anti-parallel β-sheets [21].

For the preparation of drug delivery systems or when intended for human implantation, purification of SF is mandatory due to immunogenicity in presence of sericin [154]. This extraction and purification process (frequently referred to as degumming) is usually characterized by quite harsh conditions (elevated temperature, alkaline pH), resulting not only in sericin degradation but also partial hydrolysis of fibroin [155]. Longer degumming in boiling sodium carbonate solution was reported to result in reduction of average molecular weight of SF [15, 156]. While degumming using sodium carbonate solution is the most common process applied for preparation of silk fibroin for biomedical applications, various alternative degumming conditions and processes were published, e.g. degumming with citric acid [157], urea [158], tartaric acid [155], different enzymes [17, 159] and ionic liquids [160]. Besides the different degumming reagents, different solvents for subsequent dissolution of SF were tested and compared, e.g. lithium bromide, Ajisawa's reagent and formic acid [158, 161] and the influence of dissolution time was studied [162].

The degumming process conditions are known to primarily affect molecular structure of SF. Besides general reduction of average molecular weight depending on degumming time using sodium carbonate, it has been found that SF degradation appears to specifically occur in amorphous regions while crystalline Gly-X domains are largely unaffected [15, 156]. As a result, formation of beta-sheets is virtually unaffected by degumming process duration using sodium carbonate [156]. Besides reduction

of molecular weight and despite unchanged beta-sheet formation, changes in the ability to form higher order structures were observed [156]. Furthermore, degumming was shown to affect *in vitro* cytocompatibility. SF treated with alkali for extended durations showed inhibitory effects on fibroblast cell growth compared to fibroin taken directly from gland [163]. Additionally, the degradation profile and drug release kinetics play a key role for the use as scaffold in tissue engineering and drug delivery applications. Variation of degumming time was found to affect *in vitro* degradation and drug release kinetics of various model compounds [164]. Recently, we studied the impact of different degumming times on the release of differently charged high molecular weight compounds and reported that degumming not only influenced SF integrity but also SF charge distribution and hence release of charged compounds [156]. Finally, degumming influences SF tensile properties, resulting in reduction of failure strength and yield point [16].

In summary, degumming process conditions substantially change physicochemical and mechanical properties of SF which in turn significantly affects the performance of SF as a scaffold in various biomedical applications such as drug delivery and tissue engineering. However, to our knowledge no comprehensive study on the effect of different degumming processes and process conditions has been performed for regenerated SF in the context of biomedical applications. Therefore, we herein investigate the effect of different degumming strategies such as enzymatic and alkali degumming as well as degumming using ionic liquid (IL) and process conditions on physicochemical, mechanical and optical properties of SF relevant for biomedical applications.

2. Materials and methods

2.1. Materials

Silkworm cocoons were purchased from Wollspinnerei Vetsch (Pragg-Jenaz, Switzerland). All other chemicals were ordered from Sigma Aldrich (Buchs, Switzerland).

2.2. Methods

2.2.1. Silk fibroin extraction

SF was extracted using various degumming reagents and process conditions (**Table 1**). In brief, SF cocoons were cut into small pieces and incubated in the respective solution at 5 g l^{-1} under constant stirring at 300 rpm at the temperature and time as detailed in **Table 1**. Afterwards, SF fibers were dried at room temperature in a fume hood overnight and dissolved in Ajiwasa's reagent (calcium chloride:ethanol:water at a molar ratio of 1:2:8) at 65 °C. The solution was filtered through syringe filter with nominal pore size of 5 µm (Yeti PVDF HPLC syringe filter, Infochroma AG, Zug, Switzerland) and dialyzed against purified water (Spectra/Por dialysis tubes MWCO 6-8 kDa, Spectrum Laboratories, Rancho Domingez, CA, USA). The mass of silk fibroin contained in a known volume of the solution was determined gravimetrically after evaporation of water at 65 °C for 24 h. For further processing, all silk fibroin solutions were adjusted to 10.0 g l^{-1}.

Table 1. *Degumming reagents and process conditions.*

Sample	**C5**	**C30**	**C60**	**C120**	**OL**	**T120**	**T180**	**IL**
Degumming reagent	0.02 M Sodium carbonate	0.02 M Sodium carbonate	0.02 M Sodium carbonate	0.02 M Sodium carbonate	1% Sodium oleate	1% Trypsin in 67 mM phosphate buffer pH 8	1% Trypsin in 67 mM phosphate buffer pH 8	90 % 1-butyl-3-methyl-imidazolium bromide
Degumming time / min	5	30	60	120	60	120	180	420
Temperature / °C	100	100	100	100	90	37	37	85

2.2.2. Scanning Electron Microscopy

The morphology of differently degummed fibers was studied by scanning electron microscopy (SEM). The fibers were sputter coated with gold and characterized with an accelerating voltage of 5 kV using a Hitachi TM3030 plus (Hitachi, Krefeld, Germany).

2.2.3. Mass loss

Before and after the degumming step the dry mass of the material was determined for 4 individual samples (IL: 2 individual samples) and percentage mass loss (m%) was calculated according to equation 1, where $m_{\text{before degumming}}$ is the dry mass before and $m_{\text{after degumming}}$ the dry mass after the degumming process.

$$m\% = \frac{m_{before\ degumming} - m_{after\ degumming}}{m_{before\ degumming}} \cdot 100\ \% \qquad (1)$$

Degumming efficiency based on mass loss was calculated by setting mass loss observed for C120 as 100% degumming efficiency.

2.2.4. Amino acid composition

To determine the amino acid composition, degummed samples (**Table 1**) were hydrolyzed according to USP 41 [165]. In brief, to one gram of degummed sample or sericin (Sericin *Bombyx mori*, order number S5201, Sigma Aldrich, Buchs, Switzerland), 200 µl 6 M hydrochloric acid (containing 0.5 % phenol) was added and incubated at 115 °C for 16 h. Hydrochloric acid was removed using speed vacuum. To each sample 200 µl 0.02 M hydrochloric acid was added and incubated at 50 °C for 10 minutes. Standard solutions with 50, 100, 200, 300, 400, 500, 600 and 1000 µM of amino acids (glycine, alanine, tyrosine, serine, glutamic acid, aspartic acid), chosen based on the significant difference in weight percentage found in sericin compared to fibroin, were prepared. Samples and standard solutions were derivatized using 70 µl borate buffer (pH 8.8), 10 µl sample or standard solution and 20 µl 6-aminoquinolyl-*N*-hydroxysuccinimidyl carbamate, vortexed for 10 s and heated at 55 °C for 10 minutes. Then, the samples and standards were analyzed by RP HPLC (Agilent 1260 Infinity, Agilent Technologies, Santa Clara, CA, USA; Acquity UPLC column, BEH shield RP 18, 1.7 µm, 2.1 x 100 mm, Waters Corporation Milford, MA, USA) at 55 °C with a flow rate of 0.4 ml min^{-1} (gradient steps **Table 2**). Buffer A consisted of a pre-prepared solution of acetonitrile, formic acid and 100 mM ammonium formate (10:6:84), which

was diluted with water (5:95). Buffer B consisted of acetonitrile and formic acid (98:2). The proportion of sericin and fibroin in the samples was calculated by setting SF 120 as 100 % fibroin and sericin to 0% fibroin. Degumming efficiency was calculated based on SF content by setting cocoons to 0% degumming efficiency and SF 120 to 100 % degumming efficiency.

Table 2. *RP HPLC step gradients.*

Time / min	**Buffer A / %**	**Buffer B / %**
0	99.9	0.1
0.54	99.9	0.1
5.74	90.9	9.1
7.74	78.8	21.2
8.04	40.4	59.6
8.64	40.4	59.6
8.73	99.9	0.1
9.5	99.9	0.1

2.2.5. Size exclusion chromatography

The chromatographic system (Agilent 1260 Infinity, Agilent Technologies, Santa Clara, CA, USA) used for size exclusion chromatography (SEC) was equipped with a quaternary pump, auto sampler, column oven, diode array detector (DAD) and a static and dynamic light scattering detector (SLS and DLS). The separation was performed using an Agilent Bio SEC-3 column (3 µm, 300 Å, 4.6 x 300 mm, Agilent Technologies, Santa Clara, CA, USA) with 0.1 M sodium chloride as mobile phase and a flow rate of 0.3 ml min^{-1} at 30 °C.

2.2.6. Weak anion exchange chromatography

For weak anion exchange chromatography (WAX) the same chromatographic system as for SEC was used. The separation was performed using a Bio WAX ion-exchange column (3 µm, 4.6 x 150 mm, Agilent Technologies, Santa Clara, CA, USA) with step gradients (**Table 3**). Buffer A consisted of 20 mM tris-(hydroxymethyl)-aminomethan (Tris) pH 8.5 and buffer B 20 mM Tris and 2 M sodium chloride pH 8.5. The separation was performed with a flow rate of 0.5 ml min^{-1} at 30 °C.

***Table 3**. Weak anion exchange chromatography step gradients.*

Time / min	**Buffer A / %**	**Buffer B / %**
5	100	0
5.01	80	20
10	80	20
10.01	60	40
15	60	40
15.01	40	60
20	40	60
20.01	0	100

2.2.7. Tensile testing

Single silk baves were unreeled from cocoons mounted into steel frames and degummed according to **Table 1**. To avoid batch-to-batch variability, one cocoon was unreeled and samples, taken from this cocoon, were measured in triplicates. Afterwards, degummed fibers were rinsed with water and dried in a fume hood over night. Then the frames with the fibers were fixed in a Texture Analyser TA-XT2i (Stable Microsystems Ltd., Surrey, UK) with grips and the frames were opened laterally to allow pulling. Test speed was set to 0.17 mm s^{-1} until rupture of the fibers.

2.2.8. Ellipsometry

Silicon wafers (2.25 cm^2, thickness: 675 □m, polished on one side from Silicon Materials, Kaufering, Germany) were washed with acetone and ethanol (ultrasound (SW 3 by Sonoswiss AG, Ramsen, Switzerland) each 15 min) and cleaned with carbon dioxide snow. Overcoats of silk fibroin of various degumming times and concentrations were prepared by spin casting the fibroin solutions onto the SiO_2 surface at a spin speed of 4000 rpm for 40 s (WS 650-MZ-23NPPB, Laurell Technologies Corporation, North Wales, USA). The samples were dried under vacuum in a desiccator over CaH_2 for at least 3 h. To induce β-sheet formation, samples were placed in methanol for 15 min and again dried under vacuum in a desiccator over night.

The refractive indices of dry silk fibroin films on silicon wafers were measured using an alpha-SE Ellipsometer (J. A. Woollam, Lincoln, USA). Experimental data were modelled by the Cauchy fit for transparent films using the software Complete EASE, Version 5.19, choosing 1.50 as starting point for

the fit of the refractive index of the protein. Refractive index measurements were taken at three different angles (65°, 70°, 75°) on three different spots on each film, and the measurements were repeated on 10 different films of each sample.

2.2.9. Statistical analysis

All measurements were performed in triplicates unless stated otherwise and results are presented as mean ± standard deviation. Two-tailed Student's t-test or one-way ANOVA with Tukey´s test (mass loss, SF content) or Dunnett's test (amino acid composition, untreated cocoons as control) was performed to identify statistical significance. Probability values of $p \leq 0.05$ were considered statistically significant.

3. Results

3.1. Microscopic characterization

Scanning electron micrographs of individual fibers after degumming were recorded to visually evaluate the removal of sericin as well as the microstructure of SF filaments (**Figure 1 A-I**). The native, untreated bave (**Figure 1 A**) showed two fibroin filaments, which are coated with and connected by sericin. After degumming using sodium carbonate (**Figure 1 B-E**), filaments without sericin coating were found and after extended degumming duration fibril formation at the surface of individual filaments was observed (**Figure 1 C and E**). After treatment with sodium oleate (**Figure 1 F**) filaments were partly disconnected and spots were visible on the filament surface, likely representing sericin residues. After enzyme treatment with trypsin for two and three hours (**Figure 1 G and H**), the fiber appeared cracked with a puckered surface. Degumming with ionic liquid (**Figure 1 I**) resulted in filaments, which partly appeared to be still connected and coated with sericin, and spots were visible on the fiber surface. **Figure S1** in supporting information provides additional micrographs of the samples after degumming.

3.2. Mass loss

SF degumming efficiency was assessed by the mass lost during the degumming process (**Figure 1 J and K**). However, it should be highlighted that mass loss during degumming may represent sericin and fibroin degradation. Mass loss may therefore be indicative of efficient removal of sericin but excessive mass loss may indicate substantial hydrolysis of fibroin. Sodium carbonate treatment resulted in overall

highest mass loss and highest degumming efficiency, whereas the degumming with sodium oleate lead to the lowest mass loss. Within the different degumming times with sodium carbonate, treatment for 5 minutes resulted in significantly lower mass loss than longer degumming times. No statistically significant difference was observed for mass loss for C30, C60 and C120. Treatment with trypsin resulted in statistically significantly higher mass loss than sodium oleate treatment. Incubation with trypsin for 2 or 3 hours lead to similar mass loss with statistically insignificant differences between the incubation times. Ionic liquid degumming lead to statistically insignificant different mass loss as treatment with trypsin and was also similar to C5.

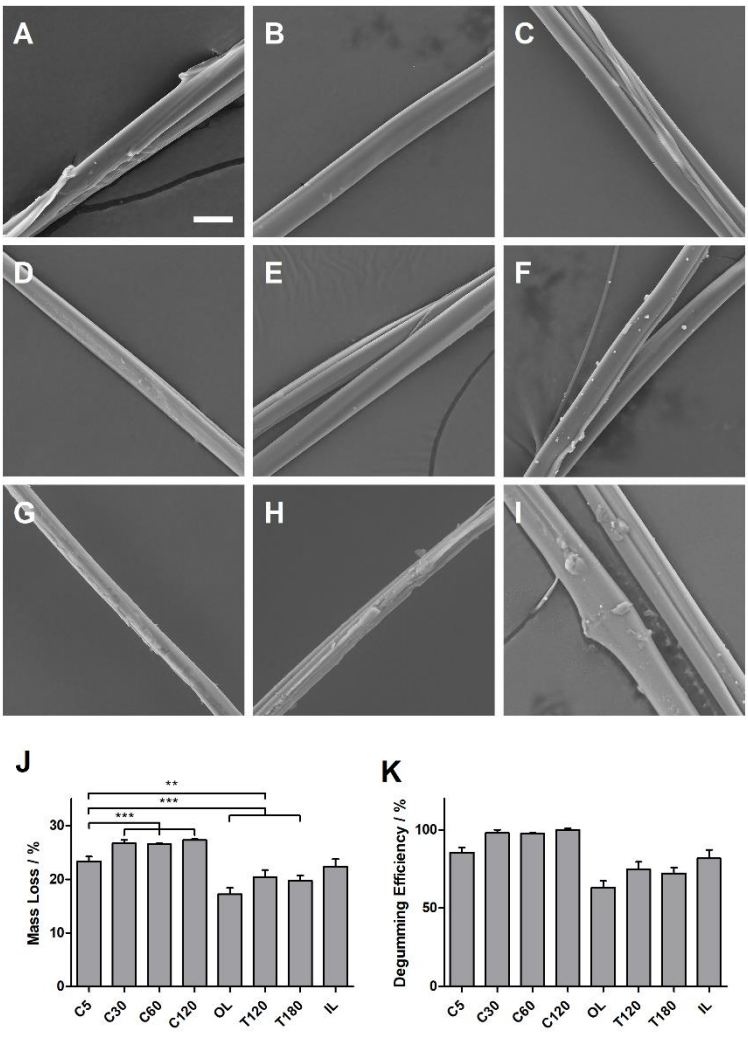

Figure 1. *(A-I) Scanning electron micrographs of native and degummed fiber samples. (A) native silk fiber, (B) C5, (C) C30, (D) C60, (E) C120, (F) OL, (G) T120, (H) T180 and (I) IL. Bar in (A) represents 20 µm and applies to all micrographs. (J) Mass loss during degumming process and (K) degumming efficiency calculated based on mass loss. Asterisks indicate significance level: ** $p \leq 0.01$; $p \leq 0.001$.*

3.3. Amino acid composition

Amino acid composition was determined focusing on glycine, alanine, tyrosine, serine, aspartic acid and glutamic acid because the amino acid content differed significantly between in SF and sericin (**Figure 2 A and B**). Glycine content differed significantly between cocoon and sericin. All degummed samples showed statistically significantly higher glycine content than untreated cocoon due to partial or complete hydrolysis of sericin. Similarly, statistical significant differences in alanine content were found between untreated cocoons and sericin as well as degummed samples except OL and IL. Variation of tyrosine content between cocoons and sericin was rather small but significant. Major differences between cocoons and sericin as well as degummed samples were observed in serine content. Serine content in all degummed samples was significantly lower than in cocoons, again confirming partial or complete hydrolysis of sericin. The same was found for aspartic acid and glutamic acid.

Determination of the amino acid composition allowed calculation of fibroin content and degumming efficiency (**Figure 2 C and D**). Fibroin content was statistically significantly higher than in cocoons for all degummed samples except OL. No significant differences were observed for fibroin content after treatment with sodium carbonate for different durations or fibroin content after treatment with trypsin for different durations. Since fibroin content in untreated cocoons was already approx. 80 %, differences between the degumming processes are more evident if degumming efficiency is assessed (**Figure 2 D**). Complete degumming is observed after 30 minutes treatment with sodium carbonate. Incomplete degumming is found only after treatment with sodium oleate and to a smaller extend trypsin for 2 hours.

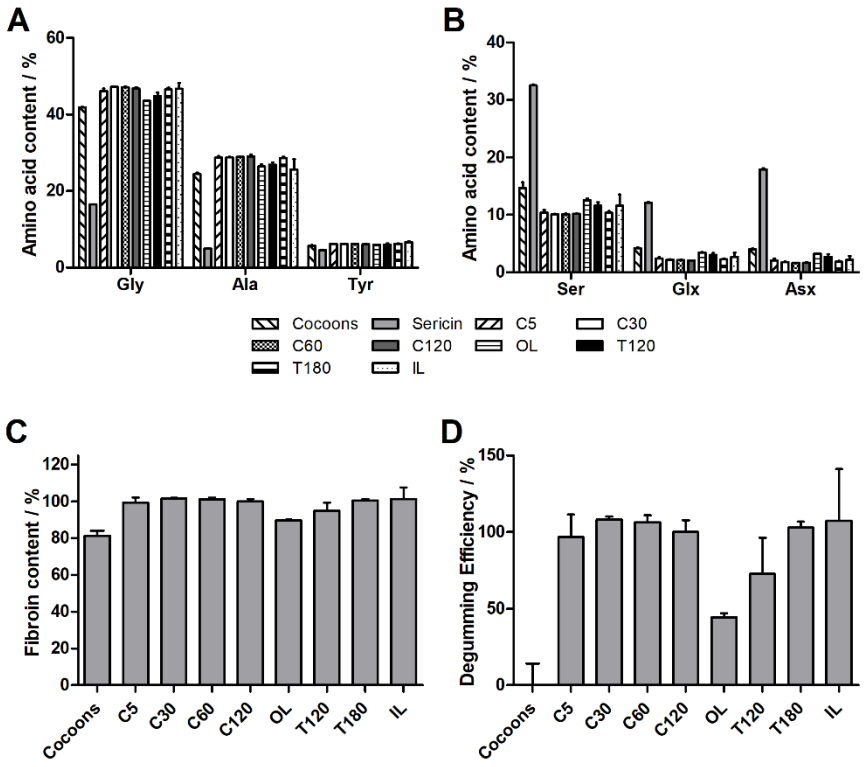

Figure 2. *Amino acid content for (A) glycine, alanine, tyrosine and (B) serine, aspartic acid and glutamic acid of cocoons, sericin and degummed samples. Fibroin content (C) and degumming efficiency (D) of cocoons and samples as calculated based on amino acid composition analysis.*

3.4. Size exclusion and weak anion exchange chromatography

Silk cocoons showed a single peak at 5.6 minutes in size exclusion chromatography using UV detection (**Figure 3 A**). With longer degumming time in sodium carbonate (C5, C30, C60 and C120) the main peak became smaller and a second broad peak appeared at longer retention times (lower molecular weight). In addition, a small leading peak was observed at approx. 5.0 minutes. OL exhibited similar results compared to cocoon sample but in addition a small shoulder appeared at approx. 5.4 minutes. T120 and T180 did not show peaks at the same position as the other samples, but peaks at longer retention times were observed. IL exhibited a similar chromatogram as untreated cocoons.

Using static light scattering detection (**Figure 3 B**), the main peak observed by UV detection at approx. 5.6 minutes was confirmed but in addition the small leading peak at approx. 5.0 minutes was more pronounced. OL showed three peaks, the retention time of two of them was comparable to carbonate-degummed samples (peaks at 5.0 and 5.6 minutes). In addition, a new peak was observed at 5.3 minutes

(potentially corresponding to the shoulder observed using UV detection). Virtually no static light scattering signals were obtained in the case of T120, T180 and IL.

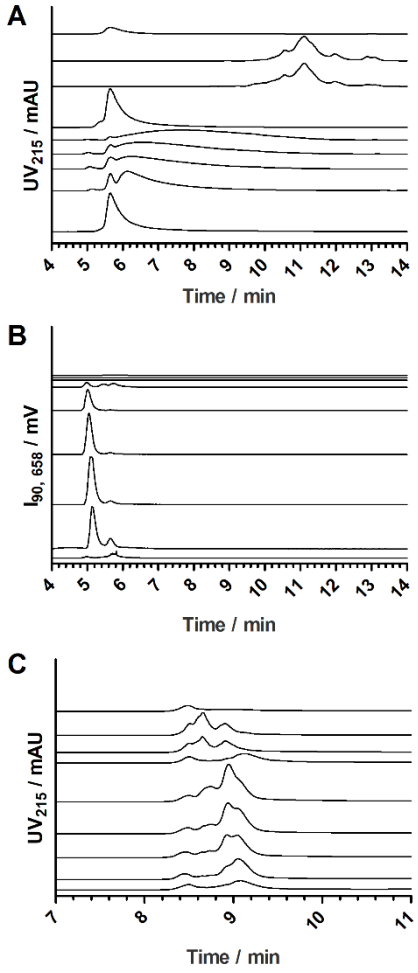

Figure 3. *Chromatography of cocoons, C5, C30, C60, C120, OL, T120, T180 and IL (traces from bottom to top in each panel). Size exclusion chromatography with (A) UV detection at 215 nm and (B) light scattering detection at 90°. (C) Weak anion exchange chromatography with UV detection at 215 nm.*

Weak anion exchange chromatography of cocoon and sodium carbonate treated samples revealed a main peak at approx. 9.1 minutes with side peak (less acidic variants) at approx. 8.4 minutes (**Figure 3 C**). With increasing degumming time with sodium carbonate, the main peak area was reduced and new variant peaks at approx. 8.6, 8.7 and 8.9 minutes appeared and became more prominent. OL showed a similar chromatogram as the cocoon sample with slightly more pronounced variant peaks at 8.4 minutes. Chromatograms of T120 and T180 were comparable to C120 with even more pronounced variants showing shorter retention times. Finally, IL only showed the variant peak at approx. 8.4 minutes.

3.5. Tensile testing

In **Figure 4** the maximum rupture forces and yield points are displayed. Native, untreated fibers had the highest rupture force (~ 150 mN) and yield point (~ 60 mN), whereas sodium carbonate treatment resulted in significant reduction of both rupture force and yield point with increasing degumming time. No significant differences were observed between C60, C120, OL and IL. However, trypsin treatment resulted in further significant reduction of mechanical properties, especially comparing C120 with T180.

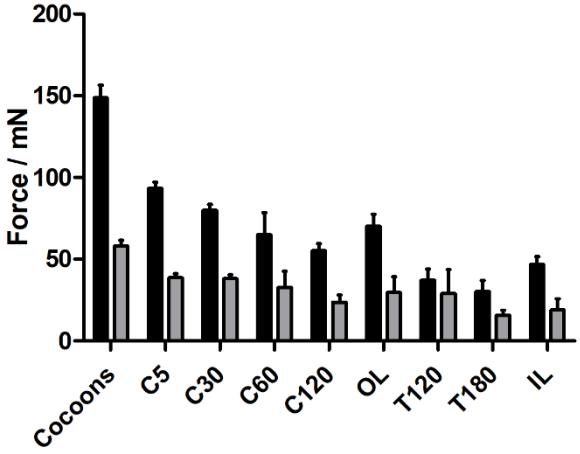

Figure 4. *Tensile testing of native silk and differently degummed samples: rupture force (black bars) and yield point (grey bars).*

3.6. Refractive index

Within the margin of error of the measurements, no major variation of refractive index with degumming method and -duration were observed, neither before nor after methanol treatment to induce beta sheet formation (**Figure 5**). Comparing the results before and after treatment with methanol, no significant differences were observed between the two groups either.

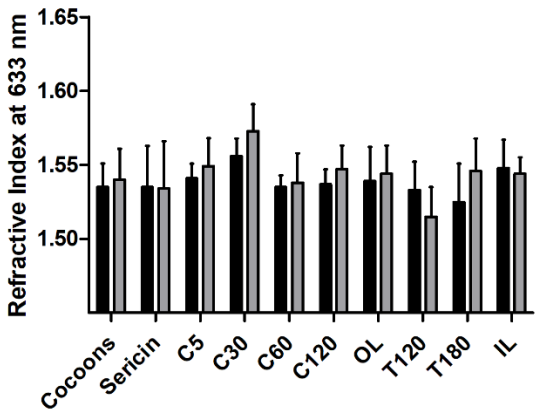

Figure 5. *Refractive indices of native silk, sericin and differently degummed samples before (black bars) and after (grey bars) treatment with methanol.*

4. Discussion

The degumming process, i.e. the removal of sericin from virgin silk, is one of the most critical process steps during preparation of regenerated SF, which is increasingly used as a biomaterial for tissue engineering, implantable devices, disease models and for drug delivery systems [166].

Depending on degumming process conditions, various material properties such as tensile strength, molecular weight distribution and micelle formation of SF are affected, ultimately affecting performance in biomedical applications such as tissue engineering and drug delivery [16, 156, 164]. Furthermore, efficient degumming is crucial with regards to the biocompatibility and immunogenicity of SF [15]. Therefore, it is necessary to completely remove sericin, while preserving or controlling SF integrity.

Numerous different processes and conditions have been published for silk fibroin extraction from virgin silk, the most common of these processes uses boiling sodium carbonate solution for degumming. Traditionally, silk textiles have been treated after weaving with alkali-free olive oil soap (Marseilles soap) at 90-98°C for several hours to remove sericin and resulting in reduced brittleness, improved handling and characteristic luster of silk textiles [167]. Common alternative degumming processes, especially in the context of SF extraction for biomedical applications include enzymatic degradation of sericin and, more recently, degumming using ionic liquids [159, 160].

Degumming using sodium carbonate solution efficiently hydrolyzed and removed sericin after 30 minutes as evidenced by evaluation of degumming efficiency based on mass loss (**Figure 1 K**) and

amino acid analysis (**Figure 2 D**). Extending the process duration beyond 30 minutes did not significantly improve degumming efficiency based on either analysis. Published analysis of degumming efficiency showed variable results ranging from complete degumming after 5 minutes at 100 °C [15] to complete degumming after 40 minutes at 80°C [168], presumably due to variable process conditions such as temperature, agitation and silk concentration. Increasing degumming time using sodium carbonate on the other hand substantially affected SF integrity. In agreement with previous reports, average molecular weight of SF was reduced, and molecular weight distribution increased with increasing degumming time (**Figure 3 A**) [15, 156, 164, 169, 170]. Interestingly, incubation in sodium carbonate also resulted in a shift towards less acidic charge variants with increasing degumming time (**Figure 3 C**), suggesting predominant degradation of the light subunit and/or C-terminal region of the heavy chain of SF [171]. This conclusion corresponds with the previous finding that beta-sheet content of SF is not significantly affected by degumming time [15, 156]. Tensile testing revealed reduction of both rupture force and yield point with increasing degumming time. The elastic behavior of silk was related to the amorphous phase as well as beta-sheet crystals [172], while rupture force is mainly governed by failure of crystalline units [173]. Therefore, it may be hypothesized that degumming in addition to degradation of amorphous regions also reduced crystallite integrity resulting in the reduction of both yield point and rupture force [16]. Finally, changes in amino acid composition of proteins may result in small but significant differences of refractive indices [174]. However, refractive indices showed no significant changes in response to increasing degumming time (**Figure 4 B**), in line with recently published results [175] and potentially due to the fact that the contribution of repetitive elements of SF heavy chain dominate refractive index. This finding contributes to the conclusion that degradation primarily affected non-repetitive regions of SF.

Oleate degumming was significantly less efficient than other methods and resulted in incomplete removal of sericin with degumming efficiency in the range of 44 to 63% (**Figures 1 K and 2 D**) with remnants of sericin coating visible in micrographs (**Figure 1 F**). In contrast, mass losses of approx. 22 to 24 % were reported for degumming using Marseille's soap at 5 g l^{-1} or 25 % of weight of the fabric at 93 or 95 °C and 90 minutes [176, 177], which would be comparable to degumming efficiency achieved for C5 in the present study. While SEC and anion exchange chromatography revealed no major

degradation and despite incomplete degumming, oleate treated sample showed significantly reduced yield point as well as rupture force. Degumming with Marseille's soap was reported to similarly result in pronounced strength loss, even at still incomplete degumming [176].

Numerous alternative degumming processes applying various enzymes have been published [176-178]. We herein focused on trypsin, due to its wide availability and its reported high degumming efficiency [159]. However, in the present study, only moderately efficient degumming of 75 % and 72 % after incubation for 120 minutes and of 72 % and 103 % after incubation for 180 minutes was achieved based on mass loss and amino acid composition, respectively, which is in good agreement with previous findings in another study [179]. Additionally, degumming using trypsin resulted in pronounced SF degradation observed in scanning electron micrographs, SEC as well as anion exchange chromatography. Tensile testing similarly showed the lowest rupture forces and low yield points after degumming with trypsin. Based on these results it is concluded that trypsin under the conditions chosen not only degrades sericin but also fibroin, resulting in formation of protein fragments and limiting its suitability for degumming of silk for biomedical applications. This result may not be surprising in view of numerous studies, which successfully used trypsin for silk fibroin digestion [180, 181].

Degumming with ILs may represent another promising degumming approach due to their specific properties, e.g. tunability, versatility and low melting point (below 100 °C). IL consist of an inorganic ion and an organic, bulky counterion carrying a delocalized charge, which prevents the formation of a stable crystal lattice. Long alkyl chains of the organic cation, e.g. 1-butyl-3-methylimidazolium (Bmim), are able to interact with the protein, leading to participation or competition of the solvent with intra- and intermolecular protein interactions and therefore, to dissolution [182]. In the present study treatment with [Bmim]Br resulted in similar degumming efficiency to C5, both by mass loss and amino acid analysis (**Figure 1 K and 2 D**), while SEC showed no major degradation of SF (**Figure 3 A**). However, micrographs (**Figure 1 I**) showed remnants of sericin on the fiber surface and tensile testing revealed substantially reduced rupture force and yield point. Reports in the literature on the effects of ILs on silk are controversial. Treatment with [Bmim]OAc resulted in visually complete dissolution of silk fibers within 4 minutes at 120 °C [183] while it was reported in another study that only 0.7 % of silk fibroin was soluble in [Bmim]Br [160]. Differences in water content of ILs may significantly change the

dissolution properties and therefore result in different dissolution characteristics. Furthermore, silk fibers were subjected to degumming prior to incubation in ILs in one of the studies, potentially resulting in improved SF dissolution due to partial degradation induced by prior degumming.

5. Conclusion

Degumming of SF using sodium carbonate not only results in fast sericin removal after 30 minutes but also affects SF average molecular weight, molecular weight distribution, isoelectric point and mechanical properties. All these properties significantly influence the performance in various biomedical applications and may be employed for tuning of SF material characteristics for specific applications. As an example, drug release from SF matrices was shown to depend on SF isoelectric point, resulting in more sustained release of positively charged propranolol hydrochloride compared to negatively charged salicylic acid [184]. Similarly, SF average molecular weight was shown to affect drug release kinetics [156].

Degumming with sodium oleate and trypsin was only moderately efficient but resulted in significant SF degradation and/or substantially reduced yield point and rupture strength. On the contrary, degumming with IL was quite efficient but requires further optimization to improve tensile properties of SF after degumming.

In summary, degumming using sodium carbonate solution for 30 minutes appears the best degumming process among the studied alternatives allowing to retain SF integrity and achieve complete sericin removal.

Supporting Information

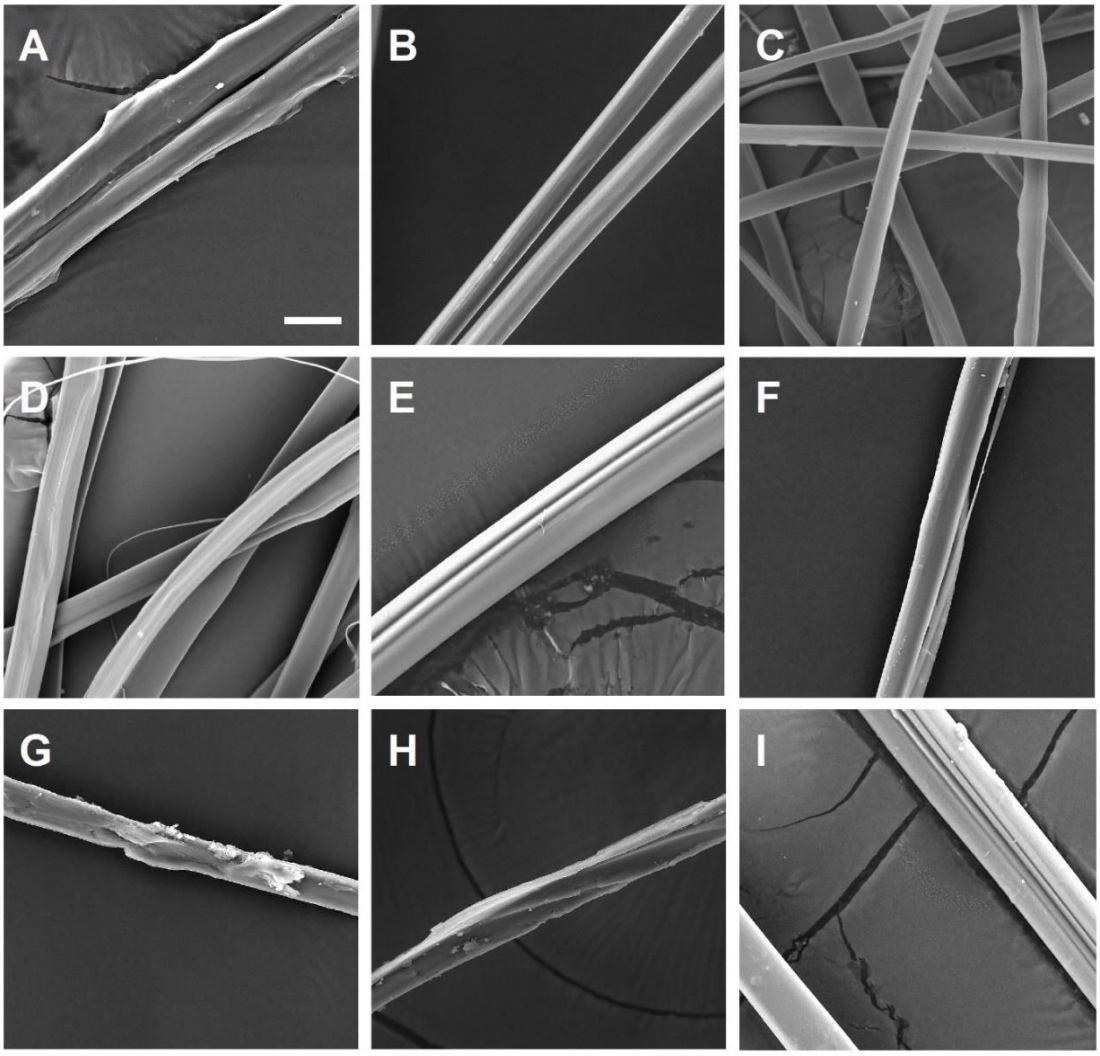

Figure S1. *Scanning electron micrographs of native and degummed fiber samples. (A) native silk fiber, (B) C5, (C) C30, (D) C60, (E) C120, (F) OL, (G) T120, (H) T180 and (I) IL. Bar in (A) represents 20 µm and applies to all micrographs.*

Acknowledgements

We thank Dr. Bodo Wilts (Adolphe Merkle Institute, Fribourg, Switzerland) for scientific discussions along this project as well as for reading the manuscript. KN and OG gratefully acknowledge financial support by the Swiss National Science Foundation (SNSF) under grant number 157890. LKB and NB received funding from the European Union's Horizon 2020 research and innovation program under the Marie Skłodowska-Curie grant agreement No. 722842, and from the SNSF under grant number PP00P2_172927 and the NCCR Bio-Inspired Materials.

3.2. Silk Fibroin Degumming affects Scaffold Structure and Release of Macromolecular Drugs

The experimental part, data analysis and writing of the manuscript were my contribution. The manuscript was finalized by Prof. Dr. Oliver Germershaus.

– Kira Nultsch –

Published in: European Journal of Pharmaceutical Sciences, June 2017

Silk Fibroin Degumming Affects Scaffold Structure and Release of Macromolecular Drugs

Kira Nultsch [†,¥], *Oliver Germershaus* [*,¥]

[†] Institute of Pharma Technology, University of Applied Sciences, Gründenstrasse 40, 4132 Muttenz, Switzerland

[¥] Department of Pharmaceutical Sciences, University of Basel, Klingelbergstrasse 50, 4056 Basel, Switzerland

* Corresponding author:

E-mail address: oliver.germershaus@fhnw.ch (Oliver Germershaus)

Abstract

Silk fibroin (SF) is a natural polymer with tremendous potential as a matrix for drug delivery systems as well as for tissue engineering. Silk sericin (SS) removal (degumming) is a critical step during SF purification, potentially affecting SF integrity and resulting in structural changes such as partial hydrolysis and inhibition of micelle formation. In addition to SF composition itself, the molecular weight and charge of encapsulated drugs may significantly affect drug release from SF matrices. The effect of these parameters on drug release was investigated by varying SF degumming time and charge of the model compound encapsulated in SF films. With increasing degumming time, average SF molecular weight decreased, molecular weight distribution became broader and formation of SF micelles was impaired. However, β-sheet content was not affected by degumming time, suggesting that degradation occurred mainly in hydrophilic domains of SF. The release of differently charged dextran derivatives, used as macromolecular model drugs, was significantly affected by SF degumming. Release of neutral dextran increased with increasing degumming time. In contrast, negatively charged dextran showed an inverse effect potentially due to reduced SF charge density with increased degumming time. Interestingly, positively charged dextran were shown to partly form polyelectrolyte complexes with SF by isothermal titration calorimetry but also exhibited phase separation during film drying resulting in fast burst release. These results demonstrate that both, SF preparation as well as drug charge significantly affect drug release from SF matrices.

KEYWORDS

Silk Fibroin; Controlled Release; Biologic Drug; Biopolymer; Biodegradable Films; Drug Delivery

1. Introduction

Silk obtained from cocoons of the domesticated silk worm *Bombyx mori* was the most common suture material since the early 20th century but was largely replaced after the advent of synthetic sutures [185]. However, silk was in recent years rediscovered as a natural material for various biomedical applications [110]. Silk was applied in numerous drug delivery systems due to its biocompatibility and biodegradability [28] and was identified as a promising biopolymer for regenerative medicine [186] and the stabilization of biologicals [6]. Preparation of silk-based materials can be performed under very mild conditions, i.e. in an entirely aqueous environment and applying no or very low shear force [5, 187].

Silk fibers (bave) consist of two individual silk fibroin (SF) filaments (brins) that are coated with the glue-like protein silk sericin (SS). SF comprises a light chain (~25 kDa) and a heavy chain (~350 kDa) which are connected by a single disulfide bond. The heavy chain of SF is characterized by repeating sequences of GAGAGS, GAGAGY and GAGAGVGY, resulting in formation of antiparallel β-sheets and being ultimately responsible for crystalline regions in SF [188]. SF has an approximately isoelectric point (IEP) of 4.6 [62], leading to an overall negative charge at physiological pH.

The presence of SS was associated with lack of biocompatibility and hypersensitivity to silk and hence, SS must be efficiently removed in a so called degumming process [14]. This purification process is frequently carried out by alkali treatment at elevated temperature, hydrolyzing the amid bonds of sericin. However, the degumming process step is assumed to affect the SF integrity. Commonly, 0.02 M sodium carbonate is used for degumming [189] whereby higher concentrations and elevated pH values were found to increasingly result in SF degradation [190, 191]. Other degumming agents were studied, such as formic acid [192], citric acid [157], urea [16], boric acid [16] and different enzymes [17, 178]. Apart from type of degumming agent, concentration and pH value, degumming time is a potential major factor affecting SF integrity [15, 193].

Even though the impact of degumming time on physicochemical properties of silk has been investigated in the past, little research has been conducted regarding a) the impact of the degumming time on SF-based drug delivery system performance and b) how the properties of encapsulated, macromolecular

compounds affect the release pattern. Hines et al. investigated the influence of the molecular weight of fluorescein labelled dextran on the release pattern as well as the release of negatively charged small molecules (dyes) [194, 195].

Pritchard et al. looked into the effects of the degumming on the SF material and in consequence, the influence of the material properties on small molecule drug delivery [164]. However, no studies regarding the release of high molecular weight compounds and the effect of differently charged compounds have been performed to date. Dextrans are suitable model compounds to study drug delivery matrices due to their defined molecular weight and straightforward modification with different residues [196]. Dextran derivatives (**Figure 1**) with similar average molecular weight of 10 kDa and the same backbone, but differently charged residues, were chosen to investigate the influence of drug charge on release. To assess whether the degumming time and charge of the encapsulated, macromolecular compound influence the release pattern, we investigated the release of neutral, positively and negatively charged dextran from films, prepared from SF extracted from silk cocoons using increasing degumming

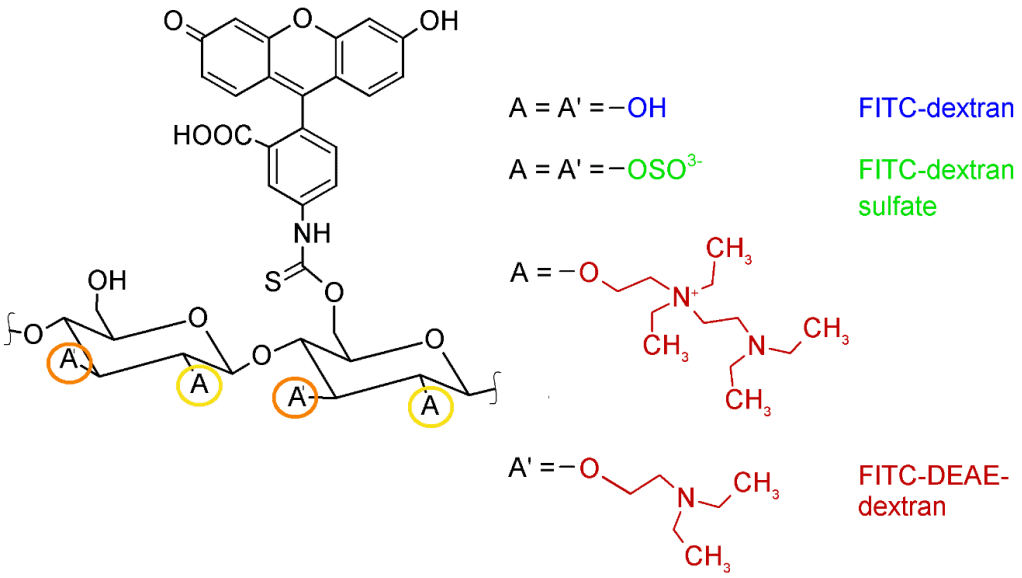

Figure 1. *Structural formula of the differently charged dextran derivatives.*

time.

2. Materials and Methods

2.1 Materials

Cocoons of the silkworm (*Bombyx mori*) were supplied by Wollspinnerei Vetsch (Pragg-Jenaz, Switzerland) and Swiss Silk – Vereinigung Schweizer Seidenproduzenten (Hinterkappelen, Switzerland). Fluorescein isothiocyanate-dextran (FITC-dextran) 10 kDa, fluorescein isothiocyanate-2-(diethylamino) ethyl-dextran (FITC-DEAE-dextran) 10 kDa and fluorescein isothiocyanate-dextran sulfate (FITC-dextran sulfate) 10 kDa were purchased from TdB Consultancy AB (Uppsala, Sweden). Bio-Safe™ Coomassie Stain G-250 was supplied by Bio-Rad Laboratories (Cressier, Switzerland). Cell culture plates (6-well-plates) were obtained from Vaudaux-Eppendorf AG (Basel, Switzerland). All other chemicals were purchased from Sigma Aldrich (Buchs, Switzerland).

2.2 Methods

Gel Electrophoresis. Molecular weight distribution was investigated by sodium dodecyl sulfate poly(acrylamide) gel electrophoresis (SDS PAGE) according to the protocol of Laemmli under reducing conditions [197]. Briefly, for each sample 20 µg dialyzed SF per band was loaded on a 12% gel and run for 90 minutes. The samples were stained with Bio-Safe™ Coomassie for 1 h and then rinsed with water for 30 min.

Size-Exclusion-Chromatography. The chromatographic systems consisted of a quaternary pump, auto sampler, column oven, diode array detector (DAD) and a static and dynamic light scattering detector (SLS and DLS) (Agilent 1260 Infinity, Agilent Technologies, Santa Clara, CA, USA). The separation was performed on an Agilent Bio Sec-3 column (3 µm, 300 Å, 4.6 x 300 mm, Agilent Technologies, Santa Clara, CA, USA) with 0.1 M sodium chloride as mobile phase and flow rate of 0.3 mL/min at 25 °C. The dialyzed SF solution was diluted with the mobile phase to 0.1% solution.

Fourier Transform Infrared Spectroscopy (FT-IR). To investigate the differences between the degumming times, ATR FT-IR spectroscopy using an Agilent Cary 620/670 (Agilent Technologies, Santa Clara, CA, USA) was performed. The blank SF films were either left untreated or treated with methanol (preparation as described further below) and after drying, measured in a range of 400 cm^{-1} to 4000 cm^{-1} in 4 cm^{-1} resolution. The spectra were baseline corrected and β-sheet content of the SF films

was calculated by Fourier-self deconvolution using Omnic™ Spectra Software (Thermo Fisher, Waltham, MA, USA). Amide I (1600 – 1700 cm^{-1}) was chosen for the calculation since the band is characteristic for β-sheets.

SF Film Preparation. SF solution (6% w/w) was mixed with either FITC-dextran, FITC-DEAE-dextran or FITC-dextran sulfate (aiming a 15 mg/mL solution) and subsequently, 2.5 mL were dried in 6-well-plates overnight, resulting in a 25% (w/w) loading [194]. After drying, the films were cut into (commensurate) samples of the same size with a hole punch and transferred into glass vials (6 mL). Triplicates of each film type (DEAE-D, D and DS) were prepared. The films were treated with 300 µl of methanol to induce β-sheets and dried in a fume hood overnight.

Release Studies. For the *in vitro* release studies the films were placed in fresh 6 mL glass vials with 2.5 mL phosphate buffered saline (PBS) and incubated in the dark at 37°C and 30 rpm in an orbital incubator shaker (IKA®-Werke, Staufen, Germany). Sink conditions were maintained throughout the release studies. After 150 h incubation, the films were collected and dissolved in 2.5 mL Ajiwasa's reagent to determine the unreleased amount of the model compounds. The amount of the released compounds was measured by UV/Vis spectroscopy (VWR UV 6300PC, VWR, Dietikon, Switzerland) at 494 nm for each time point. To compare the drug release differently charged dextran derivatives, the mean dissolution time (MDT) was calculated (Equation 1), where *i* is the sample number, *n* is the dissolution sample times, M_i is the amount of drug released between t and (t-1), *t* is the midpoint between t and (t-1). Statistical significance was calculated by using student's t-test to compare two groups with a significance level of p = 0.05.

$$MDT = \frac{\sum_{i=1}^{n} t\Delta M_i}{\sum_{i=1}^{n} \Delta M_i} \qquad \textbf{Equation 1}$$

Table 1. *Overview of the varying treatments of the SF films: different degumming times and differently loaded SF films.*

Degumming time / min	*Blank films*	*Films loaded with FITC-DEAE-dextran*	*Films loaded with FITC-dextran*	*Films loaded with FITC-dextran sulfate*
30	SF 30	DEAE-D 30	D 30	DS 30
60	SF 60	DEAE-D 60	D 60	DS 60
120	SF 120	DEAE-D 120	D 120	DS 120

Scanning Electron Microscope (SEM). Cross sections of the SF films were sputter coated and characterized by SEM (Hitachi TM3030 plus, Hitachi, Krefeld, Germany).

Confocal Laser Scanning Microscope (CLSM). SF films loaded with FITC-DEAE-dextran, FITC-dextran or FITC-dextran sulfate were imaged by CLSM (Olympus FV1000, Olympus, Center Valley, PA, USA). The CLSM micrographs were recorded using an objective with 10x magnification (NA 0.30) and an excitation laser wavelength of 488 nm, a pinhole size of 80 µm, resulting in an optical slice thickness of 6.51µm. Emission was detected using a band-pass filter (500-600 nm).

FT-IR Imaging Analysis. The differently loaded SF films were measured with an FT-IR microscope equipped with an ATR germanium crystal (Agilent Cary 620 FT-IR microscope, Agilent Technologies, Santa Clara, CA, USA) to investigate the distribution of the model compounds in the SF films. The images were collected using the following parameters: resolution 4 cm^{-1}, scan from 4000 to 400 cm^{-1} and 64 images per step. Mapping of the SF films was performed using 1520 cm^{-1} as SF specific wavenumber, while dextrans were mapped at ~1000 cm^{-1}. The colors respectively the concentration/absorption are not comparable in between the differently loaded films.

Isothermal Titration Calorimetry (ITC). ITC measurements were performed on a nano ITC (TA instruments, New Castle, DE, USA). A 1.5 mM FITC-DEAE-dextran solution was titrated into 30 µM SF solution to measure the enthalpy of the reaction. The experiment was conducted at 37°C and the solution was stirred at 300 rpm. 20 injections with each 2 µL and 300 s spacing between the injections were carried out.

3. Results

Figure 2A shows SDS PAGE analysis of SF after degumming for 30, 60 and 120 minutes (SF 30, SF 60, SF 120). In general, longer degumming times led to a broader molecular weight distribution. After 30 minutes the molecular weight was distributed over a range of approximately 75 to 360 kDa whereas SF 120 resulted in a broad smear and a shift of the protein distribution to predominantly smaller molecular weights (approximately 10 to 75 kDa). After 30 minutes degumming time, SF light chain was still detectable at approximately 25 kDa but was barely visible at 60 minutes degumming and entirely degraded at 120 minutes. These results were confirmed by SEC analysis. With increasing degumming time, main peaks as detected by UV absorption (**Figure 2B**) shifted to longer retention time due to increasing protein degradation. Furthermore, a leading peak at 6.3 minutes was observed, whose height decreased with increasing degumming time. Static light scattering detection (**Figure 2C**) showed

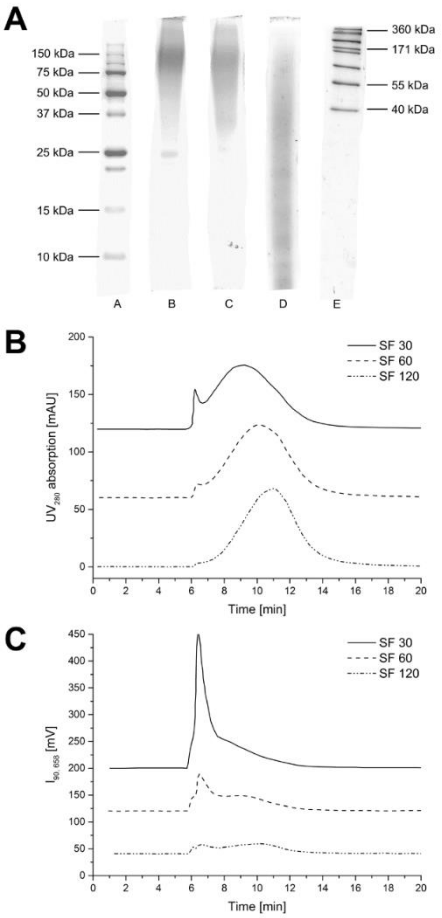

Figure 2. *Influence of the degumming time on the molecular weight distribution. A) SDS PAGE. A and E indicate the marker. SF 30 (B), SF 60 (C) and SF 120 (D). The graphs B) and C) depict the result of the size exclusion chromatography, where B) shows the UV detection and C) the light scattering.*

a peak at 6.4 minutes with tailing up to a retention time of approximately 13 minutes. As with UV detection, peak height was decreased with SF 60 and almost disappeared in the case of SF 120.

Figure 3A presents the FT-IR spectrum of SF 30, before and after methanol treatment to induce β-sheet formation. Untreated SF 30 showed bands for amide I (C=O stretching) at 1635 cm^{-1}, amide II (secondary N-H bending) at 1515 cm^{-1} and amide III (C-N stretching) at 1232 cm^{-1}. Methanol treatment induced a shift of the amide I band to 1619 cm^{-1} (amide II 1513 cm^{-1}, amide III 1230 cm^{-1}), indicating β-sheet formation [198, 199]. No shift in the amide III band suggested that besides β-sheets there were also remaining random coil structures in the protein. Untreated SF120 showed bands at 1638 cm^{-1} (amide I), 1514 cm^{-1} (amide II) and 1235 cm^{-1} (**Figure 3B**), similar to untreated SF 30. Methanol treated SF 120 showed bands at 1621 cm^{-1} (amide I), 1517 cm^{-1} (amide II) and 1235 cm^{-1} (amide III), suggesting β-sheet formation. The β-sheet content of methanol treated SF films ranged between 0.39 and 0.47 and no significant differences between SF30, SF60 and SF120 were observed.

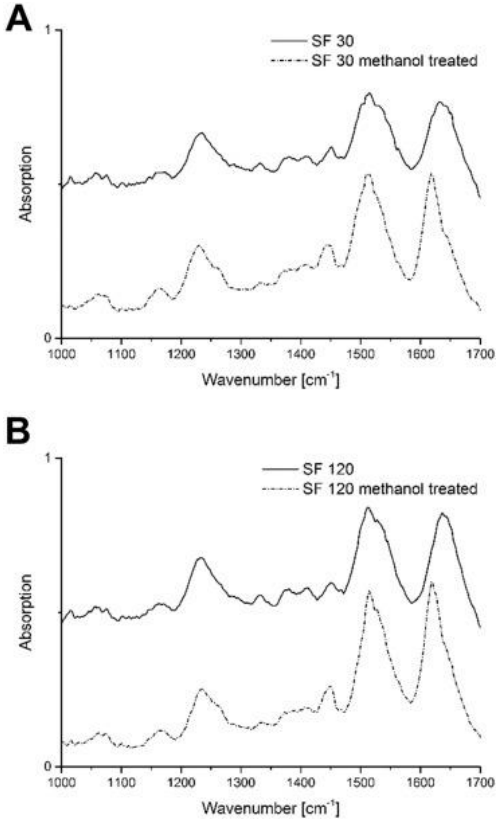

Figure 3. *FT-IR spectra of SF after different degumming times. A) SF 30, untreated (solid line) and ethanol treated (dotted line). B) SF 120, before (solid line) and after methanol treatment (dotted line).*

No significant differences between the release profiles from SF films were found for FITC-DEAE-dextran (**Figure 4A**). The MDT of FITC-DEAE-dextran loaded films was also not significantly different between the different degumming times (DEAE-D 30: 5.732 h ± 1.891 h, DEAE-D 60: 4.470 h ± 4.356 h, DEAE-D 120: 6.678 h ± 3.640 h). The release profiles obtained with FITC-dextran showed increasing burst release with increasing degumming time (**Figure 4B**). Longer degumming times overall led to reduced MDT, whereby the MDT of D 30 compared to D 120 and D 60 compared to D 120 differed significantly (D 30: 40.530 h ± 7.760 h, D 60: 36.913 h ± 5.126 h, D 120: 17.755 h ± 3.553 h).

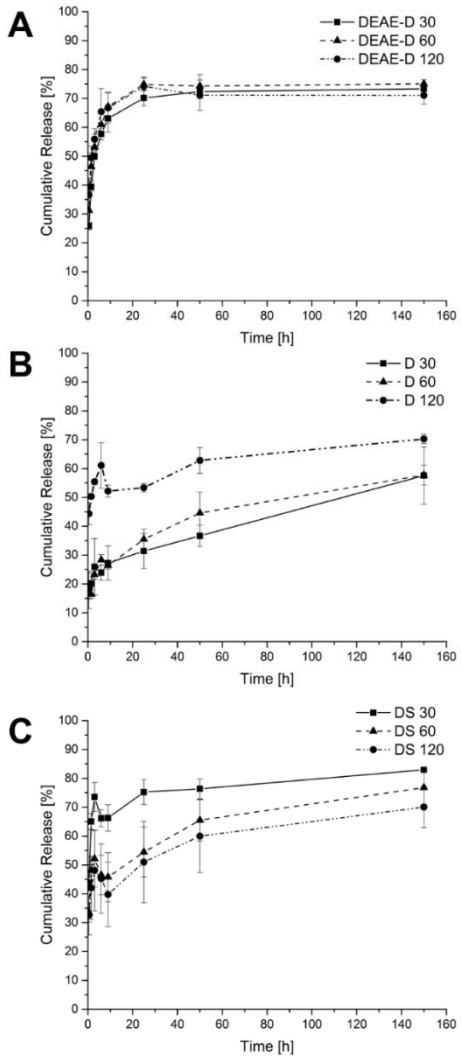

Figure 4. *Cumulative release profiles from SF films applying degumming time of 30, 60, and 120 minutes and loaded with A) FITC-DEAE-dextran, B) FITC-dextran, and C) FITC-dextran sulfate.*

For films loaded with negatively charged FITC-dextran sulfate the order of the release was inversed compared to FITC-dextran (**Figure 4C**). Shorter degumming times resulted in a more pronounced burst release compared to longer degumming times. The MDT increased with longer degumming time,

whereby the release rate of DS 30 compared to DS 120 differed significantly (DS 30: 10.545 h ± 2.977 h, DS: 22.115 h ± 7.271 h, DS 120: 29.278 h ± 1.566 h).

Cross-sections of the blank and loaded films were imaged using SEM (**Figure 5**). The porosity of blank films appeared to decrease with increasing degumming time (**Figure 5A SF30, B SF 60, C SF 120)**. Films loaded with FITC-DEAE-dextran were more compact and less porous than all other films and instead had numerous large holes on the surface and within the films.

Films loaded with FITC-dextran and FITC-dextran sulfate appeared less porous than the blank films, with small pores visible on the surface and within the films.

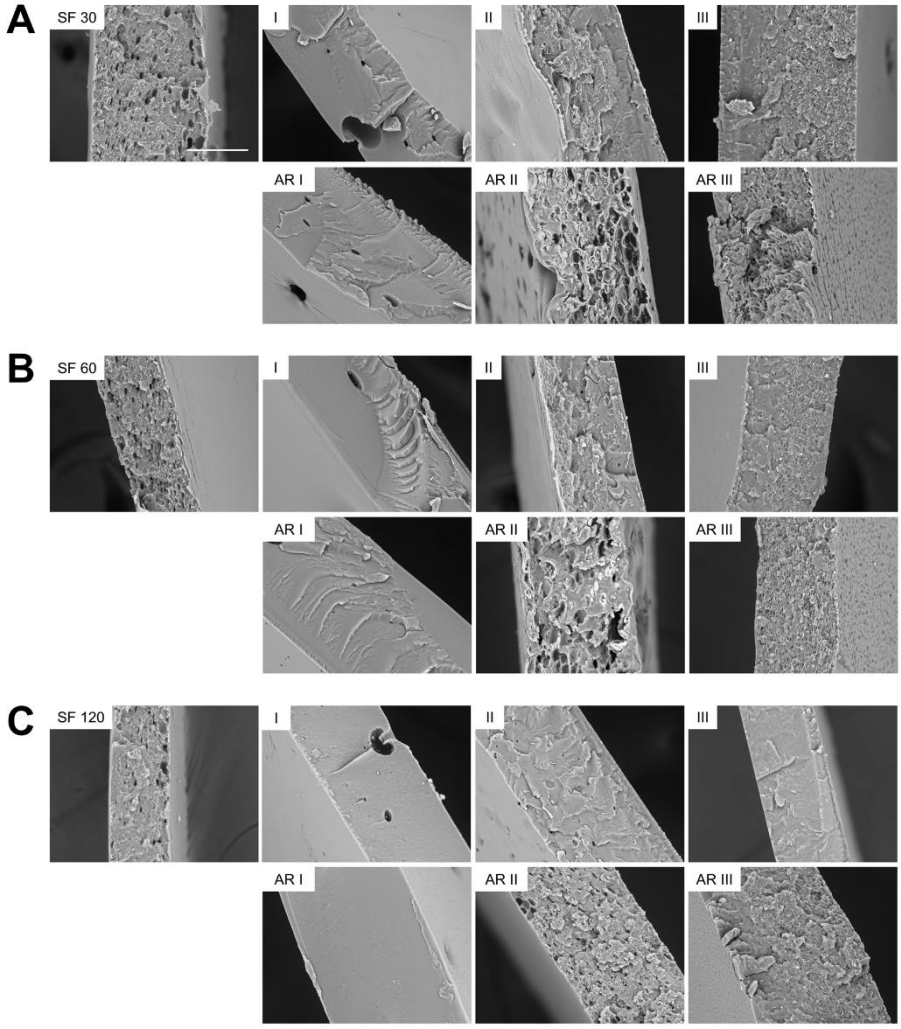

Figure 5. *Cross-sections of SF films after different degumming times. A) 30min. B) 60 min. C) 120 min. SF 30, SF 60 and SF 120 depict blank films. SF films loaded with I) FITC-DEAEdextran, II) FITC-dextran and III) FITC-dextran sulfate before release studies, whereas SF films loaded with AR I)FITC-DEAE-dextran, AR II) FITC-dextrana nd AR III) FITC-dextran sulfate after release are showed. Scale bar in SF30 represents 50 µm and is valid for all pictures.*

After drug release, with longer degumming times the films loaded with FITC-dextran appeared more compact (**Figure 5A, B, C AR II**), whereby FITC-dextran sulfate loaded films appeared more porous than before the release and more pores were visible on the surface (**Figure 5A, B, C AR III**). Films loaded with FITC-DEAE-dextran appeared still solid after release, showing no major differences compared to the appearance before drug release.

CLSM micrographs showed that FITC-dextran and FITC-dextran sulfate were distributed evenly in the films (**Figure 6**). FITC-DEAE-dextran accumulated on the film surface (red arrows). After release, the accumulation of FITC-DEAE-dextran on the film surface disappeared whereas the FITC-dextran and FITC-dextran sulfate was still equally distributed.

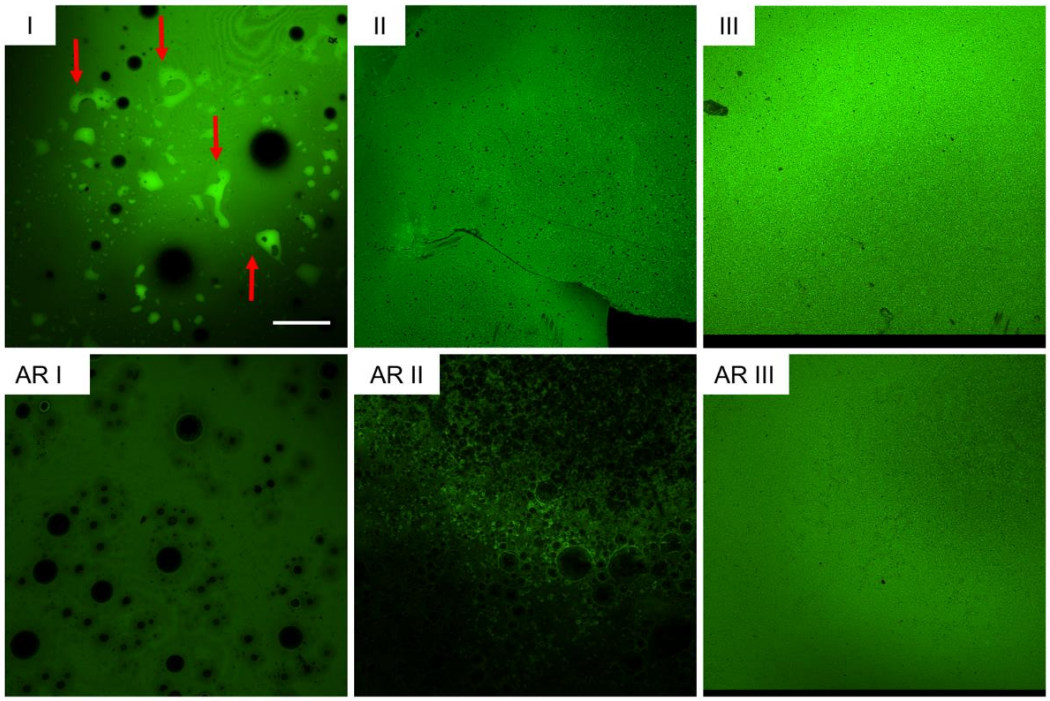

Figure 6. *CLSM pictures of SF 60 loaded with (I) FITC-DEAE-dextran, (II) FITC-dextran and (II) FITC-dextran sulfate, before release (first row) and after release studies (AR). Scale bar in I indicates 250 µm and is valid for all pictures.*

FT-IR mapping was used to study the distribution of SF and dextrans on the film surface after film preparation (**Figure 7**). While SF and FITC-dextran or FITC-dextran sulfate were evenly distributed, SF films loaded with FITC-DEAE-dextran showed phase separation and spot-like accumulation of

dextran on the film surface (**Figure 7 B I**), confirmed by the absence of SF (**Figure 7 A I**) in these spots (red arrows).

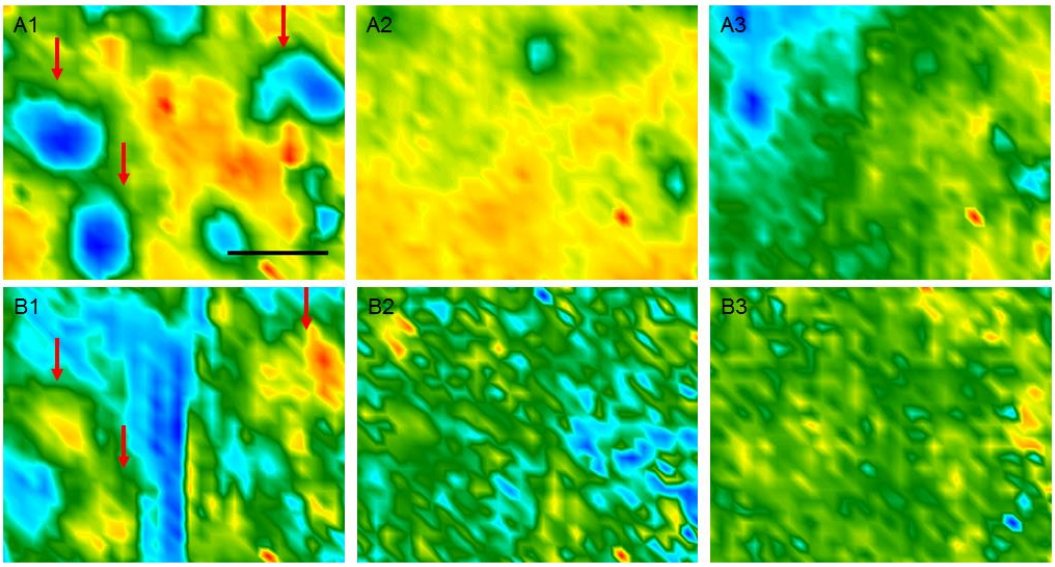

Figure 7. *FT-IR mapping of SF 60 loaded with (1) FITC-DEAE-dextran, (2) FITC-dextran and (3) FITC-dextran sulfate, mapping using wavenumbers specific for (A) SF and (B) dextrans. Scale bar in A1 represents 10 µm, magnification of all micrographs is equal.*

The interaction between FITC-DEAE-dextran and SF were measured by ITC (**Figure 8**). A maximum heat liberation was observed at a molar ratio of 6:1 FITC-DEAE-dextran:SF. With a higher molar ratio than 6 a regression of the liberated heat was observed.

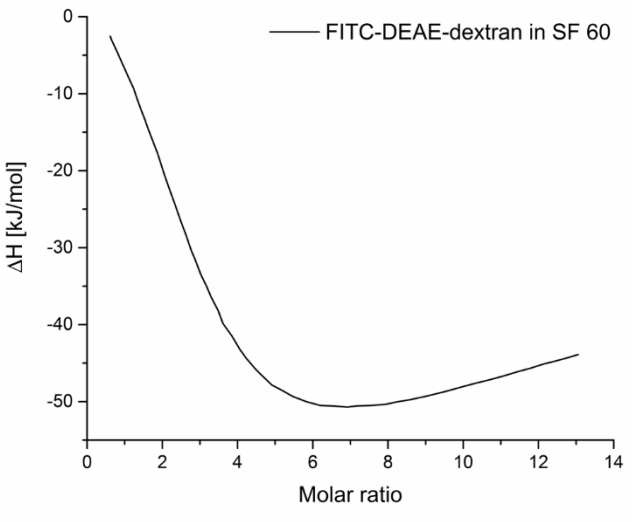

Figure 8. *Interaction of FITC-DEAE-dextran and SF 60 in PBS.*

4. Discussion

Degumming is a crucial process step in the purification of SF where sericin is removed by treating SF with alkaline solution at elevated temperature, resulting in hydrolytic cleavage of amid bonds. This process step is inherently unspecific and therefore threatens SF integrity. The degumming time considerably affected molecular weight distribution of SF (**Figure 2**). Shorter degumming times resulted in a narrower distribution of molecular weights, while longer degumming times caused more pronounced SF degradation signified by broader molecular weight distribution and a shift towards low molecular weight fragments. These observations are well in line with results obtained in previous studies [15, 164, 200, 201]. Static light scattering detection employed during SEC revealed the presence of structures with very high molecular weight, close to the exclusion limit of the column. These species were detectable by UV absorption in the case of silk degummed for 30 minutes but only detectable as a small shoulder in the case of 60 or 120 minutes degumming samples. Again, these findings are in line with data published by Wray et al. but the presence of additional species in SEC analysis was not further discussed in this paper [15]. Being an amphiphile, SF forms micellar structures of approximately 100 to 200 nm in water, where large hydrophilic N- and C-termini form the hydrophilic shell and large hydrophobic blocks with small interspersed hydrophilic blocks form the core of the micelle [2, 62, 202]. It is therefore assumed that the very high molecular weight structures eluting close to the exclusion limit of the column represent SF micelles. Interestingly, the concentration of these species is reduced with increasing degumming time both in the present study (**Figure 2B**) as well as in the data published by Wray et al. [15], assuming that longer degumming times led to higher protein degradation and as a result, to aggravated micelle formation.

Treatment of SF with methanol or water vapor induces β-sheet formation, whereupon methanol treatment was shown to be more effective (β-sheet content 0.4 - 0.53 [199]) and resulted in a higher surface hydrophobicity [200]. FT-IR spectra (**Figure 3**) did not show relevant differences between the different degumming times nor any relevant changes of β-sheet content (0.39 - 0.47) despite pronounced SF degradation as detected by SEC and SDS-PAGE (**Figure 2**). These findings suggest that the crystalline Gly-X domains are less likely to be degraded during degumming, still allowing formation of β-sheeted crystalline regions after regeneration and point to region-specific degradation of SF primarily

in the amorphous regions as well as N- and C-termini during degumming [15]. Based on this interpretation of the data it seems reasonable to hypothesize that regio-specific degradation of hydrophilic domains of SF leads to alteration or even inhibition of SF micelle assembly, which would explain the reduction of concentration of very high molecular weight structures with increasing degumming time as detected by static light scattering. This interpretation could also serve to further explain the microstructural differences between films obtained from differently degummed SF as observed by SEM in the present study (**Figure 5 A SF 30, B SF 60, C SF 120** and by Wray et al. [15]. In their study on silk fibroin self-assembly, Lu et al. studied SF, obtained by using short degumming time (20 minutes), and showed that SF micelles assemble into fibrils at concentrations above approximately 20% (w/w) [202]. Such fibril formation would be inhibited if micelle concentration is reduced or no micelles are present at all, resulting in pronounced differences in film microstructure.

In the next step, the effect of variation of degumming conditions on drug release was investigated using neutral and charged 10 kDa dextrans as model drugs. Drug release from silk fibroin film was shown to be driven by diffusion and only marginally by matrix degradation due to very slow degradation of SF in the release medium [194, 195]. Region-specific degradation of SF was assumed to change the molecular as well as microscopic structure of SF films and hence, affect diffusion driven release of model compounds. Mean dissolution time of FITC-dextran, representing a virtually uncharged compound, was shorter after longer degumming times, meaning a faster release, which is assumed to be due to higher diffusivity of FITC-dextran in the SF matrix. Similar results were obtained by Pritchard et al. studying diffusion of indigo carmine (466.35 g/mol), rifampicin (822.94 g/mol), reactive-red 120 (1469.98 g/mol), and azoalbumin (66.4 kDa) through SF films, where the release of all compounds increased for methanol treated SF films with increasing degumming time [164]. Furthermore, loading of SF films with FITC-dextran changed the microscopic structure of film cross sections compared to blank films. However, no pronounced differences of the microscopic structure were observed between loaded films prepared using SF obtained using different degumming times in contrast to blank films.

Interestingly, using negatively charged FITC-dextran sulfate an inversed effect of degumming time on drug release was observed compared to neutral FITC-dextran. We interpret this finding as an effect of

regional degradation of SF as outlined above affecting mainly the charge bearing N- and C- termini and hydrophilic, non-repetitive domains of SF, which contribute to the net negative charge of SF at physiological pH [203]. As described above, increasing degumming time results in increased hydrolytic degradation of hydrophilic regions of SF, which are also the regions comprising charged amino acids, and therefore, potentially reduce net charge of the matrix. Hence, electrostatic repulsion between negatively charged dextrans and SF matrix is reduced with increasing degumming time, leading to shorter MDT (faster release) of FITC-dextran sulfate. This finding and interpretation correlates well with the study of Hines et al., in which loading of SF films with negatively charged dyes lead to increased diffusion coefficients, which was attributed to electrostatic repulsion between negatively charged dyes and negatively charged SF [195].

FITC-DEAE-dextran is a polycationic dextran derivate containing three basic groups (pK_{a1} = 9.5; pK_{a2} = 5.7, pK_{a3} = 14). Therefore, release profile of FITC-DEAE-dextran was expected to be slowest (highest MDT) due to attractive electrostatic interactions between positively charged DEAE residues and negatively charged domains of SF. Indeed, attractive interaction between FITC-DEAE-dextran and SF was confirmed by ITC (**Figure 8**), showing complex formation in PBS up to a molar ratio of 6:1 FITC-DEAE-dextran:SF. In contrast, no interaction was observed by ITC between either FITC-dextran or FITC-dextran sulfate and SF (data not shown). Similar complex formation between SF and polycationic compounds was observed by ITC in a previous study [204]. In contrast to our expectations, we found that the MDT of FITC-DEAE-dextran from SF was shorter than uncharged and negatively charged dextran due to supersaturation of binding sites between FITC-DEAE-dextran and SF. The MDT was not significantly affected by degumming time. Similar release profiles were obtained with an alternative polycationic dextran derivative (FITC-Q-dextran, see supporting information). Furthermore, in contrast to SF films loaded with FITC-dextran or FITC-dextran sulfate, films loaded with FITC-DEAE-dextran appeared compact and non-porous by SEM. Confocal microscopy and FT-IR-imaging further showed that phase separation occurred in the case of FITC-DEAE-dextran loaded films, but FITC-dextran and FITC-dextran sulfate appeared to be homogenously distributed within the SF matrix. These results suggest that FITC-DEAE-dextran forms polyelectrolyte complexes with SF and/or charged SF fragments, inhibiting micelle formation and resulting in compact, non-porous films independent of

degumming time. Furthermore, only a fraction of FITC-DEAE-dextran may form polyelectrolyte complexes with SF as shown by ITC, resulting in exclusion of the remaining FITC-DEAE-dextran and hence, phase separation as observed by FT-IR-imaging and CLSM. Finally, phase-separated FITC-DEAE-dextran is rapidly released (burst release) while complexed DEAE-dextran is not released (steady release) within the timeframe of the release study. These results are in line with the findings of He et al. showing that only a part of carboxymethyl chitosan was able to interact with silk fibroin, higher concentrations led to phase separation [205]. Therefore, the interaction between SF and the model compound plays a key role for controlled release.

5. Conclusions

The degumming time is an important parameter to influence drug release from SF-based drug delivery systems. Degumming time not only affected molecular weight distribution of SF but also charge distribution of the matrix as well as micelle formation. Release of differently charged dextrans from SF-based films was significantly affected by these changes of SF characteristics. While release of neutral dextran was mainly related to SF molecular weight-dependent diffusivity in the matrix, the release of negatively charged dextran appeared to depend on matrix charge. Finally, positively charged dextrans formed polyelectrolyte complexes with SF, resulting in significantly changed film morphology, phase separation and rapid release.

Supporting Information

Release studies of FITC-Q-dextran were depicted to compare two different, positively charged dextran derivatives, since FITC-DEAE-dextran made an exception regarding the release studies.

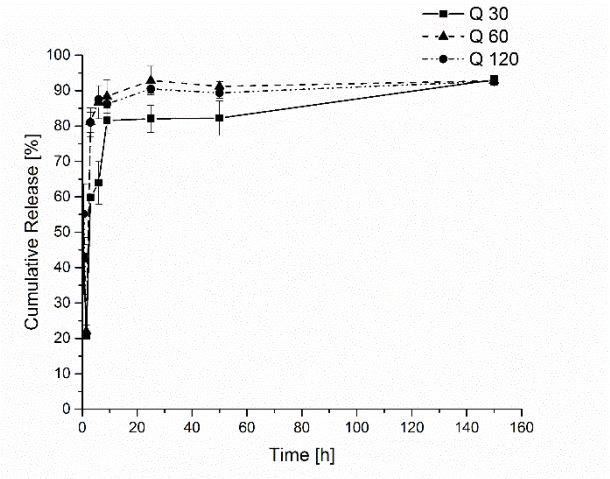

Figure S1. *Release studies of SF with different degumming times, loaded with FITC-Q-dextran.*

Acknowledgements

We acknowledge financial support from Swiss National Science Foundation under grant number 157890.

3.3. Crosslinking of Silk Fibroin via Click Chemistry to Control Drug Delivery

The experimental part, data analysis and writing of the manuscript were my contribution. The manuscript was finalized by Prof. Dr. Oliver Germershaus.

– Kira Nultsch –

To be submitted

Crosslinking of Silk Fibroin via Click Chemistry to Control Drug Delivery

Kira Nultsch [1, 2], Oliver Germershaus [2, *]

[1] *Department of Pharmaceutical Sciences, University of Basel, Klingelbergstrasse 50, 4056 Basel, Switzerland*

[2] *Institute of Pharma Technology, University of Applied Sciences and Arts Northwestern Switzerland, Gründenstrasse 40, 4132 Muttenz*

* Corresponding author:

E-mail address: oliver.germershaus@fhnw.ch (Oliver Germershaus)

Abstract

Silk fibroin (SF) extracted from the silkworm *Bombyx mori* was processed into films and the use as potential drug delivery system was studied. In this study, we demonstrate a new way to control the release of macromolecular compounds by chemical modification. For this, the tyrosine residues of SF were coupled with a diazonium salt in a first step and the efficiency of the reaction was studied with UV/Vis. Films were loaded with FITC-dextran derivatives of different molecular weights (10, 20 and 70 kDa) and charges and the release was investigated by comparison of virgin films (vSF) with different degrees of modification (0.1 (cSF_0.1) and 1.0 (cSF_1.0) equivalents added). Therefore, the films were crosslinked with a poly (ethylene glycol) crosslinker via click chemistry (copper (I) catalyzed alkyne azide cycloaddition CuAAC). The latter provides a powerful tool to tailor the characteristics of biomacromolcules. By introduction of the hydrophilic crosslinker, film properties could be tailored, resulting in a decreased contact angle and higher degree of film swelling. Mean dissolution time (MDT) could be significantly increased, allowing a more sustained release. In conclusion, these findings provide a promising tool for controlling the release from silk-based drug delivery systems.

KEYWORDS

Biomaterial, Silk Fibroin, Chemical Modification, Click Chemistry

1. Introduction

The use of natural and semi-synthetic polymers for tissue engineering and drug delivery has received increasing interest in recent years [110]. They have to meet several requirements, for example biocompatibility, biodegradability into non-toxic products, economical production and possible fabrication for a broad range of applications (films, foams, particles and gels) [6, 206]. Silk fibroin (SF) derived from silk of the silk worm (*Bombyx mori*) is a suitable candidate for a wide variety of applications ranging from textiles to biomedical use [5]. Silk fibroin comprises excellent properties for drug delivery systems, e.g. mechanical stability, slow degradation, biocompatibility and processability in aqueous medium [6].

In general, functionalization of natural polymers can widen the range of "smart" and "interactive" materials [207]. The most common way to functionalize proteins, especially SF, is the activation of carboxylic groups with a carbodiimide (1-ethyl-3-(3-dimethylaminopropyl) carbodiimide EDC) and the coupling via N-hydroxysuccinimide (NHS) [208]. However, only 0.5 mol % (corresponds to 25 residues per fibroin molecule) aspartic acid, 0.6 mol % (corresponds to 30 residues per fibroin molecule) glutamic acid and 0.3 mol % (corresponds to 12 residues per molecule) lysine are exhibited within SF, making only 1.5 mol % accessible to be modified via EDC/NHS chemistry [208]. Tyrosine residues represent approximately 5 mol % (corresponds to 125 residues per SF molecule) and are homogeneously distributed within SF, therefore modification of tyrosine residues is more efficient and achieves higher degrees of modification [208]. Different strategies have been investigated, including cyanuric chloride-activated coupling [209], enzyme catalyzed reactions [207, 210-212] and sulfatation of tyrosine residues with chlorosulfonic acid [213, 214]. However, these reactions are limited in yield and/or the specificity. To overcome these drawbacks copper (I)-catalyzed azide alkyne cycloaddition (CuAAC, click chemistry) was introduced to modify tyrosine residues of silk fibroin [215-217]. This reaction is conducted in two steps: firstly, the phenolic group of the tyrosine residue is activated by diazonium coupling and secondly, the formed azo derivative is coupled with the alkyne group.

Murphy et al. studied the diazonium coupling with regard to the change of overall hydrophilicity by the introduction of different aniline derivatives and the effect on attachment, growth and differentiation of human bone marrow-derived mesenchymal [215]. After 7 days of incubation, all azo SF derivatives

showed the same cell growth, whereas after 12 days of incubation SF decorated with negatively charged aniline derivatives exhibited the highest proliferation. On the other hand, drug release of dextran derivatives with different molecular weight (4, 20 and 40 kDa) was studied from photo-crosslinked hydrogels based on inter-penetrating poly (vinyl alcohol) methacrylate/SF network [218]. All hydrogels showed an initial burst release due to the release of the surface bound dextran. The release could be decreased by increasing the amount of poly (vinyl alcohol) methacrylate. Since SF was not covalently bound to the poly (vinyl alcohol) methacrylate matrix, SF was supposed to be released together with the dextran derivative and therefore, decreasing SF amount in the matrix resulted in a faster release [212].

Due to the slow degradation rate of SF, drug release kinetics is mainly determined by passive diffusion [194]. As a result, the release of drugs from SF matrices strongly depends on process conditions and on drug properties such as molecular weight and charge [156, 194, 195]. To further control drug delivery, either the drug can be covalently bound to the SF matrix or drug diffusion can be controlled by crosslinking of the SF matrix. Previous studies showed that covalent attachment of drug to SF matrices is a promising approach to increase stability and extend half life [219].

In this study, SF was chemically modified to extend its excellent intrinsic properties and enhance its performance as drug delivery system. In our previous study, we investigated the influence of SF purification on its physicochemical properties and its effect on drug release [156]. To expand the use of SF as scaffold for drug delivery, tyrosine residues were crosslinked, mainly on the film surface via click chemistry, so that the release of encapsulated drugs can be controlled resulting in a more sustained release. Differently charged dextran derivatives and dextran derivatives with different molecular weights were used as macromolecular model compounds and the release in relation to the degree of modification was studied. As a crosslinker, poly (ethylene glycol) (PEG, 1000 Da) was applied since PEG is biocompatible, non-immunogenic, and is frequently used for biomedical applications [220]. In this report, we demonstrate a new approach to control drug delivery and, additionally, tailor the properties of fibroin, e.g. introduction of hydrophilicity.

2. Materials and Methods

2.1 Materials

Cocoons of the silkworm (*Bombyx mori*) were supplied by Wollspinnerei Vetsch (Pragg-Jenaz, Switzerland). Fluorescein isothiocyanate-dextran (FITC-dextran) 10 kDa, fluorescein isothiocyanate-2-(diethylamino) ethyl-dextran (FITC-DEAE-dextran) 10 kDa and fluorescein isothiocyanate-dextran sulfate (FITC-dextran sulfate) 10 kDa were purchased from TdB Consultancy AB (Uppsala, Sweden). All other chemicals were purchased from Sigma Aldrich (Buchs, Switzerland).

2.2 Methods

2.2.1 Silk fibroin purification and film preparation

Fibroin was degummed as described elsewhere [156]. In brief, the cocoons were cut into small pieces and boiled in 0.02 M sodium carbonate solution for 60 minutes at a concentration of 5 g l^{-1} under constant stirring (300 rpm). Afterwards the residual fibers were dried in a fume hood overnight and then dissolved in Ajisawa's reagent (1 mol calcium chloride, 2 mol ethanol, 8 mol water). The solution was filtered through a 5 µm syringe filter (Yeti PVDF, HPLC syringe filter, Infochroma AG, Zug, Switzerland) and dialyzed against ultrapure water for 48 hours, using a SpectraPor® dialysis tube (SpectraPor® dialysis tubes MWCO 6–8 kDa, Spectrum Laboratories, Rancho Dominguez, CA, USA). Dialyzed SF solution was concentrated against 10 % poly (ethylene glycol) 35 KDa solution and the mass of a known volume of concentrated SF solution was determined gravimetrically and adjusted to a final concentration of 6% (w/v). Silk fibroin solution was mixed with FITC-dextran of different molecular weights (10, 20 and 70 kDa) and charges (positively charged FITC-DEAE-dextran, negatively charged FITC-dextran sulfate) to result in loading of 25% (w/w). Subsequently, 2.5 ml of the solution were transferred into one well of a 6-well plate and dried overnight at room temperature. After drying, the films were cut into samples of 1 cm in diameter with a hole punch and treated with methanol to induce β-sheet formation overnight.

2.2.2. Modification of tyrosine residues

Modification of tyrosine residues by diazonium salt formation was performed and monitored by UV/Vis spectroscopy as described previously with slight modifications [215]. In brief, 1.25 ml of 0.2 M 4-azidoaniline (in acetonitrile:water 1:1) was mixed with 625 µl of 1.6 M p-toluenesulfonic acid (aqueous

solution) in an ice bath (diazonium salt stock solution). Afterwards, 625 µl of 0.8 M sodium nitrite was added, vortexed for 15 seconds, and the mixture was allowed to react for 15 minutes. After extraction from cocoons and dialysis (vide supra), SF solution was diluted to a concentration 0.5 % (w/v) and incubated with diazonium salt solution, aiming a conversion of 0.1 or 1.0 equivalents of tyrosine residues, respectively. The concentration of azo fibroin was calculated using Lambert-Beer law with an estimated extinction coefficient of 22000 $M^{-1}cm^{-1}$ and a peak maximum at λ=329 nm [221].

2.2.3 Chemical modification of films via click chemistry

Tyrosine residues of SF were chemically modified as described in [215, 216] (**Scheme 1**). In all experiments, the films were incubated in 500 µl solution, therefore the diazonium salt stock solution was diluted in order to modify different fractions of tyrosine residues, 0.1 and 1.0 equivalents of diazonium salt, relative to the total number of 125 tyrosine residues per fibroin molecule. After adding the appropriate volume of diazonium salt solution, the reaction was allowed to proceed for 30 minutes in an ice bath. In the next step, the modified tyrosine residues were crosslinked with alkyne-PEG (1000 Da)-alkyne (Creative PEGWorks, Chapel Hill, NC, USA) as described in (**Scheme 1**) [222]. The modified films were washed three times with water to remove residual reagents. Stock solutions of 20 mM copper sulfate ($CuSO_4$), 50 mM tris (3-hydroxypropyltriazolyl-methyl) amine (THPTA), 100 mM sodium ascorbate and alkyne-PEG-alkyne (all in water) were prepared. CuAAC reaction was performed using a premixed solution of $CuSO_4$ and THPTA stock solutions (2.5 and 5 µl), 25 µl sodium ascorbate stock solution and 457.5 µl alkyne-PEG-alkyne (with the desired concentration to achieve different degrees of modification: $6.5 \cdot 10^{-6}$ respectively $6.5 \cdot 10^{-8}$ mol) and modified fibroin films were incubated with the solution for two hours at room temperature. Subsequently, the films were washed three times with water to remove residual reagents. Films were designated vSF for virgin, unmodified SF films, cSF_0.1 for SF films with 0.1 equivalents of tyrosine modified after crosslinking and cSF_1.0 for SF films with 1.0 equivalents of tyrosine modified after crosslinking.

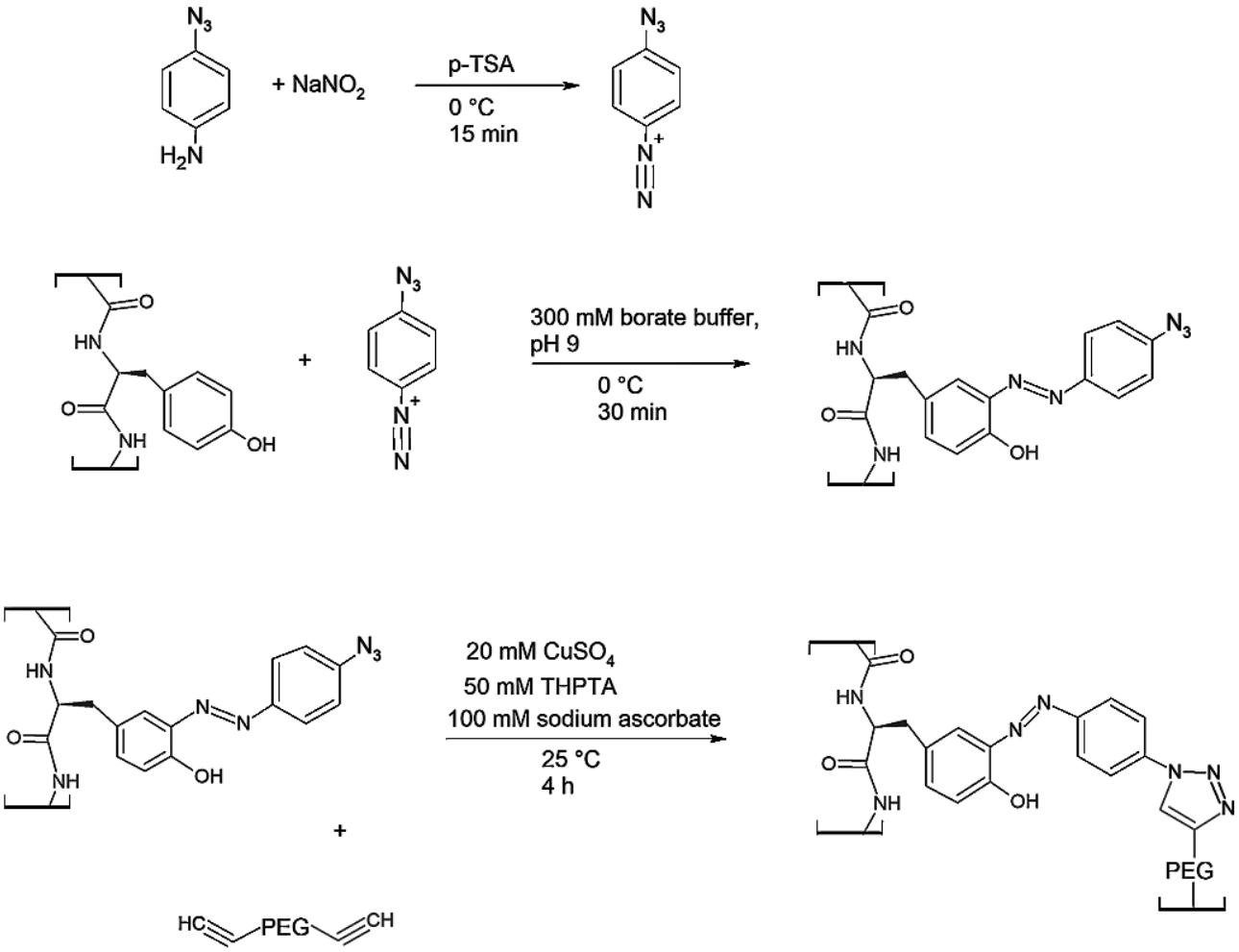

Scheme 1. *Modification of the tyrosine residues by diazonium coupling and crosslinking of SF via click chemistry.*

2.2.4 Swelling

SF films without drug (vSF, cSF_0.1 and cSF_1.0) were incubated for 24 hours in water. Afterwards non-absorbed surface water on the films was removed with a paper towel, films were weighted, and water content was determined by thermogravimetric analysis (Perkin Elmer TGA 4000, Wellesley, MA, USA). For TGA measurements, samples were heated to from 30 to 150 °C at a rate of 10 °C min^{-1} and nitrogen flow of 20 ml min^{-1} and temperature was kept constant until sample weight was constant. Water content was determined according to **Equation 1**.

$$m\% = \frac{m_{before\,TGA} - m_{after\,TGA}}{m_{before\,TGA}} \cdot 100\ \%$$ Equation 1

2.2.5 Contact angle measurement

Contact angle measurements of films without drug (vSF, cSF_0.1 and cSF_1.0) were performed using sessile drop method (DSA 100, Krüss GmbH, Hamburg, Germany). Measurements were performed by deposition of a drop of deionized water (4 µl) onto the surface of SF films. Evaluation of the contact angle was done after 20 seconds, since no change of the droplet shape occurred thereafter. The static contact angle was acquired by fitting the symmetric water drop with conic section method (assuming an ellipse as drop shape). The contact angle was determined as angle between the baseline and the tangent at the conical section of the curve.

2.2.6 Release studies

Fibroin films loaded with different dextran derivatives were placed in 6 ml glass vials and incubated with phosphate buffered saline (pH 7.4) at 37 °C in an orbital shaker (IKA®Werke, Staufen, Germany) at 30 rpm. Release studies were conducted under sink conditions. After 96 hours, fibroin films were dissolved in Ajisawa's reagent to determine the amount of unreleased model compound. Release media samples were analyzed with UV/Vis spectroscopy (VWR UV 6300PC, VWR, Dietikon, Switzerland) at λ=494 nm. To compare release characteristics of different molecular weights and charges, mean dissolution time (MDT) was calculated for each sample (KinetDS v3.0, (https://sourceforge.net/projects/kinetds/) according to **Equation 2**. Herein, *i* describes the sample number, *n* the dissolution sample times, M_i the amount of drug released between time point *t* and (t-1) and *t* is the midpoint between t and (t-1).

$$MDT = \frac{\sum_{i=1}^{n} t\Delta M_i}{\sum_{i=1}^{n} \Delta M_i} \qquad \text{Equation 2}$$

2.2.7 Statistical Analysis

All measurements were performed in triplicates unless stated otherwise and all results are presented as mean ± standard deviation. In order to identify statistically significance, Student's t-test (release studies) or one-way ANOVA with Tukey's test was performed. Probability values with $p \leq 0.05$ were considered statistically significant.

3. Results

3.1 Diazonium coupling reaction and degree of modification

In order to investigate the conversion of tyrosine residues into the azobenzene derivative, different equivalents of diazonium salt (0, 0.1 and 1.0 equivalents) were added to a SF solution and analyzed by UV/Vis spectroscopy. After nucleophilic substitution reaction the color of the solution changed from colorless to yellow-brownish (**Figure 1A**) and a strong absorption with a peak maximum at $\lambda = 329$ nm appeared due to the newly formed azobenzene chromophor ($\pi - \pi^*$, $n - \pi^*$ transitions; **Figure 1B**). Furthermore, the percentage of modified tyrosine residues was determined by comparison of molar concentration of the azobenzene derivative with the theoretical molar concentration of tyrosine residues present in SF (assuming 125 tyrosine residues per SF molecule). After addition of 0.1 equivalents, approximately 9 % of the tyrosine residues were converted, whereas after addition of 1.0 equivalents approximately 86 % of the tyrosine residues were converted. These results indicate that the reaction proceeds almost completely (~ 90 %).

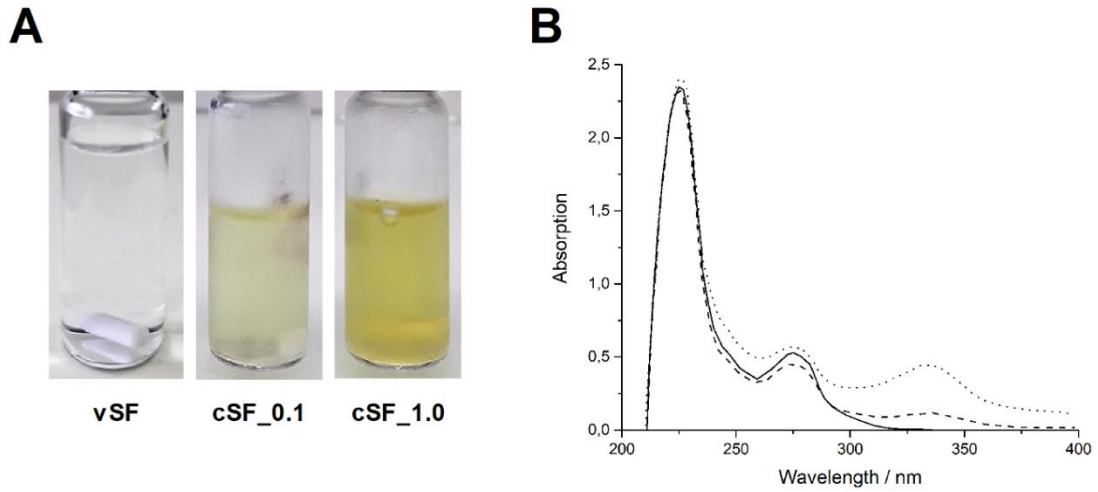

Figure 1. *Formation of azobenzene derivative with SF tyrosines. (A) Virgin SF solution, 0.1 and 1.0 equivalents added to the SF solution. (B) UV/Vis spectrum of the virgin SF solution (black line), and after addition of 0.1 (dashed line) and 1.0 (dotted line) equivalents of diazonium salt.*

3.2 Swelling

The ability of SF films to absorb water was measured using TGA. While in the case of vSF water absorption was 14.9 ± 1.0 %, statistically significantly higher swelling was observed for crosslinked films (21.8 ± 0.2 % for cSF_0.1 and 24.0 ± 1.8 % for cSF_1.0).

3.3 Contact angle

The change in SF film surface hydrophilicity was quantified by contact angle measurement. vSF exhibited the highest contact angle (75.8 ± 2.0 °), whereas the introduction of the PEG crosslinker led to a decrease of the contact angle to 70.5 ± 0.5 ° in the case of cSF_0.1 and 54.3 ± 6.4 ° for cSF_1.0.

3.4 Drug release

In general, the release profiles of vSF were characterized by burst release. Crosslinking of 0.1 or 1.0 tyrosine equivalents resulted in reduction of burst release (**Figure 2A**), whereby the MDT of vSF compared to cSF_0.1 and cSF_1.0 differed significantly (**Table 1**). FITC-dextran with a molecular weight of 20 kDa showed in general a slower release compared to FITC-dextran with a molecular weight of 10 kDa. MDT was significantly increased within a higher crosslinking degree (**Figure 2B**). Results obtained with FITC-dextran 70 kDa showed an even lower burst release compared to the other two molecular weight dextrans, though MDT was only significantly decreased when comparing vSF to cSF_0.1 (**Figure 2C**). MDT of the positively charged dextran from vSF films was the lowest, equivalent to the fastest release and MDT was significantly decreased after crosslinking (**Table 1**). In line with results obtained with neutral dextran, the burst release was significantly decreased after crosslinking, confirmed by prolonged MDT (**Figure 2D, Table 1**). Similar results were obtained with the negatively charged FITC-dextran sulfate (**Figure 2E**). MDT significantly increased when comparing vSF to cSF_1.0 and cSF_0.1 to cSF_1.0 (**Table 1**).

Table 1. *Mean dissolution time of different dextran derivatives from non-crosslinked and crosslinked SF films.*

	Mean dissolution time / h				
	FITC-dextran 10 kDa	**FITC-dextran 20 kDa**	**FITC-dextran 70 kDa**	**FITC-DEAE-dextran 10 kDa**	**FITC-dextran sulfate 10 kDa**
vSF	10.034 ± 0.658	12.994 ± 1.502	12.290 ± 0.864	5.378 ± 2.016	17.781 ± 1.464
cSF_0.1	16.079 ± 0.104	16.937 ± 0.239	10.790 ± 0.082	11.053 ± 3.511	17.000 ± 0.159
cSF_1.0	16.757 ± 0.682	21.099 ± 1.961	11.569 ± 1.504	19.077 ± 4.096	29.260 ± 0.272

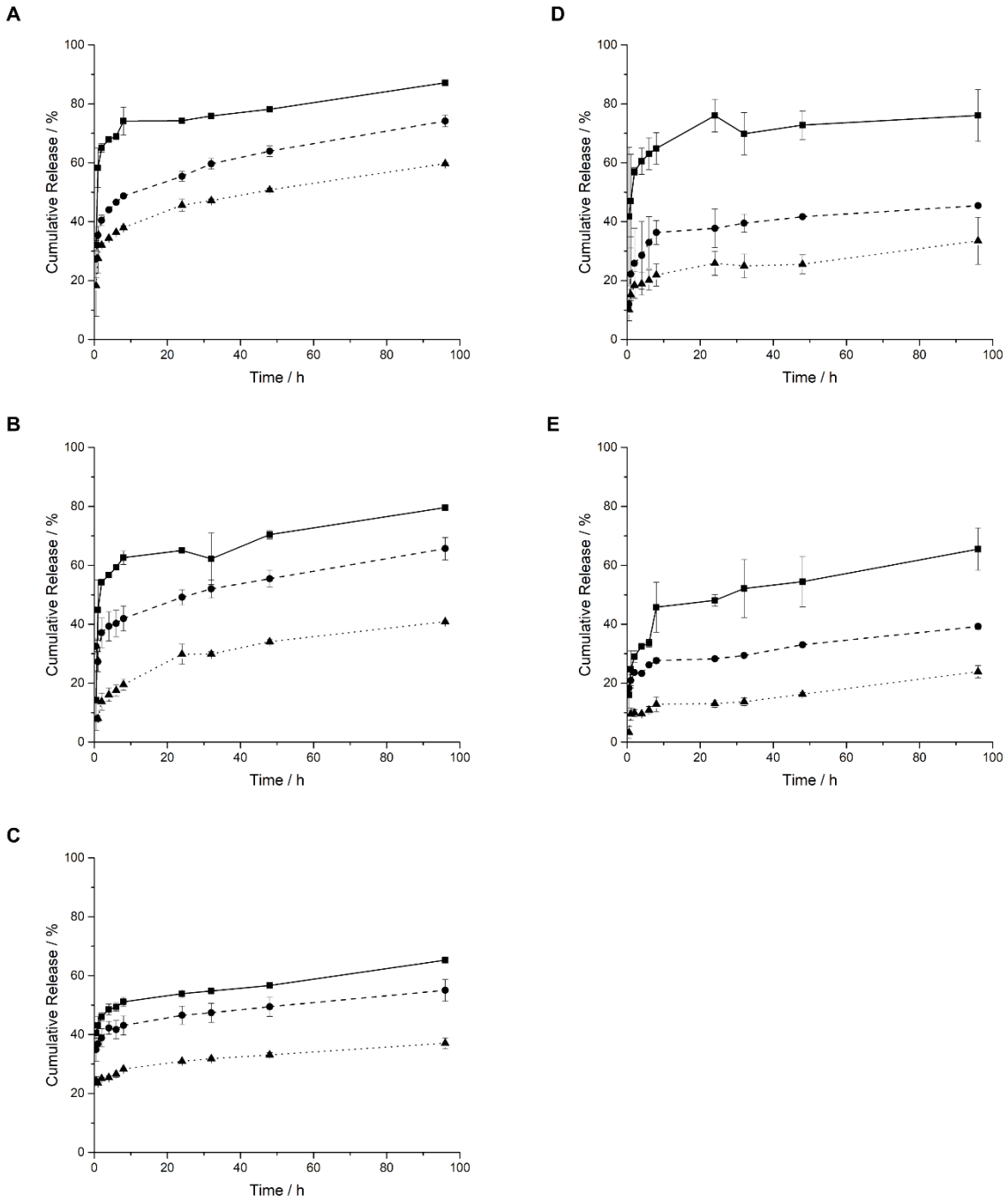

Figure 2. *Cumulative release of (A) FITC-dextran 10 kDa, (B) FITC-dextran 20 kDa, (C) FITC-dextran 70 kDa, (D) FITC-DEAE-dextran 10 kDa and (E) FITC-dextran sulfate 10 kDa from vSF (black line), cSF_0.1 (dashed line) and cSF_1.0 (dotted line).*

4. Discussion

A novel approach for controlling the drug release from silk fibroin scaffolds is presented in this study. SF comprises only limited options for functionalization due to the low mol percentage of amino acids allowing straightforward modification. However, SF contains approx. 5 mol % tyrosine residues, which can be efficiently modified by diazonium coupling allowing straightforward introduction of a click handle. Reaction conditions are compatible with the fibroin properties, i.e. SF shows good stability at basic pH [208, 215]. In addition, the reaction is fast and efficient, requiring 15 minutes for diazonium coupling and two hours for the crosslinking by click chemistry.

Azobenzene derivative formation was found to be efficient, with degrees of conversion of approx. 90 %. These results are in line with previous studies [215, 216]. When tyrosine residues were modified with different aniline derivatives, the highest level of modification were obtained for aniline derivatives with electron-withdrawing groups (~ 70 % efficiency) [215]. Hence, modification with azidoaniline can provide the necessary specificity compared to other modification options (e.g. EDC/NHS chemistry) [216]. On the contrary, only approx. 1.5 mol% of SF amino acids can be modified by EDC/NHS chemistry, significantly limiting the degree of modification [208]. Furthermore, instability of SF in the presence of EDC/NHS in 2-(N-morpholino) ethanesulfonic acid (MES) buffer due to formation of intra- and intermolecular beta-sheet structures was observed [216].

In the second step, the films were crosslinked with a PEG linker (**Scheme 1**) to control drug release and to tailor SF properties. The incorporation of PEG led to an overall increased hydrophilicity of crosslinked SF compared to vSF, which is in agreement with results obtained for similar SF-PEG conjugates [209, 215, 220]. The incorporation of cyanuric acid activated PEG 10 kDa led to a decrease of the contact angle of up to 33 ° [209], resulting in significantly lower contact angle compared to our study due to the higher hydrophilicity of PEG. Similar results were obtained in another study where SF was modified with PEG 2 kDa via click chemistry [220]. For this, azido modified SF was reacted with acetylene terminal PEG and after SF modification, films were prepared, resulting in contact angles between 30 and 44.3 ° (dependent on degree of modification). A possible explanation for differences in the contact angle is that methanol treatment to induce β-sheet formation was done after modification with PEG [220], leading to different arrangement of β-sheet and therefore, different surface

hydrophilicity [220]. The ability to absorb water was significantly higher compared to our results (44 – 66 % vs. 21 – 24 %). In contrast to this study, we firstly prepared the films, followed by β-sheet formation with methanol and then, the films were crosslinked. One hypothesis is that the SF chains are less flexible (when crosslinked after β-sheet formation), therefore the penetration of the crosslinking reagents into films was aggravated, resulting in modification of SF films mainly on the film surface. Since SF is in general a hydrophobic protein [62, 223] and if the core of the SF films are not or less crosslinked (with the hydrophilic PEG crosslinker), water penetration into the film matrix will be prohibited.

In previous studies, it was found that on the one hand, degumming time during SF preparation and on the other hand, charge of encapsulated compounds affects release of different model compounds [156, 164]. Longer degumming time led to a pronounced burst release of the neutral dextran derivative. The positively charged dextran derivative stated an exception since the release was faster compared to the other dextran derivatives. These findings are in line with our previous studies [156]. In the previous study, positively charged dextran derivative formed polyelectrolyte complexes with silk fibroin. As a result, only a part of the dextran was able to interact with silk fibroin, whereas the rest of positively charged dextran underwent phase separation, resulting in a burst release.

In this study, we compared not only differently charged dextran derivatives, but also different molecular weights, and additionally, tailored the release by the modification of silk fibroin. Drug release from silk fibroin films was found to be mainly driven by diffusion since the degradation rate of silk fibroin is negligible in the release medium [194, 195]. With increasing molecular weight, the remaining amount of dextran derivative in the silk fibroin film increased due to limited diffusion through the film (**Figure 2A, B, C**). Additionally, the charge of the released compound plays a key role and these findings are again in line with our previous study [156], where the release of the negatively charged dextran derivative was characterized by matrix diffusion and electrostatic repulsion. The release of the positively charged dextran derivative stated an exception, since the release was slower compared to the other dextran derivatives. By introduction of 0.1 or 1.0 equivalents of crosslinker, MDT could be significantly increased. Our hypothesis stats that the crosslinking of SF films takes mainly place on the film surface.

With a higher degree of crosslinking, the film becomes denser and therefore, diffusion is more and more aggravated.

To expand this functionalization strategy, the PEG linker can be replaced by a bioresponsive crosslinker, e.g. a peptide crosslinker. This peptide crosslinker is then cleaved in presence of e.g. inflammatory mediators and the encapsulated drug is release in response, whereas in absence of the trigger no or very slow release takes place. This strategy could path a new way for controlled and self-regulating drug release.

5. Conclusion

Properties of the encapsulated compound (molecular weight, charge) as well as the interaction of the latter with the polymer matrix were found to be key factors for drug release from SF matrices. With a higher molecular weight, the release of dextran derivative was slower due to the limited diffusion through the SF matrix. Crosslinking of the tyrosine residues of SF via click chemistry was found to offer an additional option to control drug release. Especially, the mild reaction conditions (aqueous solution, room temperature) are an advantage compared to other possible modifications. With the introduction of the PEG crosslinker, the properties of silk fibroin could be tailored, a higher hydrophilicity and swelling was achieved. Finally, the PEG linker could be exchanged with a bioresponsive linker, resulting in an endogenous release of the encapsulated compound.

Acknowledgements

We acknowledge financial support from Swiss National Science Foundation under grant number 157890.

4. Conclusion and Outlook

The most straightforward way for drug incorporation is the simple mixing of the drug with the matrix and then, further processing into the final drug delivery system. Therefore, the integrity of the matrix and the preservation of the biological activity has to be ensured. Other possibilities to incorporate the drug into the matrix are e.g. by adsorption or covalent binding. Currently, 50 to 60% of the active pharmaceutical ingredients available on the market are poorly water-soluble. Therefore, the formulation of these ingredients is one of the major challenges in the pharmaceutical industry. Silk fibroin can provide a range of properties to meet these expectations, allowing the encapsulation of differently charged and high molecular weight compound and due to its amphiphilic character additionally the encapsulation of hydrophobic compounds.

The aim of this thesis was to establish a silk fibroin based drug delivery system that can be produced and loaded under aqueous conditions, while allowing the encapsulation of drugs with different properties. Therefore, SF was characterized regarding different degumming time with the standard degumming reagent sodium carbonate, other degumming reagents (enzymes, ionic liquids) were considered as alternative and the influence of these factors on molecular weight distribution and mechanical strength were studied. We found that with longer degumming times, the molecular weight distribution became broader. However, SF was still able to form β-sheets to the same extend, suggesting that during degradation the hydrophobic blocks of SF remain intact. Anion exchange chromatography showed a shift in retention time, stating that the degradation takes mainly place in the hydrophilic segments of SF.

High levels of drug loading (up to 25%) were possible, when using SF films as carrier system. Longer degumming times led to a faster burst release of the neutral dextran derivative compared to shorter degumming times due to the higher diffusivity through the film. As opposed to this, the negatively charged dextran showed an over-all fast release and with longer degumming times a slower release because of the decrease of matrix charge. Interestingly, the positively charged dextran stated an exception, since it showed an over-all faster release compared to all other dextran derivatives. This is due to the fact that only a part of the positively charged dextran can interact with the negatively charged

SF, leading to phase separation and as a result, to a burst release. Besides the different charges, different molecular weights were studied, ranging from 10 to 70 kDa, whereas a higher molecular weight led to a sustained release, showing that the release from SF films is mainly diffusion controlled. These studies showed that on the one hand, the purification process is a key factor for the use of SF as drug delivery system and on the other hand, the properties of the encapsulated compound. However, to limit the diffusion controlled release, SF can be chemically modified, either by covalent binding of the drug to the drug delivery system or by crosslinking of the drug delivery system. We were able to successfully incorporate a PEG crosslinker to the tyrosine residues of the SF and significantly decrease the release rate of the dextran derivatives. The advantage of this crosslinking procedure is the processing under very mild conditions (room temperature, aqueous conditions) and furthermore, the surface of the films can be tailored according to the application form and target location.

As mentioned above, silk fibroin and other biomaterials possess the advantage, among others, of good biocompatibility, non-toxicity and biodegradability. Thus, they are versatile carriers for drug delivery for small molecules, genes and biologicals. With a fully characterized SF starting material, the further formulation work can be conducted in a systematic manner, beginning with the appropriate SF matrix, the selection of the processing parameters and subsequent with a suitable drug candidate in order to achieve targeting and to control the pharmacokinetics. Furthermore, the potential Silk fibroin based drug delivery has to show significantly improvement regarding clinical outcome and patient compliance compared to already existing drug delivery systems. Where other polymers like PLGA (due to the acidic degradation products or the need of organic solvents) failed, there might the opportunity to use SF.

For each drug candidate, not only its potency, but also the physicochemical properties (hydrophilicity, molecular weight and charge) have to be taken into consideration, since the SF-drug interactions strongly affect the release mechanism and the pharmacokinetics. In addition, immediate burst release might result from insufficient drug encapsulation and/or phase separation due to either supersaturation of binding sites or other occurring events during formulation. While these classic drug delivery systems control location and time of the released drug, a novel approach for drug delivery will be a bioresponsive, on-demand system that can respond to its environment. In our third study, we incorporated a PEG crosslinker in the SF films, aiming for more sustained release. In pre-trials, we exchanged the PEG

crosslinker for an MMP-sensitive linker. Unfortunately, we could not control the MMP-dependent release of the dextran derivatives. MMP-9 has a molecular weight of 92 kDa. When comparing this molecular weight to the molecular weight of the encapsulated compound, it can be seen that the release of 70 kDa dextran is already very slow. This means that the diffusion through the silk fibroin matrix is already limited; conversely, this suggests that the diffusion of the MMP into the SF film is restricted by its size. Additionally, to the limited space to diffuse into the film, the enzyme needs to partly unfold to bind to its substrate, meaning that even more space is needed. As a result, only the MMP-sensitive crosslinker at the surface are accessible for the enzyme. Therefore, further studies regarding the porosity and how to control it should be conducted. Alternatively, the drug could be directly bound to the MMP-sensitive linker, virtually the drug delivery system would become a prodrug.

Another promising approach is treatment of chronic wounds (e.g. diabetic ulcer) and tumor tissue, since they are characterized by high MMP levels, making them an attractive target. The high MMP level can be used to trigger the localized release of e.g. siRNA for specific MMP inhibition. The ability of siRNA to inhibit protein expression on a transcriptional level is an attractive option for the treatment of many diseases that are characterized by e.g. an overexpression of enzymes. The advantage of this specific and localized treatment is the reduced side effects compared to systemically administered formulations.

In general, this thesis provides a toolbox for a more precise characterization of the starting material silk fibroin that can be used as for initial quality assessment as well as for in-process controls, and in addition, provides an insight into the future possibilities for bioresponsive drug delivery.

5. References

[1] L.-D. Koh, Y. Cheng, C.-P. Teng, Y.-W. Khin, X.-J. Loh, S.-Y. Tee, M. Low, E. Ye, H.-D. Yu, Y.-W. Zhang, M.-Y. Han, Structures, mechanical properties and applications of silk fibroin materials, Progress in Polymer Science (2015).

[2] H.J. Jin, D.L. Kaplan, Mechanism of silk processing in insects and spiders, Nature 424(6952) (2003) 1057-61.

[3] J.W. Boretos, M. Eden, Contemporary biomaterials: material and host response, clinical applications, new technology and legal aspects, Elsevier, 1984.

[4] D. Liu, F. Yang, F. Xiong, N. Gu, The smart drug delivery system and its clinical potential, Theranostics 6(9) (2016) 1306.

[5] G. Altman, F. Diaz, C. Jakuba, T. Calabro, R. Horan, J. Chen, H. Lu, J. Richmond, D. Kaplan, Silk-based biomaterials, Biomaterials 24(3) (2003) 401-416.

[6] E. Wenk, H.P. Merkle, L. Meinel, Silk fibroin as a vehicle for drug delivery applications, J Control Release 150(2) (2011) 128-41.

[7] T. Yucel, M.L. Lovett, D.L. Kaplan, Silk-based biomaterials for sustained drug delivery, J Control Release 190 (2014) 381-97.

[8] Q. Lu, X. Wang, X. Hu, P. Cebe, F. Omenetto, D.L. Kaplan, Stabilization and release of enzymes from silk films, Macromolecular bioscience 10(4) (2010) 359-68.

[9] K.S. Soppimath, T.M. Aminabhavi, A.R. Kulkarni, W.E. Rudzinski, Biodegradable polymeric nanoparticles as drug delivery devices, J Control Release 70(1-2) (2001) 1-20.

[10] E.J.W. Barber, Prehistoric textiles: the development of cloth in the Neolithic and Bronze Ages with special reference to the Aegean, Princeton University Press1991.

[11] N. Yonemura, F. Sehnal, The design of silk fiber composition in moths has been conserved for more than 150 million years, Journal of molecular evolution 63(1) (2006) 42-53.

[12] F. Vollrath, D. Porter, Spider silk as a model biomaterial, Applied Physics A 82(2) (2006) 205-212.

[13] J. Pérez-Rigueiro, M. Elices, J. Llorca, C. Viney, Effect of degumming on the tensile properties of silkworm (Bombyx mori) silk fiber, Journal of Applied Polymer Science 84(7) (2002) 1431-1437.

[14] G.H. Altman, F. Diaz, C. Jakuba, T. Calabro, R.L. Horan, J.S. Chen, H. Lu, J. Richmond, D.L. Kaplan, Silk-based biomaterials, Biomaterials 24(3) (2003) 401-416.

[15] L.S. Wray, X. Hu, J. Gallego, I. Georgakoudi, F.G. Omenetto, D. Schmidt, D.L. Kaplan, Effect of processing on silk-based biomaterials: reproducibility and biocompatibility, Journal of biomedical materials research. Part B, Applied biomaterials 99(1) (2011) 89-101.

[16] P. Jiang, H. Liu, C. Wang, L. Wu, J. Huang, C. Guo, Tensile behavior and morphology of differently degummed silkworm (Bombyx mori) cocoon silk fibres, Materials Letters 60(7) (2006) 919-925.

[17] G. Freddi, R. Mossotti, R. Innocenti, Degumming of silk fabric with several proteases, Journal of Biotechnology 106(1) (2003) 101-112.

[18] A. Zvonar, J. Kristl, J. Kerc, P.A. Grabnar, High celecoxib-loaded nanoparticles prepared by a vibrating nozzle device, J Microencapsul 26(8) (2009) 748-59.

[19] S. Inoue, K. Tanaka, F. Arisaka, S. Kimura, K. Ohtomo, S. Mizuno, Silk fibroin of Bombyx mori is secreted, assembling a high molecular mass elementary unit consisting of H-chain, L-chain, and P25, with a 6:6:1 molar ratio, J Biol Chem 275(51) (2000) 40517-28.

[20] Y. Takahashi, M. Gehoh, K. Yuzuriha, Structure refinement and diffuse streak scattering of silk (Bombyx mori), International journal of biological macromolecules 24(2-3) (1999) 127-138.

[21] C.-Z. Zhou, F. Confalonieri, M. Jacquet, R. Perasso, Z.-G. Li, J. Janin, Silk Fibroin: Structural Implications of a Remarkable Amino Acid Sequence, Proteins: Structure, Funtion, and Bioinformatics 44 (2001) 119-122.

[22] M.T. Krejchi, S.J. Cooper, Y. Deguchi, E.D. Atkins, M.J. Fournier, T.L. Mason, D.A. Tirrell, Crystal structures of chain-folded antiparallel β-sheet assemblies from sequence-designed periodic polypeptides, Macromolecules 30(17) (1997) 5012-5024.

[23] R. Valluzzi, S.P. Gido, W. Muller, D.L. Kaplan, Orientation of silk III at the air-water interface, International journal of biological macromolecules 24(2-3) (1999) 237-242.

[24] H.-J. Jin, D. Kaplan, Mechanism of silk processing in insects and spiders, Nature 424 (2003) 1057-1061.

[25] A. Motta, L. Fambri, C. Migliaresi, Regenerated silk fibroin films: thermal and dynamic mechanical analysis, Macromolecular Chemistry and Physics 203(10-11) (2002) 1658-1665.

[26] D. Kaplan, K. McGrath, Protein-based materials, Springer Science & Business Media2012.

[27] D. Coleman, F. Howitt, Studies on silk proteins I. The properties and constitution of fibroin. The conversion of fibroin into a water-soluble form and its bearing on the phenomenon of denaturation, Proc. R. Soc. Lond. A 190(1021) (1947) 145-169.

[28] C. Vepari, D.L. Kaplan, Silk as a Biomaterial, Prog Polym Sci 32(8-9) (2007) 991-1007.

[29] J. Sirichaisit, V.L. Brookes, R.J. Young, F. Vollrath, Analysis of structure/property relationships in silkworm (Bombyx mori) and spider dragline (Nephila edulis) silks using Raman spectroscopy, Biomacromolecules 4(2) (2003) 387-394.

[30] S. Xiao, W. Stacklies, M. Cetinkaya, B. Markert, F. Gräter, Mechanical response of silk crystalline units from force-distribution analysis, Biophys J 96(10) (2009) 3997-4005.

[31] A. Nova, S. Keten, N.M. Pugno, A. Redaelli, M.J. Buehler, Molecular and nanostructural mechanisms of deformation, strength and toughness of spider silk fibrils, Nano letters 10(7) (2010) 2626-2634.

[32] A.R. Choudhury, Textile preparation and dyeing, Science publishers2006.

[33] S. Kurosaki, H. Otsuka, M. Kunitomo, M. Koyama, R. Pawankar, K. Matumoto, Fibroin allergy IgE mediated hypersensitivity to silk suture materials, Journal of Nippon Medical School 66(1) (1999) 41-44.

[34] D.H. Hollander, Interstitial cystitis and silk allergy, Medical hypotheses 43(3) (1994) 155-156.

[35] C. Wen, S. Ye, L. Zhou, Y. Yu, Silk-induced asthma in children: a report of 64 cases, Annals of allergy 65(5) (1990) 375-378.

[36] J.C. Celedón, L.J. Palmer, X. Xu, B. Wang, Z. Fang, S.T. Weiss, Sensitization to silk and childhood asthma in rural China, Pediatrics 107(5) (2001) e80-e80.

[37] P. Aramwit, A. Sangcakul, The effects of sericin cream on wound healing in rats, Bioscience, biotechnology, and biochemistry 71(10) (2007) 2473-2477.

[38] A.E. Thurber, F.G. Omenetto, D.L. Kaplan, In vivo bioresponses to silk proteins, Biomaterials 71 (2015) 145-157.

[39] D. Greenwald, S. Shumway, P. Albear, L. Gottlieb, Mechanical comparison of 10 suture materials before and after in vivo incubation, J Surg Res 56(4) (1994) 372-377.

[40] R.L. Horan, I. Toponarski, H.E. Boepple, P.P. Weitzel, J.C. Richmond, G.H. Altman, Design and characterization of a scaffold for anterior cruciate ligament engineering, The journal of knee surgery 22(01) (2009) 82-92.

[41] U.J. Kim, J. Park, H.J. Kim, M. Wada, D.L. Kaplan, Three-dimensional aqueous-derived biomaterial scaffolds from silk fibroin, Biomaterials 26(15) (2005) 2775-85.

[42] U.-J. Kim, J. Park, C. Li, R. Valluzzi, D.L. Kaplan, Structure and Properties of Silk Hydrogels, Biomacromolecules 5(3) (2004) 786-792.

[43] R. Nazarov, H.-J. Jin, D.L. Kaplan, Porous 3-D scaffolds from regenerated silk fibroin, Biomacromolecules 5(3) (2004) 718-726.

[44] Q. Zhang, S. Yan, M. Li, Silk fibroin based porous materials, Materials 2(4) (2009) 2276-2295.

[45] A.J. Meinel, K.E. Kubow, E. Klotzsch, M. Garcia-Fuentes, M.L. Smith, V. Vogel, H.P. Merkle, L. Meinel, Optimization strategies for electrospun silk fibroin tissue engineering scaffolds, Biomaterials 30(17) (2009) 3058-67.

[46] S. Zarkoob, R.K. Eby, D.H. Reneker, S.D. Hudson, D. Ertley, W.W. Adams, Structure and morphology of electrospun silk nanofibers, Polymer 45(11) (2004) 3973-3977.

[47] J. Ayutsede, M. Gandhi, S. Sukigara, M. Micklus, H.-E. Chen, F. Ko, Regeneration of Bombyx mori silk by electrospinning. Part 3: characterization of electrospun nonwoven mat, Polymer 46(5) (2005) 1625-1634.

[48] X. Wang, E. Wenk, A. Matsumoto, L. Meinel, C. Li, D.L. Kaplan, Silk microspheres for encapsulation and controlled release, J Control Release 117(3) (2007) 360-70.

[49] E. Wenk, A.J. Wandrey, H.P. Merkle, L. Meinel, Silk fibroin spheres as a platform for controlled drug delivery, J Control Release 132(1) (2008) 26-34.

[50] X. Wang, T. Yucel, Q. Lu, X. Hu, D.L. Kaplan, Silk nanospheres and microspheres from silk/pva blend films for drug delivery, Biomaterials 31(6) (2010) 1025-35.

[51] B.D. Lawrence, S. Wharram, J.A. Kluge, G.G. Leisk, F.G. Omenetto, M.I. Rosenblatt, D.L. Kaplan, Effect of hydration on silk film material properties, Macromolecular bioscience 10(4) (2010) 393-403.

[52] B. Witkop, Paul Ehrlich and his Magic bullets--revisited, Proc Am Philos Soc 143(4) (1999) 540-57.

[53] Y.H. Bae, K. Park, Targeted drug delivery to tumors: myths, reality and possibility, J Control Release 153(3) (2011) 198-205.

[54] O. Germershaus, K. Nultsch, Localized, non-viral delivery of nucleic acids: Opportunities, challenges and current strategies, Asian J Pharm Sci 10(3) (2015) 159-175.

[55] D.G. Vartak, R.A. Gemeinhart, Matrix metalloproteases: underutilized targets for drug delivery, J Drug Target 15(1) (2007) 1-20.

[56] A. Daniele, I. Abbate, C. Oakley, P. Casamassima, E. Savino, A. Casamassima, G. Sciortino, V. Fazio, G. Gadaleta-Caldarola, A. Catino, F. Giotta, R. De Luca, R. Divella, Clinical and prognostic role of matrix metalloproteinase-2, -9 and their inhibitors in breast cancer and liver diseases: A review, The international journal of biochemistry & cell biology 77(Pt A) (2016) 91-101.

[57] K. Kessenbrock, V. Plaks, Z. Werb, Matrix metalloproteinases: regulators of the tumor microenvironment, Cell 141(1) (2010) 52-67.

[58] M. Egeblad, Z. Werb, New functions for the matrix metalloproteinases in cancer progression, Nat Rev Cancer 2(3) (2002) 161-74.

[59] A. Kruger, R.E. Kates, D.R. Edwards, Avoiding spam in the proteolytic internet: future strategies for anti-metastatic MMP inhibition, Biochimica et biophysica acta 1803(1) (2010) 95-102.

[60] P.L. Carl, P.K. Chakravarty, J.A. Katzenellenbogen, M.J. Weber, Protease-Activated Prodrugs for Cancer-Chemotherapy, P Natl Acad Sci-Biol 77(4) (1980) 2224-2228.

[61] K.Y. Choi, M. Swierczewska, S. Lee, X. Chen, Protease-activated drug development, Theranostics 2(2) (2012) 156-78.

[62] C.W.P. Foo, E. Bini, J. Hensman, D.P. Knight, R.V. Lewis, D.L. Kaplan, Role of pH and charge on silk protein assembly in insects and spiders, Applied Physics A 82(2) (2005) 223-233.

[63] M. Chang, F. Zhang, T. Wei, T. Zuo, Y. Guan, G. Lin, W. Shao, Smart linkers in polymer-drug conjugates for tumor-targeted delivery, J Drug Target 24(6) (2016) 475-91.

[64] J. Vandooren, G. Opdenakker, P.M. Loadman, D.R. Edwards, Proteases in cancer drug delivery, Adv. Drug Deliv. Rev. 97 (2016) 144-155.

[65] A.S. Hoffman, The origins and evolution of "controlled" drug delivery systems, Journal of Controlled Release 132(3) (2008) 153-163.

[66] F. Kratz, J. Drevs, G. Bing, C. Stockmar, K. Scheuermann, P. Lazar, C. Unger, Development and in vitro efficacy of novel MMP2 and MMP9 specific doxorubicin albumin conjugates, Bioorganic & medicinal chemistry letters 11(15) (2001) 2001-2006.

[67] A.M. Mansour, J. Drevs, N. Esser, F.M. Hamada, O.A. Badary, C. Unger, I. Fichtner, F. Kratz, A new approach for the treatment of malignant melanoma: Enhanced antitumor efficacy of an albumin-binding doxorubicin prodrug that is cleaved by matrix metalloproteinase 2, Cancer Research 63(14) (2003) 4062-4066.

[68] L.E. Samuelson, R.L. Scherer, L.M. Matrisian, J.O. McIntyre, D.J. Bornhop, Synthesis and In Vitro Efficacy of MMP9-Activated NanoDendrons, Molecular pharmaceutics 10(8) (2013) 3164-3174.

[69] Y. Chau, R.F. Padera, N.M. Dang, R. Langer, Antitumor efficacy of a novel polymer-peptide-drug conjugate in human tumor xenograft models, Int J Cancer 118(6) (2006) 1519-1526.

[70] A.A. Lozano-Pérez, M.G. Montalbán, S.D. Aznar-Cervantes, F. Cragnolini, J.L. Cenis, G. Villora, Production of silk fibroin nanoparticles using ionic liquids and high-power ultrasounds, Journal of Applied Polymer Science 132(12) (2015) 41702-41710.

[71] Y. Cheng, F.J. Huang, X.H. Min, P.C. Gao, T.C. Zhang, X.C. Li, B.F. Liu, Y.N. Hong, X.D. Lou, F. Xia, Protease-Responsive Prodrug with Aggregation-Induced Emission Probe for Controlled Drug Delivery and Drug Release Tracking in Living Cells, Anal. Chem. 88(17) (2016) 8913-8919.

[72] Y.Z. Chen, M. Zhang, H.Y. Jin, Y.S. Tang, A.H. Wu, Y.Z. Huang, Prodrug-Like, PEGylated Protein Toxin Trichosanthin for Reversal of Chemoresistance, Molecular pharmaceutics 14(5) (2017) 1429-1438.

[73] N.Q. Shi, W. Gao, B. Xiang, X.R. Qi, Enhancing cellular uptake of activable cell-penetrating peptide-doxorubicin conjugate by enzymatic cleavage, Int J Nanomed 7 (2012) 1613-1621.

[74] Y.Z. Chen, M. Zhang, H.Y. Jin, D.D. Li, F. Xu, A.H. Wu, J.Y. Wang, Y.Z. Huang, Glioma Dual-Targeting Nanohybrid Protein Toxin Constructed by Intein-Mediated Site-Specific Ligation for Multistage Booster Delivery, Theranostics 7(14) (2017) 3489-3503.

[75] M. Moreno, E. Zurita, E. Giralt, Delivering wasp venom for cancer therapy, Journal of Controlled Release 182 (2014) 13-21.

[76] G.Y. Lee, K. Park, S.Y. Kim, Y. Byun, MMPs-specific PEGylated peptide-DOX conjugate micelles that can contain free doxorubicin, European journal of pharmaceutics and biopharmaceutics :

official journal of Arbeitsgemeinschaft fur Pharmazeutische Verfahrenstechnik e.V 67(3) (2007) 646-54.

[77] P.S. Kulkarni, M.K. Haldar, R.R. Nahire, P. Katti, A.H. Ambre, W.W. Muhonen, J.B. Shabb, S.K.R. Padi, R.K. Singh, P.P. Borowicz, D.K. Shrivastava, K.S. Katti, K. Reindl, B. Guo, S. Mallik, MMP-9 Responsive PEG Cleavable Nanovesicles for Efficient Delivery of Chemotherapeutics to Pancreatic Cancer, Molecular pharmaceutics 11(7) (2014) 2390-2399.

[78] P.F. Xu, Q.S. Meng, H.P. Sun, Q. Yin, H.J. Yu, Z.W. Zhang, M. Cao, Y.Y. Zhang, Y.P. Li, Shrapnel nanoparticles loading docetaxel inhibit metastasis and growth of breast cancer, Biomaterials 64 (2015) 10-20.

[79] W.X. Hou, F.F. Xia, C.S. Alves, X.Q. Qian, Y.M. Yang, D.X. Cui, MMP2-Targeting and Redox-Responsive PEGylated Chlorin e6 Nanoparticles for Cancer Near-Infrared Imaging and Photodynamic Therapy, Acs Appl Mater Inter 8(2) (2016) 1447-1457.

[80] L. Zhu, T. Wang, F. Perche, A. Taigind, V.P. Torchilin, Enhanced anticancer activity of nanopreparation containing an MMP2-sensitive PEG-drug conjugate and cell-penetrating moiety, Proc Natl Acad Sci U S A 110(42) (2013) 17047-52.

[81] L. Zhu, P. Kate, V.P. Torchilin, Matrix metalloprotease 2-responsive multifunctional liposomal nanocarrier for enhanced tumor targeting, Acs Nano 6(4) (2012) 3491-8.

[82] W. Gao, B. Xiang, T.T. Meng, F. Liu, X.R. Qi, Chemotherapeutic drug delivery to cancer cells using a combination of folate targeting and tumor microenvironment-sensitive polypeptides, Biomaterials 34(16) (2013) 4137-49.

[83] X.Y. Zhang, X.F. Wang, W.T. Zhong, X.Q. Ren, X.Y. Sha, X.L. Fang, Matrix metalloproteinases-2/9-sensitive peptide-conjugated polymer micelles for site-specific release of drugs and enhancing tumor accumulation: preparation and in vitro and in vivo evaluation, Int J Nanomed 11 (2016) 1643-1661.

[84] Z. Dai, Y. Tu, L. Zhu, Multifunctional Micellar Nanocarriers for Tumor-Targeted Delivery of Hydrophobic Drugs, J. Biomed. Nanotechnol. 12(6) (2016) 1199-1210.

[85] W.D. Ke, J.J. Li, K.J. Zhao, Z.S. Zha, Y. Han, Y.H. Wang, W. Yin, P. Zhang, Z.S. Ge, Modular Design and Facile Synthesis of Enzyme-Responsive Peptide-Linked Block Copolymers for Efficient Delivery of Doxorubicin, Biomacromolecules 17(10) (2016) 3268-3276.

[86] W.D. Ke, Z.S. Zha, J.F. Mukerabigwi, W.J. Chen, Y.H. Wang, C.X. He, Z.S. Ge, Matrix Metalloproteinase-Responsive Multifunctional Peptide-Linked Amphiphilic Block Copolymers for Intelligent Systemic Anticancer Drug Delivery, Bioconjugate Chemistry 28(8) (2017) 2190-2198.

[87] Q. Yao, Z. Dai, J.H. Choi, D. Kim, L. Zhu, Building Stable MMP2-Responsive Multifunctional Polymeric Micelles by an All-in-One Polymer-Lipid Conjugate for Tumor-Targeted Intracellular Drug Delivery, Acs Appl Mater Inter 9(38) (2017) 32520-32533.

[88] Q. Yao, J.H. Choi, Z. Dai, J. Wang, D. Kim, X. Tang, L. Zhu, Improving Tumor Specificity and Anticancer Activity of Dasatinib by Dual-Targeted Polymeric Micelles, Acs Appl Mater Inter 9(42) (2017) 36642-36654.

[89] M.P. Chien, A.S. Carlini, D.H. Hu, C.V. Barback, A.M. Rush, D.J. Hall, G. Orr, N.C. Gianneschi, Enzyme-Directed Assembly of Nanoparticles in Tumors Monitored by in Vivo Whole Animal Imaging and ex Vivo Super-Resolution Fluorescence Imaging, J. Am. Chem. Soc. 135(50) (2013) 18710-18713.

[90] M.M. Nguyen, A.S. Carlini, M.P. Chien, S. Sonnenberg, C.L. Luo, R.L. Braden, K.G. Osborn, Y.W. Li, N.C. Gianneschi, K.L. Christman, Enzyme-Responsive Nanoparticles for Targeted

Accumulation and Prolonged Retention in Heart Tissue after Myocardial Infarction, Adv. Mater. 27(37) (2015) 5547-5552.

[91] R. Dorresteijn, N. Billecke, M. Schwendy, S. Putz, M. Bonn, S.H. Parekh, M. Klapper, K. Mullen, Polylactide-block-Polypeptide-block-Polylactide Copolymer Nanoparticles with Tunable Cleavage and Controlled Drug Release, Advanced functional materials 24(26) (2014) 4026-4033.

[92] J. Nguyen, R. Sievers, J.P.M. Motion, S. Kivimae, Q.Z. Fang, R.J. Lee, Delivery of Lipid Micelles into Infarcted Myocardium Using a Lipid-Linked Matrix Metalloproteinase Targeting Peptide, Mol Pharmaceut 12(4) (2015) 1150-1157.

[93] N.K. Nigam, Biochemical Markers of Myocardial Injury, Indian Journal of Clinical Biochemistry 22(1) (2007) 10-17.

[94] W. Phatharajaree, A. Phrommintikul, N. Chattipakorn, Matrix metalloproteinases and myocardial infarction, The Canadian journal of Cardiology 23(9) (2007) 727-733.

[95] H. Hatakeyama, H. Akita, E. Ishida, K. Hashimoto, H. Kobayashi, T. Aoki, J. Yasuda, K. Obata, H. Kikuchi, T. Ishida, H. Kiwada, H. Harashima, Tumor targeting of doxorubicin by anti-MT1-MMP antibody-modified PEG liposomes, International journal of pharmaceutics 342(1-2) (2007) 194-200.

[96] K. Atobe, T. Ishida, E. Ishida, K. Hashimoto, H. Kobayashi, J. Yasuda, T. Aoki, K.I. Obata, H. Kikuchi, H. Akita, T. Asai, H. Harashima, N. Oku, H. Kiwada, In vitro efficacy of a sterically stabilized immunoliposomes targeted to membrane type 1 matrix metalloproteinase (MT1-MMP), Biol. Pharm. Bull. 30(5) (2007) 972-978.

[97] B. Grunwald, J. Vandooren, E. Locatelli, P. Fiten, G. Opdenakker, P. Proost, A. Kruger, J.P. Lellouche, L.L. Israel, L. Shenkman, M.C. Franchini, Matrix metalloproteinase-9 (MMP-9) as an activator of nanosystems for targeted drug delivery in pancreatic cancer, Journal of Controlled Release 239 (2016) 39-48.

[98] E. Gullotti, J. Park, Y. Yeo, Polydopamine-Based Surface Modification for the Development of Peritumorally Activatable Nanoparticles, Pharm Res-Dordr 30(8) (2013) 1956-1967.

[99] A.K. Suresh, Y.M. Weng, Z. Li, R. Zerda, D. Van Haute, J.C. Williams, J.M. Berlin, Matrix metalloproteinase-triggered denuding of engineered gold nanoparticles for selective cell uptake, J Mater Chem B 1(18) (2013) 2341-2349.

[100] C. Nazli, G.S. Demirer, Y. Yar, H.Y. Acar, S. Kizilel, Targeted delivery of doxorubicin into tumor cells via MMP-sensitive PEG hydrogel-coated magnetic iron oxide nanoparticles (MIONPs), Colloid Surface B 122 (2014) 674-683.

[101] J.H. Choi, J.S. Lee, K.M. Park, J.W. Bae, Y. Lee, K.D. Park, Multi-layered nanogels with MMP-sheddable PEG masks: Preparation and promotion of tumor cell uptake by controlling surface characteristics, Colloid Surface B 156 (2017) 71-78.

[102] C. Wong, T. Stylianopoulos, J.A. Cui, J. Martin, V.P. Chauhan, W. Jiang, Z. Popovic, R.K. Jain, M.G. Bawendi, D. Fukumura, Multistage nanoparticle delivery system for deep penetration into tumor tissue, P Natl Acad Sci USA 108(6) (2011) 2426-2431.

[103] S.B. Ruan, X. Cao, X.L. Cun, G.L. Hu, Y. Zhou, Y.J. Zhang, L.B. Lu, Q. He, H.L. Gao, Matrix metalloproteinase-sensitive size-shrinkable nanoparticles for deep tumor penetration and pH triggered doxorubicin release, Biomaterials 60 (2015) 100-110.

[104] G.Z. Gu, X.L. Gao, Q.Y. Hu, T. Kang, Z.Y. Liu, M.Y. Jiang, D.Y. Miao, Q.X. Song, L. Yao, Y.F. Tu, Z.Q. Pang, H.Z. Chen, X.G. Jiang, J. Chen, The influence of the penetrating peptide iRGD on the effect of paclitaxel-loaded MT1-AF7p-conjugated nanoparticles on glioma cells, Biomaterials 34(21) (2013) 5138-5148.

[105] E. Locatelli, M. Naddaka, C. Uboldi, G. Loudos, E. Fragogeorgi, V. Molinari, A. Pucci, T. Tsotakos, D. Psimadas, J. Ponti, M.C. Franchini, Targeted delivery of silver nanoparticles and alisertib: in vitro and in vivo synergistic effect against glioblastoma, Nanomedicine 9(6) (2014) 839-849.

[106] W. Mao, H.S. Kim, Y.J. Son, S.R. Kim, H.S. Yoo, Doxorubicin encapsulated clicked gold nanoparticle clusters exhibiting tumor-specific disassembly for enhanced tumor localization and computerized tomographic imaging, Journal of Controlled Release 269 (2018) 52-62.

[107] H.S. Kim, S. Yoon, Y.J. Son, Y. Park, Y.M. Jung, H.S. Yoo, High-yield clicking and dissociation of doxorubicin nanoclusters exhibiting differential cellular uptakes and imaging, Journal of Controlled Release 217 (2015) 64-73.

[108] J. Ritzer, T. Luhmann, C. Rode, M. Pein-Hackelbusch, I. Immohr, U. Schedler, T. Thiele, S. Stubinger, B.V. Rechenberg, J. Waser-Althaus, F. Schlottig, M. Merli, H. Dawe, M. Karpisek, R. Wyrwa, M. Schnabelrauch, L. Meinel, Diagnosing peri-implant disease using the tongue as a 24/7 detector, Nat. Commun. 8 (2017).

[109] H.L. Gao, S. Zhang, S.J. Cao, Z. Yang, Z.Q. Pang, X.G. Jiang, Angiopep-2 and Activatable Cell-Penetrating Peptide Dual-Functionalized Nanoparticles for Systemic Glioma-Targeting Delivery, Molecular pharmaceutics 11(8) (2014) 2755-2763.

[110] O. Germershaus, T. Luhmann, J.C. Rybak, J. Ritzer, L. Meinel, Application of natural and semi-synthetic polymers for the delivery of sensitive drugs, Int Mater Rev 60(2) (2015) 101-130.

[111] J. Kim, Y. Park, G. Tae, K.B. Lee, S.J. Hwang, I.S. Kim, I. Noh, K. Sun, Synthesis and characterization of matrix metalloprotease sensitive-low molecular weight hyaluronic acid based hydrogels, J. Mater. Sci.-Mater. Med. 19(11) (2008) 3311-3318.

[112] B.P. Purcell, D. Lobb, M.B. Charati, S.M. Dorsey, R.J. Wade, K.N. Zellars, H. Doviak, S. Pettaway, C.B. Logdon, J.A. Shuman, P.D. Freels, J.H. Gorman, R.C. Gorman, F.G. Spinale, J.A. Burdick, Injectable and bioresponsive hydrogels for on-demand matrix metalloproteinase inhibition, Nat. Mater. 13(6) (2014) 653-661.

[113] M. Sutter, J. Siepmann, W.E. Hennink, W. Jiskoot, Recombinant gelatin hydrogels for the sustained release of proteins, Journal of Controlled Release 119(3) (2007) 301-312.

[114] V.K. Garripelli, J.K. Kim, S. Son, W.J. Kim, M.A. Repka, S. Jo, Matrix metalloproteinase-sensitive thermogelling polymer for bioresponsive local drug delivery, Acta biomaterialia 7(5) (2011) 1984-1992.

[115] T.P. Kraehenbuehl, L.S. Ferreira, A.M. Hayward, M. Nahrendorf, A.J. van der Vlies, E. Vasile, R. Weissleder, R. Langer, J.A. Hubbell, Human embryonic stem cell-derived microvascular grafts for cardiac tissue preservation after myocardial infarction, Biomaterials 32(4) (2011) 1102-9.

[116] H.X. Wang, X.Z. Yang, C.Y. Sun, C.Q. Mao, Y.H. Zhu, J. Wang, Matrix metalloproteinase 2-responsive micelle for siRNA delivery, Biomaterials 35(26) (2014) 7622-34.

[117] K.L. Veiman, K. Kunnapuu, T. Lehto, K. Kiisholts, K. Parn, U. Langel, K. Kurrikoff, PEG shielded MMP sensitive CPPs for efficient and tumor specific gene delivery in vivo, Journal of Controlled Release 209 (2015) 238-247.

[118] H.M. Li, S.S. Yu, M. Miteva, C.E. Nelson, T. Werfel, T.D. Giorgio, C.L. Duvall, Matrix Metalloproteinase Responsive, Proximity-Activated Polymeric Nanoparticles for siRNA Delivery, Advanced functional materials 23(24) (2013) 3040-3052.

[119] L. Zhu, F. Perche, T. Wang, V.P. Torchilin, Matrix metalloproteinase 2-sensitive multifunctional polymeric micelles for tumor-specific co-delivery of siRNA and hydrophobic drugs, Biomaterials 35(13) (2014) 4213-22.

[120] G. Salzano, D.F. Costa, C. Sarisozen, E. Luther, G. Mattheolabakis, P.P. Dhargalkar, V.P. Torchilin, Mixed Nanosized Polymeric Micelles as Promoter of Doxorubicin and miRNA-34a Co-Delivery Triggered by Dual Stimuli in Tumor Tissue, Small 12(35) (2016) 4837-4848.

[121] H.S. Kim, H.S. Yoo, In vitro and in vivo epidermal growth factor gene therapy for diabetic ulcers with electrospun fibrous meshes, Acta biomaterialia 9(7) (2013) 7371-7380.

[122] H.S. Kim, H.S. Yoo, Matrix metalloproteinase-inspired suicidal treatments of diabetic ulcers with siRNA-decorated nanofibrous meshes, Gene Therapy 20(4) (2013) 378-385.

[123] H.S. Kim, H.S. Yoo, MMPs-responsive release of DNA from electrospun nanofibrous matrix for local gene therapy: In vitro and in vivo evaluation, Journal of Controlled Release 145(3) (2010) 264-271.

[124] E.I. Chen, S.J. Kridel, E.W. Howard, W. Li, A. Godzik, J.W. Smith, A unique substrate recognition profile for matrix metalloproteinase-2, J Biol Chem 277(6) (2002) 4485-91.

[125] B.E. Turk, L.L. Huang, E.T. Piro, L.C. Cantley, Determination of protease cleavage site motifs using mixture-based oriented peptide libraries, Nature biotechnology 19(7) (2001) 661.

[126] U. Eckhard, P.F. Huesgen, O. Schilling, C.L. Bellac, G.S. Butler, J.H. Cox, A. Dufour, V. Goebeler, R. Kappelhoff, U.A.D. Keller, T. Klein, P.F. Lange, G. Marino, C.J. Morrison, A. Prudova, D. Rodriguez, A.E. Starr, Y. Wang, C.M. Overall, Active site specificity profiling of the matrix metalloproteinase family: Proteomic identification of 4300 cleavage sites by nine MMPs explored with structural and synthetic peptide cleavage analyses, Matrix Biol 49 (2016) 37-60.

[127] B.I. Ratnikov, P. Cieplak, K. Gramatikoff, J. Pierce, A. Eroshkin, Y. Igarashi, M. Kazanov, Q. Sun, A. Godzik, A. Osterman, B. Stec, A. Strongin, J.W. Smith, Basis for substrate recognition and distinction by matrix metalloproteinases, Proc Natl Acad Sci U S A 111(40) (2014) E4148-55.

[128] P. Cieplak, A.Y. Strongin, Matrix metalloproteinases - From the cleavage data to the prediction tools and beyond, Biochimica et biophysica acta 1864(11 Pt A) (2017) 1952-1963.

[129] O. Schilling, C.M. Overall, Proteome-derived, database-searchable peptide libraries for identifying protease cleavage sites, Nature biotechnology 26(6) (2008) 685.

[130] J. Patterson, J.A. Hubbell, Enhanced proteolytic degradation of molecularly engineered PEG hydrogels in response to MMP-1 and MMP-2, Biomaterials 31(30) (2010) 7836-45.

[131] D.H. Nam, C. Rodriguez, A.G. Remacle, A.Y. Strongin, X. Ge, Active-site MMP-selective antibody inhibitors discovered from convex paratope synthetic libraries, P Natl Acad Sci USA 113(52) (2016) 14970-14975.

[132] U. Eckhard, P.F. Huesgen, O. Schilling, C.L. Bellac, G.S. Butler, J.H. Cox, A. Dufour, V. Goebeler, R. Kappelhoff, U.A.D. Keller, T. Klein, P.F. Lange, G. Marino, C.J. Morrison, A. Prudova, D. Rodriguez, A.E. Starr, Y.L. Wang, C.M. Overall, Active site specificity profiling of the matrix metalloproteinase family: Proteomic identification of 4300 cleavage sites by nine MMPs explored with structural and synthetic peptide cleavage analyses, Matrix Biol 49 (2016) 37-60.

[133] J.R. Tauro, R.A. Gemeinhart, Matrix metalloproteinase triggered delivery of cancer therapeutics from hydrogel matrices, Bioconjugate Chem 16(5) (2005) 1133-1139.

[134] C.N. Salinas, K.S. Anseth, Mixed mode thiol-acrylate photopolymerizations for the synthesis of PEG-peptide hydrogels, Macromolecules 41(16) (2008) 6019-6026.

[135] Y. Zhang, R.A. Gemeinhart, Improving matrix metalloproteinase-2 specific response of a hydrogel system using electrophoresis, International journal of pharmaceutics 429(1-2) (2012) 31-37.

[136] A.C. Braun, M. Gutmann, R. Ebert, F. Jakob, H. Gieseler, T. Luhmann, L. Meinel, Matrix Metalloproteinase Responsive Delivery of Myostatin Inhibitors, Pharm Res-Dordr 34(1) (2017) 58-72.

[137] J. Conde, J.T. Dias, V. Grazu, M. Moros, P.V. Baptista, J.M. de la Fuente, Revisiting 30 years of biofunctionalization and surface chemistry of inorganic nanoparticles for nanomedicine, Front Chem 2 (2014) 48.

[138] J. Conde, J.T. Dias, V. Grazu, M. Moros, P.V. Baptista, J.M. de la Fuente, Revisiting 30 years of biofunctionalization and surface chemistry of inorganic nanoparticles for nanomedicine, Front Chem 2 (2014).

[139] D. Bacinello, E. Garanger, D. Taton, K.C. Tam, S. Lecommandoux, Enzyme-Degradable Self-Assembled Nanostructures from Polymer-Peptide Hybrids, Biomacromolecules 15(5) (2014) 1882-1888.

[140] C.D. Hein, X.M. Liu, D. Wang, Click chemistry, a powerful tool for pharmaceutical sciences, Pharm Res 25(10) (2008) 2216-30.

[141] Y. Chau, F.E. Tan, R. Langer, Synthesis and Characterization of dextran-peptide-methotrexate conjugates for tumor targeting via mediation by matrix metalloproteinase II and IX, Bioconjug Chem 15 (2004) 931-941.

[142] A.E. Ross, M.Y. Tang, R.A. Gemeinhart, Effects of Molecular Weight and Loading on Matrix Metalloproteinase-2 Mediated Release from Poly(Ethylene Glycol) Diacrylate Hydrogels, Aaps J. 14(3) (2012) 482-490.

[143] B. Ganguly, D.K. Srivastava, Influence of "Flexible" versus "Rigid" Nanoparticles on the Stability of Matrix Metalloproteinase-7, J Biomed Nanotechnol 4(4) (2008) 457-462.

[144] B. Ganguly, J. Banerjee, A.I. Elegbede, D.J. Klocke, S. Mallik, D.K. Srivastava, Intrinsic selectivity in binding of matrix metalloproteinase-7 to differently charged lipid membranes, Febs Lett 581(29) (2007) 5723-5726.

[145] A.M. Grumezescu, Drug Targeting and Stimuli Sensitive Drug Delivery Systems, Elsevier Science2018.

[146] J. Xiong, H. Gao, Matrix metalloproteases-responsive nanomaterials for tumor targeting diagnosis and treatment, Journal of microencapsulation 34(5) (2017) 440-453.

[147] Y. Lu, A.A. Aimetti, R. Langer, Z. Gu, Bioresponsive materials, Nature Reviews Materials 2(1) (2017) 16075.

[148] S. Mura, J. Nicolas, P. Couvreur, Stimuli-responsive nanocarriers for drug delivery, Nat Mater 12(11) (2013) 991-1003.

[149] C.B. Borkner, M.B. Elsner, T. Scheibel, Coatings and Films Made of Silk Proteins, Acs Appl Mater Inter 6(18) (2014) 15611-15625.

[150] B.W. Zhu, H. Wang, W.R. Leow, Y.R. Cai, X.J. Loh, M.Y. Han, X.D. Chen, Silk Fibroin for Flexible Electronic Devices, Adv Mater 28(22) (2016) 4250-4265.

[151] J. Melke, S. Midha, S. Ghosh, K. Ito, S. Hofmann, Silk fibroin as biomaterial for bone tissue engineering, Acta Biomater 31 (2016) 1-16.

[152] L.D. Koh, Y. Cheng, C.P. Teng, Y.W. Khin, X.J. Loh, S.Y. Tee, M. Low, E.Y. Ye, H.D. Yu, Y.W. Zhang, M.Y. Han, Structures, mechanical properties and applications of silk fibroin materials, Progress in Polymer Science 46 (2015) 86-110.

[153] F. Mottaghitalab, M. Farokhi, M.A. Shokrgozar, F. Atyabi, H. Hosseinkhani, Silk fibroin nanoparticle as a novel drug delivery system, Journal of Controlled Release 206 (2015) 161-176.

[154] B. Panilaitis, G.H. Altman, J.S. Chen, H.J. Jin, V. Karageorgiou, D.L. Kaplan, Macrophage responses to silk, Biomaterials 24(18) (2003) 3079-3085.

[155] G. Freddi, G. Allera, G. Candiani, Degumming of silk fabrics with tartaric acid, Journal of the Society of Dyers and Colourists 112(7-8) (1996) 191-195.

[156] K. Nultsch, O. Germershaus, Silk fibroin degumming affects scaffold structure and release of macromolecular drugs, Eur J Pharm Sci 106 (2017) 254-261.

[157] M.R. Khan, M. Tsukada, Y. Gotoh, H. Morikawa, G. Freddi, H. Shiozaki, Physical properties and dyeability of silk fibers degummed with citric acid, Bioresource technology 101(21) (2010) 8439-45.

[158] H.-Y. Wang, Y.-Q. Zhang, Effect of regeneration of liquid silk fibroin on its structure and characterization, Soft Matter 9(1) (2013) 138-145.

[159] M.N. Padamwar, A.P. Pawar, Silk sericin and its applications: A review, J Sci Ind Res India 63(4) (2004) 323-329.

[160] D.M. Phillips, L.F. Drummy, D.G. Conrady, D.M. Fow, R.R. Naik, M.O. Stone, P.C. Trulove, H.C. De Long, R.A. Mantz, Dissolution and Regeneration of Bombyx mori Silk Fibroin Using Ionic Liquids, J Am Chem Soc 126(44) (2004) 14350-14351.

[161] H.J. Cho, C.S. Ki, H. Oh, K.H. Lee, I.C. Um, Molecular weight distribution and solution properties of silk fibroins with different dissolution conditions, International journal of biological macromolecules 51(3) (2012) 336-41.

[162] J. Nam, Y.H. Park, Morphology of Regenerated Silk Fibroin: Effects of Freezing Temperature, Alcohol Addition, and Molecular Weight, Journal of Applied Polymer Science 81(12) (2001) 3008-3021.

[163] K. Tsubouchi, H. Nakao, Y. Igarashi, Y. Takasu, H. Yamada, Bombyx mori Fibroin Enhanced the Proliferation of Cultured Human Skin Fibroblasts, Journal of Insect Biotechnology and Sericology 72 (2003) 65-69.

[164] E.M. Pritchard, X. Hu, V. Finley, C.K. Kuo, D.L. Kaplan, Effect of silk protein processing on drug delivery from silk films, Macromolecular bioscience 13(3) (2013) 311-20.

[165] D.M. Salvay, M. Zelivyanskaya, L.D. Shea, Gene delivery by surface immobilization of plasmid to tissue-engineering scaffolds, Gene Ther 17(9) (2010) 1134-1141.

[166] D.N. Rockwood, R.C. Preda, T. Yucel, X.Q. Wang, M.L. Lovett, D.L. Kaplan, Materials fabrication from Bombyx mori silk fibroin, Nat Protoc 6(10) (2011) 1612-1631.

[167] T. Scheibel, H. Zahn, A. Krasowski, Silk, Ullmann's Encyclopedia of Industrial Chemistry2016.

[168] M. Sah, K. Pramanik, Regenerated Silk Fibroin from B. mori Silk Cocoon for Tissue Engineering Applications, Proceedings of 2010 International Conference on Biotechnology and Food Science (Icbfs 2010) (2010) 206-212.

[169] V. Trefiletti, G. Conio, F. Pioli, B. Cavazza, A. Perico, E. Patrone, The Spinning of Silk .1. Molecular-Weight, Subunit Structure, and Molecular Shape of Bombyx-Mori Fibroin, Makromol Chem 181(6) (1980) 1159-1179.

[170] H. Yamada, H. Nakao, Y. Takasu, K. Tsubouchi, Preparation of undegraded native molecular fibroin solution from silkworm cocoons, Mat Sci Eng C-Bio S 14(1-2) (2001) 41-46.

[171] M.S. Zafar, D.J. Belton, B. Hanby, D.L. Kaplan, C.C. Perry, Functional material features of Bombyx mori silk light versus heavy chain proteins, Biomacromolecules 16(2) (2015) 606-14.

[172] I. Krasnov, I. Diddens, N. Hauptmann, G. Helms, M. Ogurreck, T. Seydel, S.S. Funari, M. Muller, Mechanical properties of silk: Interplay of deformation on macroscopic and molecular length scales, Phys Rev Lett 100(4) (2008).

[173] M. Cetinkaya, S.B. Xiao, B. Markert, W. Stacklies, F. Grater, Silk Fiber Mechanics from Multiscale Force Distribution Analysis, Biophysical Journal 100(5) (2011) 1298-1305.

[174] T.L. McMeekin, M.L. Groves, N.J. Hipp, Refractive Indices of Amino Acids, Proteins, and Related Substances, Amino Acids and Serum Proteins, AMERICAN CHEMICAL SOCIETY1964, pp. 54-66.

[175] G. Perotto, Y.J. Zhang, D. Naskar, N. Patel, D.L. Kaplan, S.C. Kundu, F.G. Omenetto, The optical properties of regenerated silk fibroin films obtained from different sources, Appl Phys Lett 111(10) (2017).

[176] M. Arami, S. Rahimi, L. Mivehie, F. Mazaheri, N.M. Mahmoodi, Degumming of Persian silk with mixed proteolytic enzymes, Journal of Applied Polymer Science 106(1) (2007) 267-275.

[177] M.L. Gulrajani, R. Agarwal, A. Grover, M. Suri, Degumming of silk with lipase and protease, Indian J Fibre Text 25(1) (2000) 69-74.

[178] M.L. Gulrajani, S.V. Gupta, A. Gupta, M. Suri, Degumming of silk with different protease enzymes, Indian Journal of Fibre and Textile Research 21 (1996) 270-275.

[179] S.V. More, H.B. Khandelwal, M.A. Joseph, R.S. Laxman, Enzymatic Degumming of Silk with Microbial Proteases, J Nat Fibers 10(2) (2013) 98-111.

[180] K. Tanaka, N. Kajiyama, K. Ishikura, S. Waga, A. Kikuchi, K. Ohtomo, T. Takagi, S. Mizuno, Determination of the site of disulfide linkage between heavy and light chains of silk fibroin produced by Bombix mori, Bba-Protein Struct M 1432(1) (1999) 92-103.

[181] K. Yamaguchi, Y. Kikuchi, T. Takagi, A. Kikuchi, F. Oyama, K. Shimura, S. Mizuno, Primary Structure of the Silk Fibroin Light Chain Determined by Cdna Sequencing and Peptide Analysis, J Mol Biol 210(1) (1989) 127-139.

[182] C. Schroder, Proteins in Ionic Liquids: Current Status of Experiments and Simulations, Top Curr Chem (Cham) 375(2) (2017) 25.

[183] J.Y. Chen, K. Vongsanga, X.G. Wang, N. Byrne, What Happens during Natural Protein Fibre Dissolution in Ionic Liquids, Materials 7(9) (2014) 6158-6168.

[184] E. Wenk, A.J. Wandrey, H.P. Merkle, L. Meinel, Silk fibroin spheres as a platform for controlled drug delivery, Journal of Controlled Release 132(1) (2008) 26-34.

[185] R.L. Moy, A. Lee, A. Zalka, Commonly Used Suture Materials in Skin Surgery, Am Fam Physician 44(6) (1991) 2123-2128.

[186] L. Fernandez-Garcia, N. Mari-Buye, J.A. Barios, R. Madurga, M. Elices, J. Perez-Rigueiro, M. Ramos, G.V. Guinea, D. Gonzalez-Nieto, Safety and Tolerability of Silk Fibroin Hydrogels Implanted into the Mouse Brain, Acta Biomater (2016).

[187] L. Uebersax, M. Mattotti, M. Papaloizos, H.P. Merkle, B. Gander, L. Meinel, Silk fibroin matrices for the controlled release of nerve growth factor (NGF), Biomaterials 28(30) (2007) 4449-60.

[188] C.-Z. Zhou, F. Confalonieri, M. Jacquet, R. Perasso, Z.-G. Li, J. Janin, Silk Fibroin: Structural Implications of a Remarkable Amino Acid Sequence, Proteins: Structure, Funtion, and Bioinformatics 44(2) (2001) 119-122.

[189] S. Sofia, M. McCarthy, G. Gronowicz, D. Kaplan, Functionalized silk-based biomaterials for bone formulation, Journal of Biomedical Materials Research 54(1) (2001) 139-148.

[190] H. Dou, B. Zuo, Effect of sodium carbonate concentrations on the degumming and regeneration process of silk fibroin, The Journal of The Textile Institute 106(3) (2014) 311-319.

[191] S.Z. Lu, X.P. Zhang, J. Wang, T.L. Xing, J. Jin, EFFECT OF DEGUMMING pH VALUE ON ELECTROSPINING OF SILK FIBROIN, Therm Sci 18(5) (2014) 1703-1704.

[192] I.C. Um, H.Y. Kweon, Y.H. Park, S. Hudson, Structural characteristics and properties of the regenerated silk fibroin prepared from formic acid, International journal of biological macromolecules 29(2) (2001) 91-97.

[193] B.P. Partlow, A.P. Tabatabai, G.G. Leisk, P. Cebe, D.L. Blair, D.L. Kaplan, Silk Fibroin Degradation Related to Rheological and Mechanical Properties, Macromol Biosci 16(5) (2016) 666-675.

[194] D.J. Hines, D.L. Kaplan, Mechanisms of controlled release from silk fibroin films, Biomacromolecules 12(3) (2011) 804-12.

[195] D.J. Hines, D.L. Kaplan, Characterization of Small Molecule Controlled Release From Silk Films, Macromolecular Chemistry and Physics 214(2) (2013) 280-294.

[196] M. Naessens, A. Cerdobbel, W. Soetaert, E.J. Vandamme, Leuconostoc dextransucrase and dextran: production, properties and applications, Journal of Chemical Technology & Biotechnology 80(8) (2005) 845-860.

[197] U.K. Laemmli, CLEAVAGE OF STRUCTURAL PROTEINS DURING ASSEMBLY OF HEAD OF BACTERIOPHAGE-T4, Nature 227(5259) (1970) 680-&.

[198] L. Li, S. Puhl, L. Meinel, O. Germershaus, Silk fibroin layer-by-layer microcapsules for localized gene delivery, Biomaterials 35(27) (2014) 7929-39.

[199] X. Hu, D.L. Kaplan, P. Cebe, Determining Beta-Sheet Crystallinity in Fibrous Proteins by Thermal Analysis and Infrared Spectroscopy, Macromolecules 39(18) (2006) 6161-6170.

[200] S. Hofmann, C.T. Foo, F. Rossetti, M. Textor, G. Vunjak-Novakovic, D.L. Kaplan, H.P. Merkle, L. Meinel, Silk fibroin as an organic polymer for controlled drug delivery, J Control Release 111(1-2) (2006) 219-27.

[201] D. Pawcenis, M.A. Koperska, J.M. Milczarek, T. Łojewski, J. Łojewska, Size exclusion chromatography for analyses of fibroin in silk: optimization of sampling and separation conditions, Applied Physics A 114(2) (2013) 301-308.

[202] Q. Lu, H. Zhu, C. Zhang, F. Zhang, B. Zhang, D.L. Kaplan, Silk self-assembly mechanisms and control from thermodynamics to kinetics, Biomacromolecules 13(3) (2012) 826-32.

[203] A. Matsumoto, A. Lindsay, B. Abedian, D.L. Kaplan, Silk fibroin solution properties related to assembly and structure, Macromolecular bioscience 8(11) (2008) 1006-18.

[204] O. Germershaus, V. Werner, M. Kutscher, L. Meinel, Deciphering the mechanism of protein interaction with silk fibroin for drug delivery systems, Biomaterials 35(10) (2014) 3427-34.

[205] J. He, Y. Wang, S. Cui, Y. Gao, S. Wang, Structure and properties of silk fibroin/carboxymethyl chitosan blend films, Polymer Bulletin 65(4) (2010) 395-409.

[206] P. Gupta, K.K. Nayak, Characteristics of Protein-Based Biopolymer and Its Application, Polym Eng Sci 55(3) (2015) 485-498.

[207] G. Freddi, A. Anghileri, S. Sampaio, J. Buchert, P. Monti, P. Taddei, Tyrosinase-catalyzed modification of Bombyx mori silk fibroin: grafting of chitosan under heterogeneous reaction conditions, J Biotechnol 125(2) (2006) 281-94.

[208] A.R. Murphy, D.L. Kaplan, Biomedical applications of chemically-modified silk fibroin, J Mater Chem 19(36) (2009) 6443-6450.

[209] Y. Gotoh, M. Tsukada, N. Minoura, Y. Imai, Synthesis of poly(ethylene glycol)-silk fibroin conjugates and surface interaction between L-929 cells and the conjugates, Biomaterials 18(3) (1997) 267-271.

[210] B. Zhou, P. Wang, L. Cui, Y. Yu, C. Deng, Q. Wang, X. Fan, Self-Crosslinking of Silk Fibroin Using H2O2-Horseradish Peroxidase System and the Characteristics of the Resulting Fibroin Membranes, Appl Biochem Biotechnol 182(4) (2017) 1548-1563.

[211] B.P. Partlow, M. Bagheri, J.L. Harden, D.L. Kaplan, Tyrosine templating in the self-assembly and crystallization of silk fibroin, Biomacromolecules (2016).

[212] J. Kundu, L.A. Poole-Warren, P. Martens, S.C. Kundu, Silk fibroin/poly (vinyl alcohol) photocrosslinked hydrogels for delivery of macromolecular drugs, Acta Biomater 8(5) (2012) 1720-1729.

[213] Y. Tamada, Sulfation of silk fibroin by chlorosulfonic acid and the anticoagulant activity, Biomaterials 25(3) (2004) 377-383.

[214] P. Taddei, C. Arosio, P. Monti, M. Tsukada, T. Arai, G. Freddi, Chemical and Physical Properties of Sulfated Silk Fabrics, Biomacromolecules 8 (2007) 1200-1208.

[215] A.R. Murphy, P. St John, D.L. Kaplan, Modification of silk fibroin using diazonium coupling chemistry and the effects on hMSC proliferation and differentiation, Biomaterials 29(19) (2008) 2829-38.

[216] H. Zhao, E. Heusler, G. Jones, L. Li, V. Werner, O. Germershaus, J. Ritzer, T. Luehmann, L. Meinel, Decoration of silk fibroin by click chemistry for biomedical application, J Struct Biol 186(3) (2014) 420-30.

[217] B. Le Droumaguet, K. Velonia, Click Chemistry: A Powerful Tool to Create Polymer-Based Macromolecular Chimeras, Macromolecular Rapid Communications 29(12-13) (2008) 1073-1089.

[218] B.B. Mandal, S. Kapoor, S.C. Kundu, Silk fibroin/polyacrylamide semi-interpenetrating network hydrogels for controlled drug release, Biomaterials 30(14) (2009) 2826-36.

[219] Y.Q. Zhang, Y. Ma, Y.Y. Xia, W.D. Shen, J.P. Mao, X.M. Zha, K. Shirai, K. Kiguchi, Synthesis of silk fibroin-insulin bioconjugates and their characterization and activities in vivo, Journal of Biomedical Materials Research Part B: Applied Biomaterials 79(2) (2006) 275-283.

[220] S. Sampaio, T.M.R. Miranda, J.G. Santos, G.M.B. Soares, Preparation of silk fibroin-poly(ethylene glycol) conjugate films through click chemistry, Polymer International 60(12) (2011) 1737-1744.

[221] M. Tabachnick, H. Sobotka, Azoproteins. I. Spectrophotometric studies of amino acid azo derivatives, J Biol Chem 234(7) (1959) 1726-1730.

[222] S.I. Presolski, V.P. Hong, M.G. Finn, Copper-Catalyzed Azide-Alkyne Click Chemistry for Bioconjugation, Curr Protoc Chem Biol 3(4) (2011) 153-162.

[223] Y. Qi, H. Wang, K. Wei, Y. Yang, R.-Y. Zheng, I.S. Kim, K.-Q. Zhang, A review of structure construction of silk fibroin biomaterials from single structures to multi-level structures, International journal of molecular sciences 18(3) (2017) 237.

6. Acknowledgements

Ganz großen Dank gilt Prof. Dr. Oliver Germershaus, der mich in seinen Arbeitskreis aufgenommen hat und mit seinem Wissen einen großen Teil zu dieser Arbeit beigetragen hat.

Auch bei Prof. Dr. Georgios Imanidis möchte ich mich ganz herzlich für die Aufnahme ins IPT bedanken. Mit den monatlichen Kolloquien hast du uns ein Einblick in die Projekte der anderen PhD Studenten gewährt und uns so dazu bewegt auch mal über den Tellerrand zu schauen.

Herzlichen Dank an Prof. Dr. Dagmar Fischer, die sich bereit erklärt hat, das Korreferat für meine Thesis zu übernehmen.

Besonders möchte ich mich bei allen IPT Arbeitskollegen bedanken. Hier gilt besonderer Dank Dominik, der mit mir das Labor stets mit guter Musik unterhalten hat und Andreas, Jonas und Felix für die durchaus produktiven Kaffeepausen, sowie die unvergesslichen Abende am Rhein und die entstandene Freundschaft.

Zu guter Letzt möchte ich meiner Familie danken, die stets an mich geglaubt haben, mich immer motiviert haben weiter zu machen und mir in jeder Lebenslage Rückhalt geben. Vor allem möchte ich mich an dieser Stelle bei meinem Vater bedanken, der mir das alles ermöglicht hat, mir immer mit Rat und Tat zur Seite steht und mit mir durch dick und dünn gegangen ist. Nicole, Werner und Renate möchte ich danken, dass wir bei euch immer eine offene Türe haben und ihr mit eurer fröhlichen Art es immer wieder schafft einen aufzumuntern. Vielen Dank Niko und Lea, dass ihr einfach immer für einen da seid. Ganz lieben Dank geht an meinen Freund Matthias, der in jeder Situation hinter mir stand, mich aufgemuntert und motiviert hat. So eine Familie zu haben ist unbezahlbar.

7. Appendix

CURRICULUM VITAE

PERSONAL DETAILS

Name	Kira Nultsch
Date of birth	24.09.1987
Place of birth	Buchen (Odenwald), Germany
Telephone number	0049 176 80042796
E-Mail-address	Kira.Nultsch@web.de

PROFESSIONAL AND ACADEMIC EXPERIENCE

03/2018 – now	Junior Project Manager Method Validation, Dottikon Exclusive Synthesis
10/2014 – 02/2018	PhD student, Department of Pharmaceutical Sciences, University of Basel *Novel Therapeutic Options for the Treatment of Chronic Wounds: Development of a bioresponsive, Silk Fibroin-based Delivery System for Sensitive Drugs*
05/2014 – 09/2014	Pharmacist (Die Odenwald Apotheke in Buchen)
11/2013 – 04/2014	Practical Training, Forensic Toxicology-Institute of Forensic Medicine (Goethe University Frankfurt) *Forensic-toxicological analysis of blood and urine samples and other body fluids and organs regarding medication and drugs*
05/2013 – 10/2013	Practical Training, *Community Pharmacy and Hospital Pharmacy*, Pharmacy (Die Odenwald Apotheke in Buchen)
03/2009 – 04/2013	Studies of Pharmacy, Julius-Maximilians-University Würzburg

PUBLICATIONS

Articles	*Matrix metalloprotease triggered bioresponsive drug delivery systems – Design, synthesis and application*. Kira Nultsch, Oliver Germershaus (2018). Eur J Pharm Biopharm *Effects of Silk Degumming Process on Physicochemical, Tensile, and Optical Properties of Regenerated Silk Fibroin*. Kira Nultsch, Livia K. Bast, Muriel Näf, Salima El Yakhlifi, Nico Bruns, Oliver Germershaus (2018). Macromol Mater Eng

Silk fibroin degumming affects scaffold structure and release of macromolecular drugs. Nultsch, K., Germershaus, O. (2017). Eur J Pharm Sci

Localized, non-viral delivery of nucleic acids: Opportunities, challenges and current strategies. Germershaus, O., Nultsch, K. (2014). Asian J Pharm Sci

Posters

Tailoring the Release Pattern by Varying the Silk Purification Process and by Chemical Modification, Annual Research Meeting University of Basel, 02/2017

Influencing the release pattern of prilled particles by varying the silk purification process, AGPI/ADRITELF: Site-specific drug-delivery, Antibes-Juan-les-Pins, 09/2016

Tailoring the drug release of silk-based drug delivery systems via silk modification, Swiss Pharma Science Day, Bern, 08/2016

Controlling the drug release characteristics of silk-based microspheres by modifying the parameters of the silk fibroin purification process, Gordon Research Conference: Bioinspired Materials, Les Diablerets, 06/2016

Elucidating the Silk Fibroin Purification Process and its Impact on Drug Delivery System Performance, Controlled Release Society Local Chapter Germany, Saarbrücken, 03/2016

The Impact of the Silk Fibroin Extraction Process on Drug Delivery System Performance, Annual Research Meeting University of Basel, 02/2016

Effect of Silk Fibroin Purification Process on the Performance of Silk-Based Drug Delivery Systems, Swiss Pharma Science Day Bern, 08/2015

Presentation

Controlled Release from Silk Fibroin based Drug Delivery Systems, Annual Research Meeting University of Basel, 02/2018

Controlling the release of silk fibroin microspheres by chemical modification, Controlled Release Society Local Chapter Germany, Marburg, 03/2017

TRANSFERABLE SKILLS

Technical Writing, Articles in the Life Sciences and Natural Sciences

Conflict Management and Facilitating Communication

Self-Branding and Self-Promotion

English: Advanced (C1/C2) Speaking and Writing

AWARDS

Travel Award, Best Poster Presentation, BioBarriers 2016 Conference and 20th Annual Meeting of CRS Local Chapter, Saarbrücken Germany